NOTICE

The quality of this microform is heavily dependent upon the quality of the original thesis submitted for microfilming. Every effort has been made to ensure the highest quality of reproduction possible.

If pages are missing, contact the university which granted the degree.

Some pages may have indistinct print especially if the original pages were typed with a poor typewriter ribbon or if the university sent us an inferior photocopy.

Previously copyrighted materials (journal articles, published tests, etc.) are not filmed.

Reproduction in full or in part of this microform is governed by the Canadian Copyright Act, R.S.C. 1970, c. C-30.

AVIS

La qualité de cette microforme dépend grandement de la qualité de la thèse soumise au microfilmage. Nous avons tout fait pour assurer une qualité supérieure de reproduction.

S'il manque des pages, veuillez communiquer avec l'université qui a conféré le grade.

La qualité d'impression de certaines pages peut laisser à désirer, surtout si les pages originales ont été dactylographiées à l'aide d'un ruban usé ou si l'université nous a fait parvenir une photocopie de qualité inférieure.

Les documents qui font déjà l'objet d'un droit d'auteur (articles de revue, tests publiés, etc.) ne sont pas microfilmés.

La reproduction, même partielle, de cette microforme est soumise à la Loi canadienne sur le droit d'auteur, SRC 1970, c. C-30.

Canada

THE UNIVERSITY OF ALBERTA

P, T, AND RELATIVE TIMING OF METAMORPHISM IN THE AUREOLE AROUND THE ANVIL BATHOLITH, SOUTH CENTRAL YUKON.

BY

JENNIFER MARGARET SMITH

A THESIS

SUBMITTED TO THE FACULTY OF GRADUATE STUDIES AND REASEARCH IN PARTIAL FULFILMENT OF THE REQUIREMENTS FOR THE DEGREE OF

MASTER OF SCIENCE

DEPARTMENT OF GEOLOGY

EDMONTON, ALBERTA

FALL 1988

ISBN 0-315-45621-3

THE UNIVERSITY OF ALBERTA

RELEASE FORM

NAME OF AUTHOR: Jennifer M. Smith

TITLE OF THESIS: P, T and relative timing of metamorphism in the aureole around the Anvil Batholith, south central Yukon.

DEGREE: Master of Science

YEAR THIS DEGREE GRANTED: Fall, 1988

Permission is hereby granted to THE UNIVERSITY OF ALBERTA LIBRARY to reproduce single copies of this thesis and to lend or sell such copies for private, scholarly or scientific research purposes only.

The author reserves other publication rights, and niether the thesis nor extensive extracts from it may be printed or otherwise reproduced without the author's written permission.

(SIGNED) Jennifer M. Smith

PERMANENT ADDRESS

540 Lakeshore Rd. W.
Appleby College,
Oakville, Ontario
L6K 3P1

DATE October 3, 1988.

THE UNIVERSITY OF ALBERTA

FACULTY OF GRADUATE STUDIES AND RESEARCH

The undersigned certify that they have read, and recommend to the Faculty of Graduate Studies and Research for acceptance a thesis entitled P, T and relative timing of metamorphism in the aureole around the Anvil Batholith, south central Yukon, submitted by Jennifer M. Smith in partial fulfillment of the requirements for the degree of Master of Science in Geology.

Philippe Erdmer
.....
(Supervisor)

John Hoeldewatt
.....

R A Burwell
.....

B. E. Nesbitt
.....

Date: 03 october, 1988.

DEDICATION

I dedicate this thesis to my parents who have been a never-ending source of enthusiasm. Always supportive of education, they inspired my curiosity and allowed me to grow to love learning independantly. With no words of strict direction and no negative feelings toward shortcomings, their positive attitudes toward my goals have always allowed me to believe that there is nothing I cannot do and nothing I must do either.

Thank you Mom and Dad.

ABSTRACT

The mid-Cretaceous Anvil batholith, located 10 km northeast of Faro in south central Yukon, intrudes late Proterozoic to late Paleozoic metasedimentary and metavolcanic rocks. Biotite, garnet and staurolite-andalusite isograds near the pluton were defined in previous work. Because of the truncation of isograds at the granitic contact, because of a marked variation in the width of the metamorphic zone, and because the mineral assemblages appeared more typical of regional than contact metamorphism, the metamorphic zone was interpreted as a contact aureole. From the nearby presence of unmetamorphosed Devonian rocks directly overlying biotite-grade rocks of Cambrian age, metamorphism was interpreted as pre-Devonian in age. A model of arching of regionally metamorphosed rocks by the pluton to produce the "isograds" was proposed.

Subsequent work has suggested that the mineral assemblages in the Cambrian schist adjacent to the intrusion represent a stable assemblage reflecting conditions at the time of emplacement.

The present study has refined the sillimanite, staurolite, andalusite, garnet and biotite isograds

which are concentric to the pluton in the study area.

The isograds dip away from the pluton at the present level of exposure and follow the contact at depth. This accounts for variation in the width of the metamorphic zone.

Porphyroblast-matrix relationships in the metamorphic rocks indicate that metamorphism occurred during the D_2 event, the intrusion of the pluton.

Geothermometry results indicate that country rock adjacent to the Anvil batholith was heated to temperatures of more than 600 ^{o}C. A consistent trend of decreasing temperatures away from the intrusive margins is recorded. Geobarometry results indicate that the average pressure was 4.9 $\pm$ 1.6 kbar and suggests a maximum thickness of cover during emplacement of about 16 km ($\pm$ 5 km).

Large-scale uplift of the Mount Mye area is implied by the geobarometry results. Previously proposed cogenetic relationships between the Anvil Plutonic Suite and the South Fork volcanics cannot be reconciled with this evidence. As there is no evidence for similar large-scale uplift since the mid-Cretaceous in the Yukon-Tanana terrane to the west, significant differential uplift across Tintina fault in this area is implied.

ACKNOWLEDGEMENTS

I thank Jim Morin for suggesting this project and for encouraging me to go on to the graduate level. My supervisor, Philippe Erdmer, provided helpful guidance throughout the duration of this project.

Field work and thin sections were financially supported by the Department of Indian and Northern Development, and by NSERC grant number A0750. Further financial support was provided through teaching assistantships and a research assistantship provided by the University of Alberta.

Dave Tomlinson was a helpful technician in the microprobe lab. Excellent field assistance and many laughs were provided by Teresa Potter. I would also like to thank supportive colleagues, Steve Johnston and Heather Plint for good advice, good times and much laughter.

Last, but far from least, I would like to thank Alex Nikolajevich for being the light at the end of the tunnel.

TABLE OF CONTENTS

LIST OF TABLES

LIST OF FIGURES

LIST OF PLATES

LIST OF ABBREVIATIONS
(used in appendices)

sch = schist
skn = skarn
int = intrusive
phyl = phyllite
lmst = limestone
amph = amphibolite
Ch = chlorite
Bt = biotite
Ms = muscovite
Gt = garnet
Si = sillimanite
An = andalusite
St = staurolite
Hb = hornblende
Qz = quartz
Fs = feldspar
Zr = zircon
Ti = sphene
To = tourmaline
Ct = calcite
Cz = clinozoisite
Di = diopside
Vs = Vesuvianite
Tr = tremolite-actinolite
Ru = rutile
Opq = opaque minerals
Pyr = pyrope
Alm = almandine
Sp = spessartine
Gro = grossular
Phl = phlogopite
Ann = annite
Mn = Manganese
Ab = albite
An = anorthite
Or = orthoclase

I. INTRODUCTION

This thesis reports on a detailed study of a metamorphic aureole developed in Hadrynian (?) to Ordovician (?) schists adjacent to the mid-Cretaceous Anvil batholith, 200 km northeast of Whitehorse, Yukon Territory (Figure 1).

Most Lower and mid-Cretaceous plutons in the eastern Canadian Cordillera were emplaced into sedimentary or greenschist-facies metasedimentary rocks. They exhibit clearly-defined metamorphic aureoles characterized by andalusite and (or) cordierite and staurolite (Reesor, 1973), as well as structural aureoles.

Tempelman-Kluit (1972) reported transgression of isograds by the Anvil pluton, and a marked variation in the width of the metamorphic zone. Mineral assemblages were interpreted as typical of regional rather than contact metamorphism and, as a result, the metamorphism of the pelitic sediments was interpreted as a regional event preceeding the intrusive event.

From the nearby presence of unmetamorphosed Devonian rocks apparently overlying biotite-grade rocks of Cambrian (?) age, the regional metamorphism was interpreted as pre-Devonian in age. A model of arching of regionally

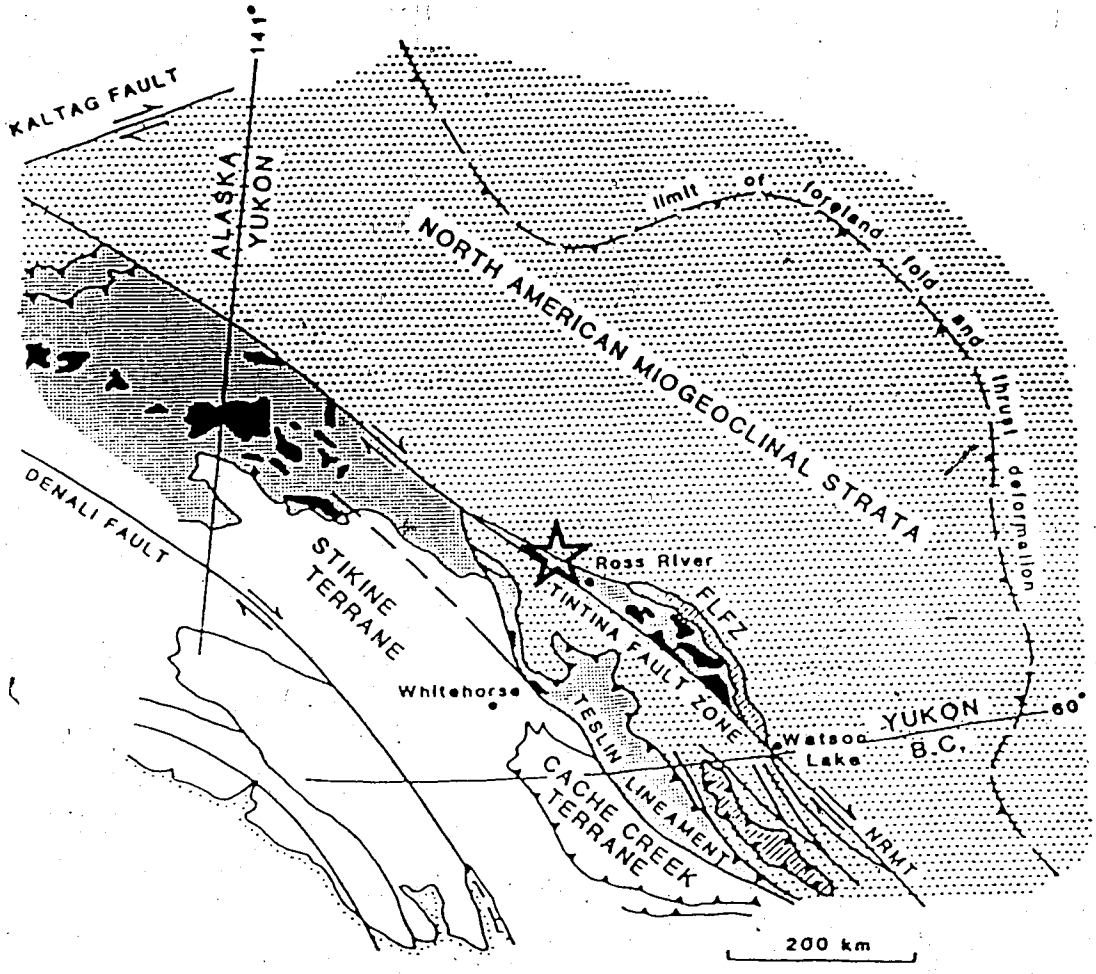

Figure 1. Location map modified after Mortensen and Jilson (1983), dense stipple = Yukon-Tanana terrane; open stipple = North American miogeoclinal strata; ruled pattern = Slide Mountain terrane; solid black = Mississippian orthogneisses; FLFZ = Finlayson Lake fault zone; NRMT = Northern Rocky Mountain Trench. The study area is indicated by the star.

metamorphos rocks by the pluton to produce the "isograds" was proposed (Tempelman-Kluit, 1972).

Pigage and Anderson (1985) suggested that the mineral assemblages in the pelitic schist adjacent to the intrusion represent a stable assemblage reflecting conditions at the time of emplacement. They concluded that the structural setting of the area indicates shallow intrusion of the Anvil plutonic suite, contemporaneous with or slightly younger than second-phase deformation in the area.

The present study was carried out to examine the relationship of the mineral isograds to the intrusive body, to determine the pressure and temperature of metamorphism, and the timing of emplacement of the Anvil batholith with respect to regional metamorphism and deformation.

Five weeks of geological mapping and sample collection from helicopter-supported fly-camps was followed by detailed petrologic work on 150 thin sections. Microprobe analyses of garnet-biotite pairs and of garnet-plagioclase-Al_2SiO_5-quartz assemblages were used in geothermo-barometry studies.

The sillimanite, staurolite, andalusite, garnet and biotite isograds are concentric to the pluton in the study area.

The Anvil batholith was emplaced under approximately 5 kilobars of pressure, and heated adjacent country rock to temperatures of more than 600 ^{o}C.

The moderately high pressures of metamorphism indicate large scale uplift since the mid-Cretaceous. Significant differential uplift since the mid-Cretaceous across Tintina fault in this area is inferred.

II. REGIONAL GEOLOGY

Setting

The Anvil Range lies on the southwestern edge of the Selwyn Basin in the Omineca Crystalline Belt (OCB). The Anvil district, is characterized by several uplifts of polydeformed and metamorphosed strata (Jennings and Jilson, 1986). Large, late- to syn-kinematic, 100 Ma-old granites form the cores of these uplifts.

The core of the Anvil Range is largely underlain by granodiorite and porphyritic quartz monzonite of the Anvil Batholith (Tempelman-Kluit, 1972).

Metasedimentary rock units that flank the Anvil Batholith range in grade from upper greenschist to almandine-amphibolite facies. They are considered to be the metamorphic equivalents of the Upper Proterozoic to Lower Paleozoic clastic and carbonate sequences in the Selwyn Basin (Tempelman-Kluit, 1972; Blusson, 1966).

The North American miogeocline is separated from the allochthonous Yukon-Tanana terrane (YTT) (Coney et al., 1980) by the steeply southwest-dipping Vangorda fault zone (Figure 1, Pigage and Anderson, 1985). Right-lateral movement on the Tintina fault system subsequently offset all units. The Anvil plutonic suite intrudes the Vangorda

fault and is displaced along the Tintina fault. Rb - Sr age determinations on the batholith by Pigage and Anderson (1985) provided an age of (100± 2 Ma). Rb - Sr geochronological results also provide a minimum age of deformation of the metasedimentary rocks and a maximum age (99± 2.5 Ma) for movement along the Tintina. K - Ar (mineral) isotopic data overlaps with the Rb - Sr (isochron) data around 100 Ma. This indicates rapid cooling and therefore, likely rapid uplift in the area (Pigage and Anderson, 1985).

Adjacent to Tintina fault, steeply-dipping northwest-trending faults splay from the Tintina and Vangorda faults and cut the Anvil Range. Movement along some of these faults involves a complex history of early reverse, strike-slip, and late normal periods of movement which may record the final stages of uplift in the area (Pigage and Jilson, 1985).

Stratigraphy

The Anvil Range was first mapped by Roddick and Green (1961). Detailed work on the stratigraphy was completed by Tempelman-Kluit (1972) and Jennings et al (1980). Gordey (1983) recognized two subhorizontal thrust faults in the area. Jennings and Jilson (1986) studied the lower portion of the Precambrian to Permian stratigraphic sequence, specifically the pre-Ordovician part in which

Pb-Zn-Ag-barite deposits occur (Figure 2, Table 1).

The Upper Proterozoic to Mississippian miogeoclinal rocks can be divided into an upper and a lower division (Jilson, 1984). The present study is concerned only with the lower division, which comprises approximately 5 km of late Precambrian to Silurian metasedimentary and lesser mafic volcanic rocks (Jennings and Jilson, 1986).

The oldest sequence is 2 km thick. It consists of lower Cambrian (?) and/or Hadrynian (?), muscovite-quartz-biotite schist, phyllite and hornfels with laminated calc-silicate rock, pale grey marble and rare lenses of amphibolite (unit 2 of Tempelman-Kluit, 1972; unit 1 of Gordey, 1983; HEmm of Jennings and Jilson, 1986). The schist generally hosts almandine-amphibolite facies assemblages which include sillimanite $\pm$ staurolite $\pm$ andalusite $\pm$ garnet + biotite + muscovite + quartz + feldspar. Schist, phyllite and calc-silicate rocks are conformably (?) overlain by Middle and Upper Cambrian (?) to lower Ordovician phyllitic rocks. The phyllite varies from 0.5 to 2 kilometers in thickness, includes 15% basic igneous rocks and becomes more calcareous up section. Regional correlation of the lower division rocks has been discussed by Jennings and Jilson (1986).

The lower division is capped by early Ordovician basalts interleaved with black phyllite. The laterally extensive volcanic rocks reach up to 1.5 kilometers in

Figure 2. Regional geology modified after Jennings and Jilson (1986).

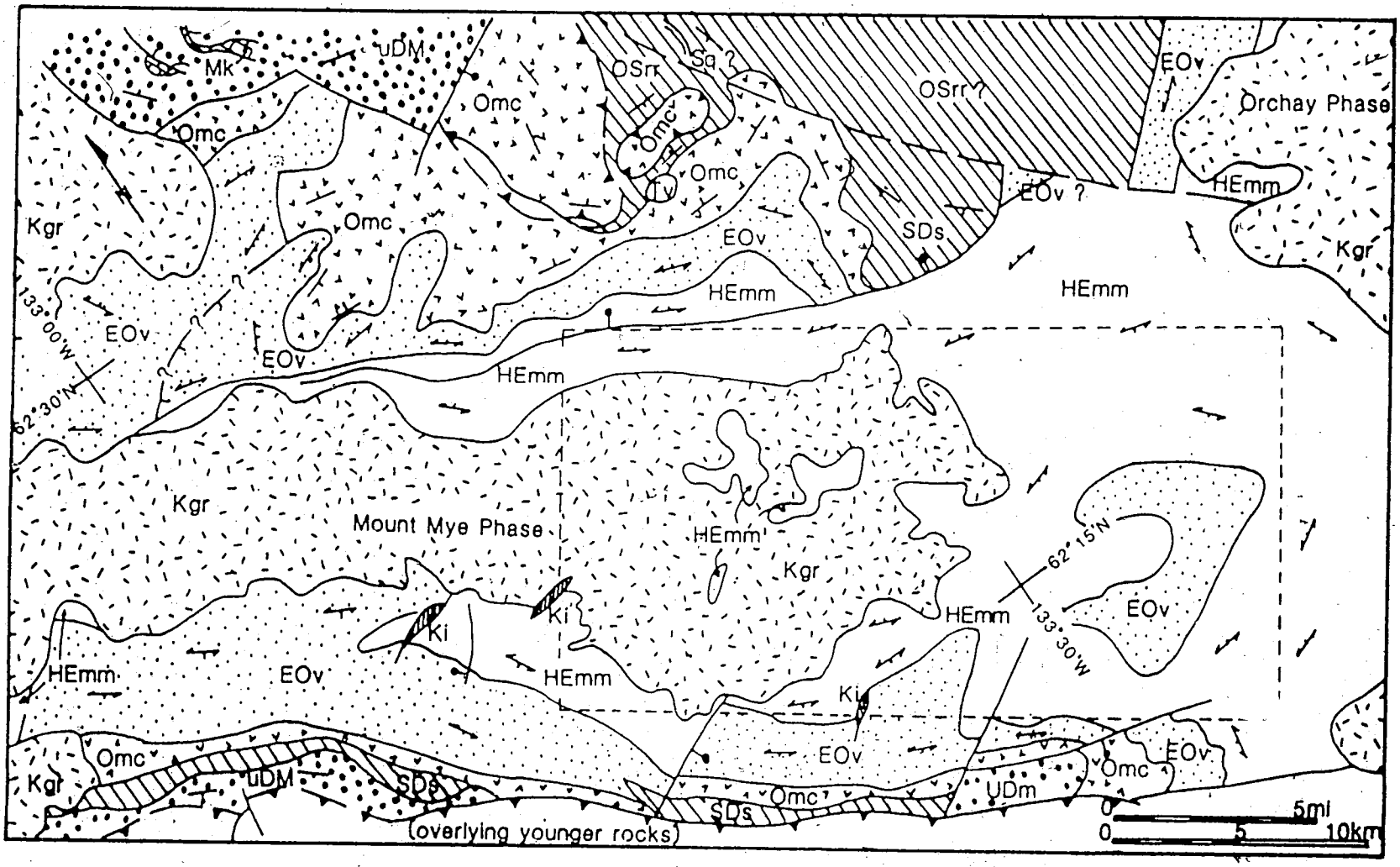

LEGEND

Tertiary (?)

Tv rhyolite plug

Cretaceous

Ki porphyritic hornblende diorite

Kgr granite (Anvil Batholith)

Devonian and Mississippian

uDm slate, chert, greywacke, conglomerte, limestone

Mk crinoidal limestone

Ordovician to Devonian

Sq medium grained orthoquartzite

SDs black phyllite with middle Devonian limestone lenses

OSrr black slate, chert

lower Ordovician (and younger?)

Omc argillite, silstone, basalt

Cambrian to lower Ordocivian (?)

EOv phyllite, chloritic tuff

lower Cambrian and Hadrynian (?)

HEmm skarn, ms-qz-bi schist, amphibolite, marble.

SYMBOLS

outline of study area

contact

normal fault, ball on downthrown side

thrust fault

moderately or shallowly dipping fault of unkonwn sense of displacement

bedding strike and dip direction (mostly 45° or less)

S_2 foliation (mostly less than 45°)

Figure 2. Continued.

TABLE OF FORMATIONS

	PERIOD/ EPOCH	MAP UNIT: Tempel-man-Kluit (1972)	MAP UNIT: Gordey (1983)	MAP UNIT: Jennings & Jilson (1986)	LITHOLOGY	THICKNESS
	T	14b		Tv	Rhyolite plug	
		intrusive into units 3, 4 of Gordey (1983)				
	K or T	13		Ki	porphyritic hornblende diorite	
		intrusive into units 1, 2, 3 of Gordey (1983)				
	K	11	9	Kgr	granite (Anvil Batholith)	
		intrusive into units 1, 2, 3 of Gordey (1983)				
Upper Division	D - M	7	8	uDM	slate, chert, grey-wacke, conglomerate, limestone	500 m +
		thrust fault contact (?) with overlying younger rocks				
	D	6	7	Mk	crinoidal limestone	0 - 30 m
	S & D	5	6	Sq	medium grained orthoquartzite	40 m +
		unconformable (?)				
	O & S	4	5	SDs(?) OSrr(?)	black slate, chert	130 m
	C - O		4	OSrr(?) Omc(?)	argillite, siltstone basalt	400 m
A.R.G. Lower divi...n		8b	3	Omc	basalt	up to 1500 m
		3, 3a	2	EOv	phyllite, chloritic tuff	500 - 2000 m
		2	1	HEmm	skarn, ms-gz-bi schist, amphibolite, marble	2000 m

TABLE 1. Table of formations modified after Jennings and Jilson (1986).

thickness (Jennings and Jilson, 1986). The volcanic rocks and underlying calcareous phyllites represent Campbell's (1967) Anvil Range Group.

The upper and lower divisions are separated by Ordovician to Silurian grey-black slate, black shale, and argillite, which contain late middle-Devonian limestone lenses and are overlain by thick-bedded orthoquartzite and by limestone and dolomite.

The lower division is unconformably overlain by a series of chert-rich clastic and carbonate strata that range in age from mid-Ordovician to Permian. All or part of this sequence may be allochthonous (Jilson, 1984). These rocks correlate with the Earn Group and include the type locality of the Anvil Range Group as defined by Jennings and Jilson (1986) after Tempelman-Kluit (1972). Detailed descriptions of the stratigraphy of the upper division are given by Tempelman-Kluit (1972), Gordey (1983), and Jennings and Jilson (1986).

Nomenclature - Anvil Range Group

Gordey (1983) determined that rocks included in Campbell's (1967) Anvil Range Group are parautochthonous in nature and Cambro-Ordovician in age. He suggested that the Upper Paleozoic volcanic rocks exposed on the southwest side of the Anvil Range have a strong affinity with the allochthonous Yukon-Tanana terrane. These should be

excluded from the Anvil Range Group since they are distinct from those rocks originally defined by Campbell (1967).

Jennings and Jilson (1986), following Tempelman-Kluit (1972), suggest that the name Anvil Range Group be applied to the upper Paleozoic basalt and underlying chert and tuffaceous chert exposed on the southwest flank of the Anvil Range.

Intrusive Rocks

The most extensive intrusive assemblage is formed of the Mid-Cretaceous granitic rocks of the Anvil plutonic suite in the core of the Anvil Range. Pigage and Anderson (1985) have mapped three distinct phases; the Orchay and Marjorie phases, hornblende-biotite granodiorite and minor granite intrusions, and the Mount Mye phase, a muscovite-biotite granite. Locally, these granitic rocks are cut by porphyritic hornblende diorite dykes and plugs.

Structure

Arching of the Paleozoic rocks that flank the Anvil intrusive forms a relatively young regional structure. Tempelman-Kluit (1972) termed this irregular, asymmetrical, northwest-trending, structural culmination, the Anvil Arch.

Evidence for four (Tempelman-Kluit, 1972) or five (Jennings and Jilson, 1986) phases of deformation in the

area has been presented. Foliation associated with the second deformation event dominates the metasedimentary package. The Anvil Arch is related to the third (or later) deformation event (Tempelman-Kluit, 1972; Pigage and Anderson, 1985).

III. GEOLOGY OF THE STUDY AREA

In the Mt. Mye area, good bedrock exposure is found along ridges and locally along streams in broad U-shaped valleys (Figure 11 in pocket). Contacts are sharp. A 600 meter-thick, 7 kilometer-wide slab of metasedimentary rocks forms a roof pendant in the Anvil Batholith and is exposed at the higher elevations in the study area.

Layering and schistosity in the metasedimentary rocks dip moderately northeast in the northeast portion of the map area and southwest in the southwest. Compositional banding defined by pelitic and calc-silicate layers likely represents premetamorphic layering. The stratigraphic thickness of the studied assemblege is approximately 2.3 km.

METASEDIMENTARY ROCKS

The metasedimentary rocks are divided into phyllite, calc-silicate and schist units.

Phyllite

Phyllitic rocks weather recessively and are exposed along Vangorda Creek road and on slopes 8 km

north-northeast of Mt. Mye. A 550 meter-thick unit of phyllite is exposed in the study area (Figure 11, in pocket).

The friable phyllite is lustrous silver-grey on fresh and weathered surfaces. The rock breaks readily along the main foliation plane and weathers to distinctive small, flat chips. The rock is locally tuffaceous, contains pods of andesitic greenstone, and is interlayered with graphitic phyllite and thinly banded calc-silicate.

Detailed petrography of this unit is reported by Tempelman-Kluit (1972) and Jennings and Jilson (1986).

The phyllitic rocks were probably originally a silty shale. The chloritic tuff is likely of volcanic derivation. The greenstone pods may be intrusive in origin (Tempelman-Kluit, 1972).

Calc-silicate Rocks

Laminated calc-silicate rock forms resistant, blocky outcrops. Calc-silicate is exposed on the south-southeastern slopes of Mt. Mye and in the roof pendant (Figure 11, in pocket). Layers of calc-silicate are over 50 m thick in the study area.

In outcrop, competent, discontinuous, light green to cream and purplish-brown bands vary in thickness from less than 1 mm to 8 mm.

Finely banded calc-silicate contains more pelitic material and commonly more graphite than coarsely banded

calc-silicate. Coarsely banded calc-silicate locally contains discontinuous schistose partings defined by parallel arrangement of micas.

Rare, foliated amphibolite pods and coarsely crystalline grey marble are included in this unit. The marble is banded (Plate 1) and generally less than 10 meters thick. Marble is locally folded into tight, disharmonic structures (Plate 2).

Detailed petrography of this unit is reported by Tempelman-Kluit (1972) and Jennings and Jilson (1986).

Contacts between alternating pelitic and calcareous layers are sharp, as are contacts with overlying and underlying units.

The calc-silicates probably represent a thin-bedded, fine-grained succession of calcareous, silty, and argillaceous sediments. The amphibolite was probably originally a volcanic rock (Tempelman-Kluit, 1972).

Schist

Grey, rusty-weathering, strongly foliated schist is generally recessive. Outcrops of schist are found on all flanks of Mt. Mye. Schist makes up a 1300 m thick (stratigraphic thickness) unit in the study area.

In outcrop, quartz stringers, veins typically less than 0.5 m in width, boudins, and fist-sized blobs stand out from the soft, dark-coloured schist. The stringers,

5

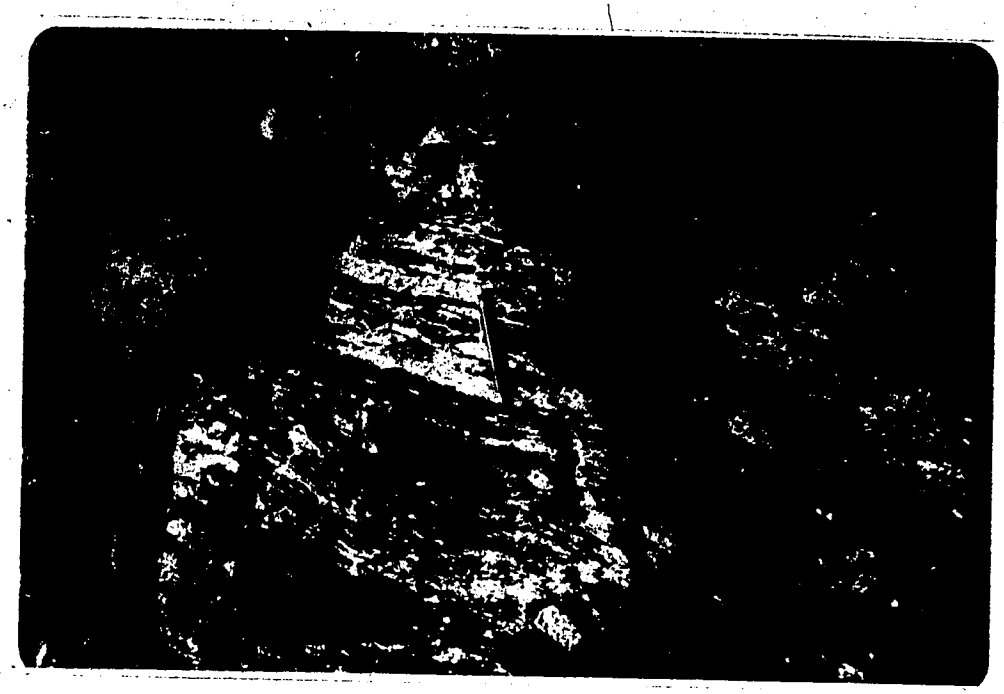

PLATE 1 Pods of coarsely crystalline banded grey marble are generally less than 10 m thick.

PLATE 2 Marble is locally folded into tight disharmonic structures.

boudins and blobs lie in the schistosity and may reflect original compositional changes, but more likely represent post-depositional quartz precipitates. Small quartz veins cut schistosity defined by the parallel arrangement of micaceous and fibrous minerals.

Sillimanite, staurolite, andalusite, garnet and biotite porphyroblasts are present in the mica-rich laminae. Sphene, tourmaline, ilmenite, zircon and varying amounts of graphite are common accessory phases.

Porphyroblasts in the schists locally preserve well-developed inclusion trails. An earlier foliation is preserved in microlithons between foliation surfaces. A discussion of microstructure is given in Chapter IV.

The schist includes foliated amphibolite bodies and thin layers of dark amphibole-rich, sulphide-bearing rock near the uppermost part of the unit. The amphibole-rich layers may be derived from tuffaceous units (Jennings and Jilson 1986).

The schist is gradational with the underlying phyllite. The appearance of large andalusite porphyroblasts and an increase in graphite content mark the gradational change in rock type. Contacts with interlayered calc-silicate horizons are sharp.

Schist and phyllite are compositionally similar, and probably represent the same pelitic package at different metamorphic grades (Jennings and Jilson 1986).

Jennings and Jilson (1986) suggested that these fine-grained, thinly banded, homogeneous rocks may have accumulated in relatively deep water on or at the foot of a continental rise.

Isograds

Metamorphic mineral assemblages in the schist vary consistently with distance from the intrusive contact. Phases include sillimanite, staurolite, andalusite, garnet, biotite, and muscovite. The mineral isograds are defined by the appearance of specific minerals in the schist and are therefore compositionally controlled (Appendix 2, Figure 13).

Sillimanite (in), staurolite (in/out), andalusite (in/out), garnet (in), and biotite (in) isograds have been recorded in the study area (Figure 12, in pocket). From present mapping, the isograds are well constrained along the north-northeast and east margins of the batholith and more loosely defined along the southern and southwestern margins. Along the north-northeast margin, isograds cut across topographic contour lines at a high angle, suggesting steeply-dipping isograd surfaces and high temperature gradients. A similar though less well-developed pattern is observed in the south (section A-B, Figure 14, in pocket). Isograds dip at progressively lower angles away from the intrusive. The underlying

intrusive contact is interpreted to dip more shallowly away from the exposed contact. The topographic trace of the contact and the wide spacing of isograds in the east and in the southwest suggest that the intrusive contact dips more shallowly than at the north-northeast and southern contacts. Staurolite persists to the east, beyond the limit of the study area. Andalusite persists to the southwest, beyond the limit of the study area.

The Anvil pluton outside the study area is elongate in a northwest-southeast direction. This supports the interpretation that the intrusive contact extends shallowly for some distance to the east. It crops out to the east.

INTRUSIVE ROCKS

Anvil Batholith

Resistant granite of the Anvil Batholith underlies Mount Mye, the highest peak in the study area. Blocky, locally castellated outcrops are characteristic.

Detailed study indicates that the batholith comprises three distinct phases which range in composition from muscovite-biotite granite to hornblende-biotite granodiorite (Pigage and Anderson, 1985).

The Mt. Mye phase underlies the study area. It is medium-grained, hypidiomorphic to granular, biotite-muscovite granite that is locally porphyritic and foliated

near the margin. The marginal foliation is defined by mica aggregates.

Granitic Sills

The intrusive's boundaries are marked by crosscutting dykes and sills (Plate 3) and by lit-par-lit layering of granite and schist. The granitic sills range from 1 m to 25 m in thickness (Plate 4), are locally foliated (Plate 5), and are commonly garnet-bearing. The foliation, defined by mica aggregates, is parallel to foliation in the adjacent schist.

In thin section, fractured euhedral garnets less than 1 to 2 mm in diameter constitute 2 - 3% of the rock. The granitic sills are otherwise petrographically similar to the Mount Mye phase.

Muscovite - biotite - potassium feldspar (with graphic intergrowth of quartz) - quartz - tourmaline dykes occur at the batholith contacts and are steeply dipping. They cut across foliation.

Diorite Dykes

Northeast-trending, grey-green diorite dykes up to 3 m across cut the Anvil batholit. They form small, blocky ridges in the schist.

Hornblende diorite dykes have been described by Tempelman-Kluit (1972), Pigage and Anderson (1985) and

PLATE 3 Locally intrusive contacts are marked by crosscutting dykes and sills.

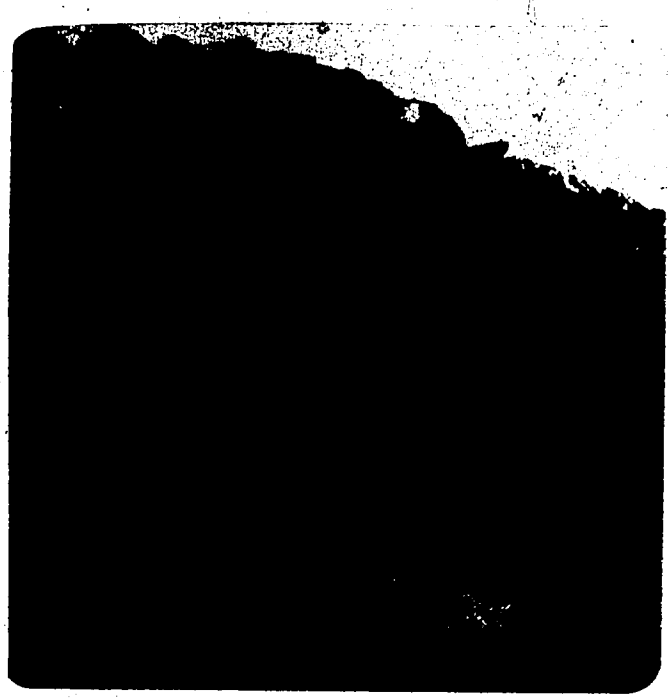

PLATE 4 Granitic sills are injected along the main foliation plane in the schist. Sills range from 1 m to 25 m in thickness.

PLATE 5 A weakly foliated a granitic sill. The foliation is defined by mica aggregates and is concordant with the main foliation plane (S_2) in the adjacent schist.

Jennings and Jilson (1986), who describe alterations including replacement of plagioclase by sausserite and replacement of hornblende phenocrysts by chlorite-epidote aggregates. Diorite dykes in the study area have less than 10% pyroxene phenocrysts that have been completely replaced by chorite ± calcite as well as strongly sausseritized plagioclase.

These late dykes may be associated with a late phase of the Anvil batholith or they may result from an entirely separate event (Tempelman-Kluit, 1972).

IV. STRUCTURE

The structure of the area has been described by Tempelman-Kluit (1972)

A detailed study of the structure on the southwest flank of the Anvil Range by Jennings and Jilson (1986) demonstrated that structural style is similar to the rest of the district.

The present study follows the structural interpretation of Tempelman-Kluit (1972).

The phyllite, schist, and calc-silicate rocks part along a well-developed crenulation foliation S_2 defined by muscovite + chlorite $\pm$ biotite in the phyllite and by the parallel arrangement of coarse-grained biotite and fine-grained muscovite $\pm$ fibrous sillimanite in the schist. Foliation planes are several millimeters thick and separate slightly thicker quartz and feldspar layers.

Locally, an older surface (S_1) defined by a compositional layering where quartz-rich layers alternate with mica-rich layers (Plate 6) and/or defined by preferred mica orientation (Plate 7) can be identified in microlithons between foliation planes. S_1 is a tectonic fabric that likely parallels original bedding (S_o). The intersection of S_1 and S_2 defines a lineation (L_2)

PLATE 6 S_1 is defined by compositional layering where quartz-rich layers alternate with mica-rich layers in the microlithons between S_2 planes. Field of view = 4.5 mm x 2.8 mm.

PLATE 7 S_1 is also defined by preferred mica orientation in the microlithons between S_2 planes. Field of view = 4.5 mm x 2.8 mm

observed most readily on S_2 cleavage surfaces.

Locally, S_2 is crenulated into symmetrical broad or open wrinkles with an amplitude of less than 2 mm and a wavelength of 4 mm or less. S_2 is locally asymmetrically crenulated into tiny folds (F_3) with amplitudes of less than 1 mm and wavelengths of less than 2 mm. Alignment of micas along the long limbs of the crenulations (incipient S_3 development) is observed (Plate 8). S_2 is also folded on a thin-section scale into sub-isoclinal folds (F_3) with amplitudes of less than 3 cm. Minor slip on S_2 surfaces indicates that S_2 is a locus of shear strain (Plate 9).

Jennings and Jilson (1986) described three late sets of crenulations affecting S_2, and corresponding foliation surfaces (S_3 through S_5) and crenulation lineations (L_3 through L_5). Evidence for the relative timing of these late crenulations is not presented. The late crenulations are only locally developed.

Plates 10 and 11 illustrate the largest-scale F_3 folds observed. In two locations a gentle warping of the F_3 axial plane surface was observed.

The final deformation event as described by Tempelman-Kluit (1972), is a regional culmination produced by arching of the Paleozoic rocks around the Anvil batholith during intrusion.

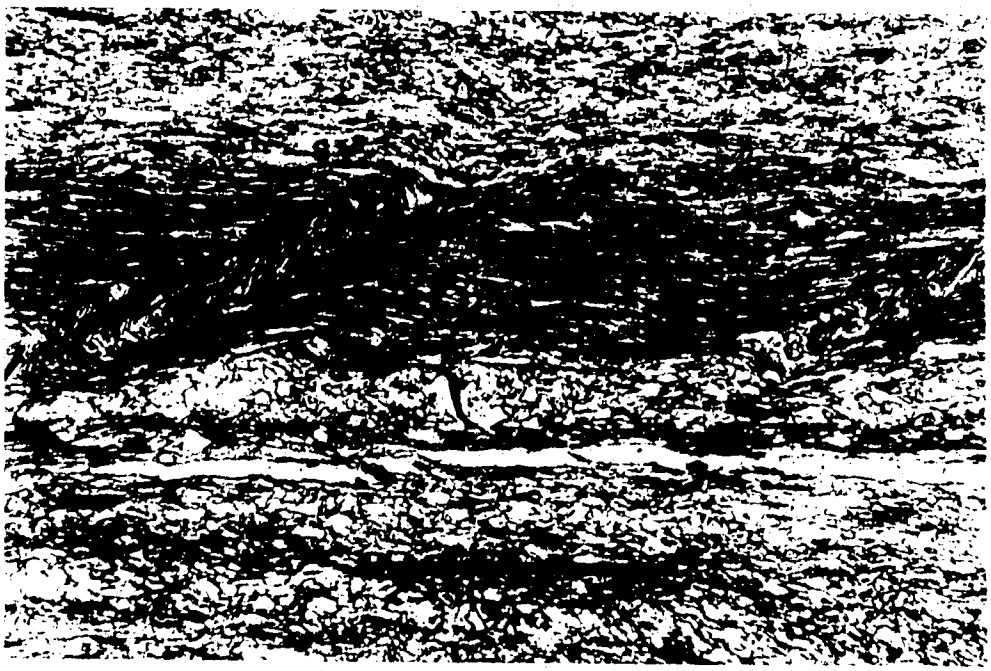

PLATE 8 Asymmetrically crenulated S_2. Incipient S_3 develops along the longer limb. Field of view = 1.8 mm x 1.0 mm

PLATE 9 S_1 is defined by compositional layering. Incipient crenulation foliation, S_2, is indicated. Minor slip (in the order of mm) occurs along S_2 locally. Field of view = 4.5 mm x 2.8 mm.

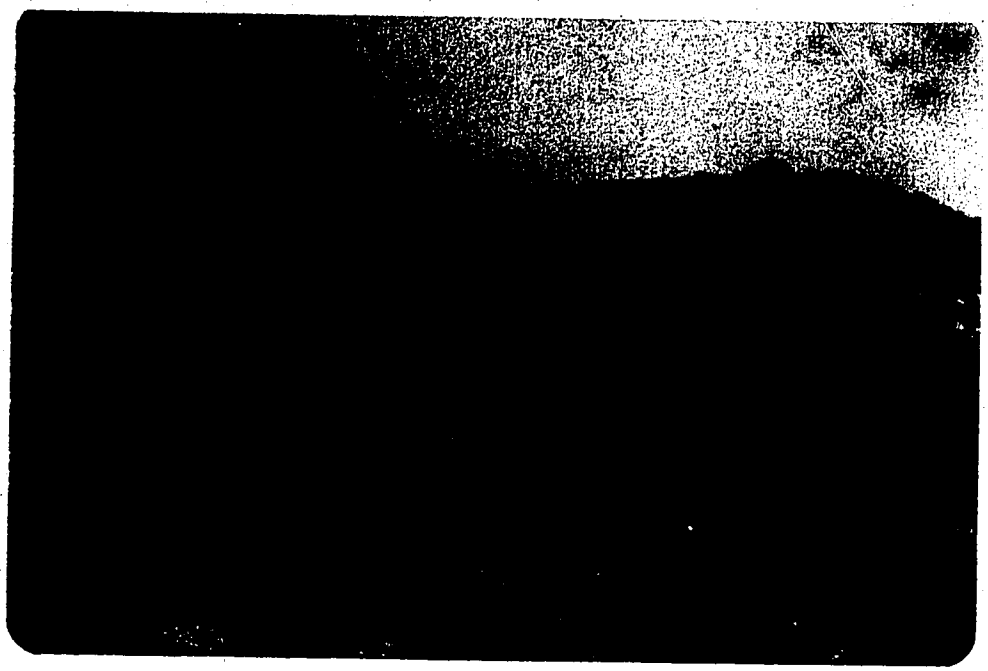

PLATE 10 A large-scale F_3 fold. The folded surface is S_2, the main schistosity in the metasedimentary rocks.

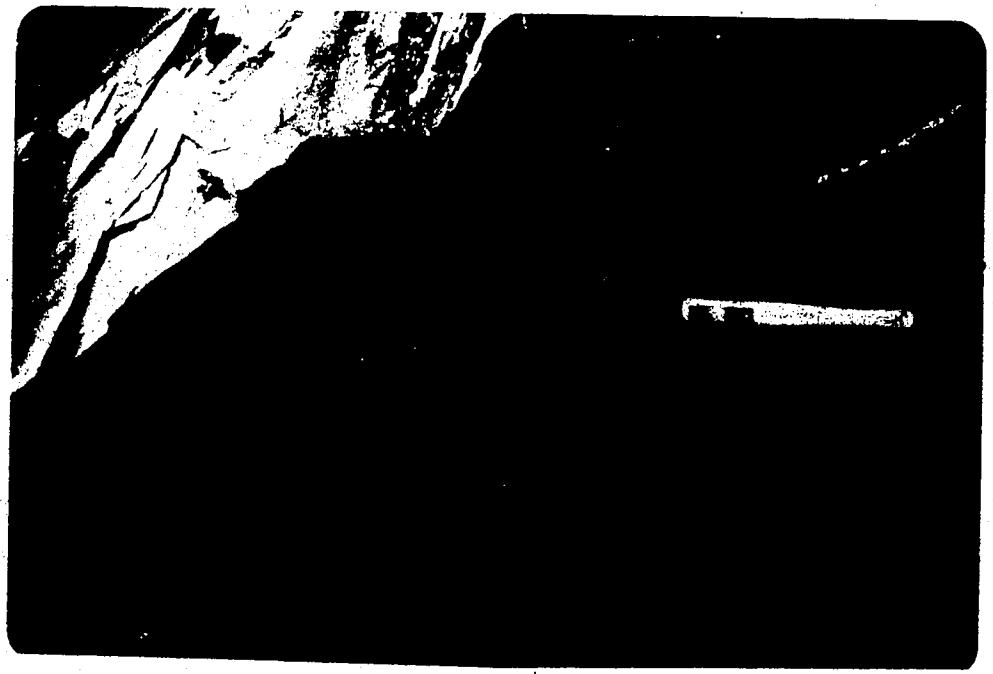

PLATE 11 F_3 folds in pelitic schist.

Porphyroblast-matrix relationships

Porphyroblast - matrix relationships can be used to understand foliation development and deformation history. Many textural criteria have been proposed for the implications of the time relationships between porphyroblast growth and foliation development (Zwart, 1960, 1962; Spry, 1969; Olesen, 1978; Vernon, 1978). Recent models for the origin of inclusion trails in crenulated rocks (Bell and Rubenach 1983; Bell, 1985) allow the relative timing of porphyroblast growth and cleavage development to be determined more precisely. Where textures allow, the petrologic determination of a simple relative time sequence of porphyroblast growth is possible.

The geometry of internal inclusion trails in porphyroblasts (S_i) and their relationship to the external foliation (S_e) has been attributed to rotation of the porphyroblasts (e.g. Spry, 1963).

A model presented by Bell (1985) suggests that porphyroblasts commonly grow syntectonically in locations controlled by strain partitioning (Figure 3). The model suggests that most porphyroblasts do not rotate during ductile deformation. Instead, the surrounding foliation rotates and reactivates due to partitioning of deformation around the porphyroblast. Commonly observed sigmoidal inclusion trails may thus represent earlier crenulations rather than a record of porphyroblast rotation.

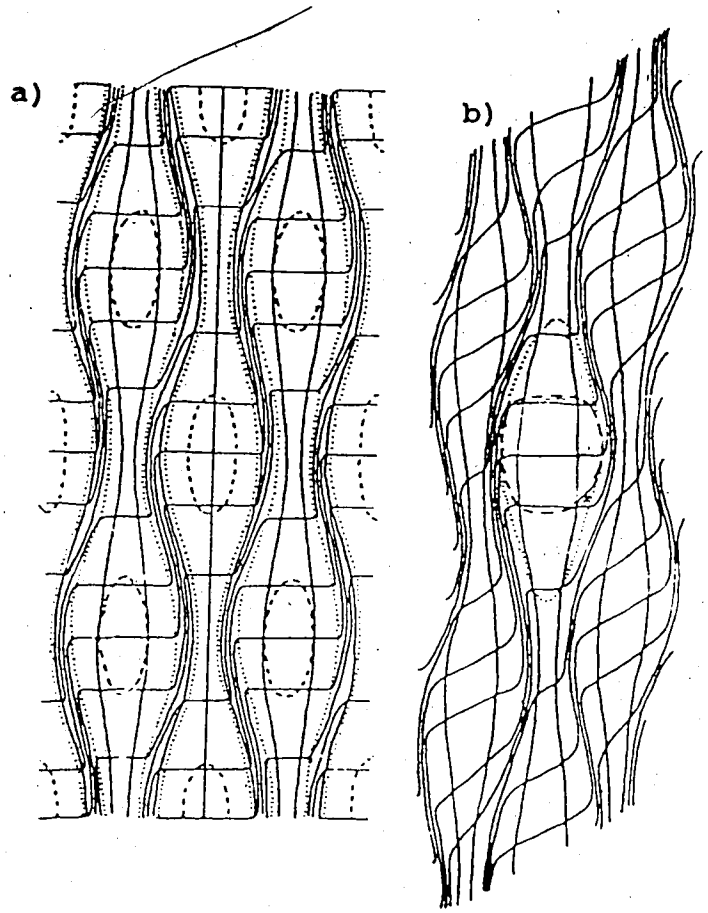

Figure 3. a) Diagram showing a distribution of deformation partitioning on a strain-field diagram constructed for the XZ plane, representing a block of rock which has undergone non-coaxial progressive bulk inhomohgeneous shortening. No strain occurred inside the dashed ellipsoid regions, progressive shortening strain dominated the region between the dashed and dotted lines; and progressive shortening plus shearing strain occurred betweer the dotted lines.
b) Sketch of strain field resulting from non-coaxial progressive bulk inhomogeneous shortening where the deformation has repartitioned about a porphyroblast. Zones of deformation partitioning are delineated as in Figure 3a. The shearing component of the deformation is partitioned about the porphyroblast which thus protects an ellipsoidal island of matrix from the effects of progressive shearing. Both modified after Bell (1985).

Helicitic and planar inclusion patterns are regarded as a syntectonically preserved foliation at one of 6 stages in the progressive process of crenulation cleavage development (Bell and Rubenach, 1983; Bell 1985, 1986; Bell et al, 1986). Figure 4 illustrates each stage of the development. A homogeneous early foliation, S_1 (stage one) is crenulated (stage two). Crenulation is eventually accompanied by metamorphic differentiation (stage three) and growth of new micas parallel to the axial plane of the crenulations forming S_2 (stage four). Finally, destruction of relict S_1 occurs in the quartz-rich domains (stage five) and a homogenized new foliation, S_2, results (stage six).

Inclusion trail fabric (S_i) may be truncated by the matrix fabric (S_e) if a reorientation of the matrix foliation or a reactivation of an earlier fabric preserved in the matrix occurs after porphyroblast growth (by continued or subsequent deformation). S_i may be oblique and discontinuous with the matrix in one porphyroblast and partially or completely continuous with S_e in another porphyroblast in the same thin section (Figure 5). Formerly this would have been interpreted as porphyroblast growth both before and after the development of the matrix foliation. Bell's model is a more simple interpretation which allows us to consider these porphyroblasts as syndeformational.

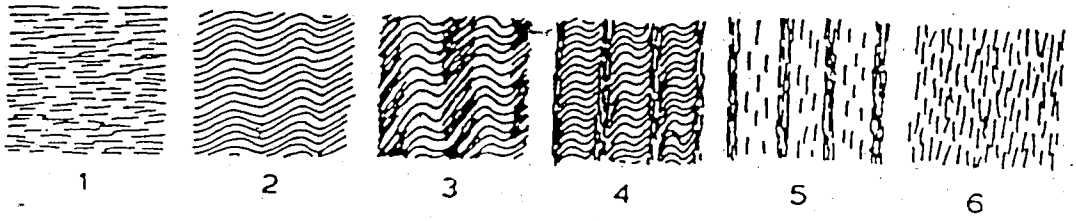

Figure 4. Six stages of development of a new schistosity via a crenulation cleavage. Stage 1 shows the original foliation S_1. Stage 2 shows crenulation of S_1. Stage 3 shows crenulation accompanied by solution transfer and consequent metamorphic differentiation. Stage 4 shows growth of new micas parallel to S_2. Stage 5 shows destruction of relic crenulations in quartz-rich domains. Stage 6 shows homogenized foliation S_2. Modified after Bell and Rubenach (1983).

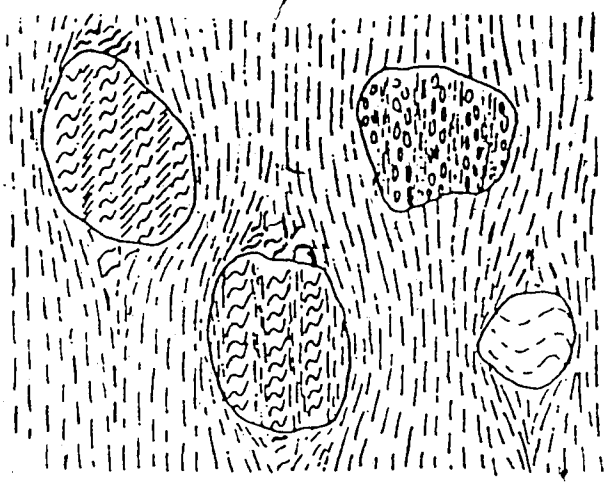

Figure 5. An example of porphyroblasts that have overgrown four stages of development of a crenulation cleavage during D_2. A fifth stage of development is shown in the matrix. The S_2 orientation revealed in each (oriented N-S) is parallel to the S_2 foliation in the matrix. Modified after Bell (1985).

Notation

S_1 is used here to refer to the earliest foliation, either in the matrix or as inclusion trails. S_2 is used for a fabric demonstrated to be a second pervasive foliation. S_i, internal foliation, and S_e, external foliation, are used for general reference to inclusion trails and matrix fabrics respectively. Bell and Rubenach's (1983) terminology for crenulation cleavage development is used here for description of inclusion trail geometry (Figure 4).

Application

The application of Bell's interpretation requires porphyroblasts with well-developed inclusion trails as in the study area.

The main schistosity in the schist is S_2. It is defined by the parallel arrangement of micas and compositional segregation. An early fabric (S_1) is similarly defined and is preserved in the microlithons between S_2 planes. S_1 is also preserved as inclusion trails in porphyroblasts.

Stages two through six of crenulation cleavage formation defined by Bell and Rubenach (1983) are recognized. Each porphyroblastic mineral may preserve different stages in different samples but the sequence of

growth is consistent.

In the study area, sillimanite is abundant in the roof pendant and adjacent to intrusive contacts. It occurs as fibrolite in bundles intergrown with biotite. More rarely, it is coarser grained (Plate 12). Fibrous sillimanite defines a foliation which wraps around porphyroblasts. Sillimanite is also present as inclusions in staurolite, andalusite, biotite and feldspar. These relationships suggest that sillimanite preceeds the growth of all other isograd-defining minerals. However, sillimanite could be a prograde product of reactions involving the aluminosilicates in which it appears to be included.

Purplish-red, subhedral to euhedral almandine porphyroblasts range from less than 1 mm to 5 mm in diameter. A few preserve stage two of crenulation cleavage development. Preservation of stage two has been observed in only one section (Plate 13). Ilmenite, graphite and quartz inclusions in the core of these garnets outline the early crenulation of S_1 indicating that these garnets formed early in the development of the crenulation cleavage (S_2). The rim of inclusion-free material (Plate 13) indicates a second phase of garnet growth.

More typically garnets preserve stage six of the crenulation cleavage development and contain inclusions (S_i) parallel to S_e (Plate 14). Some garnets contain an [illegible] at an angle to S_e.

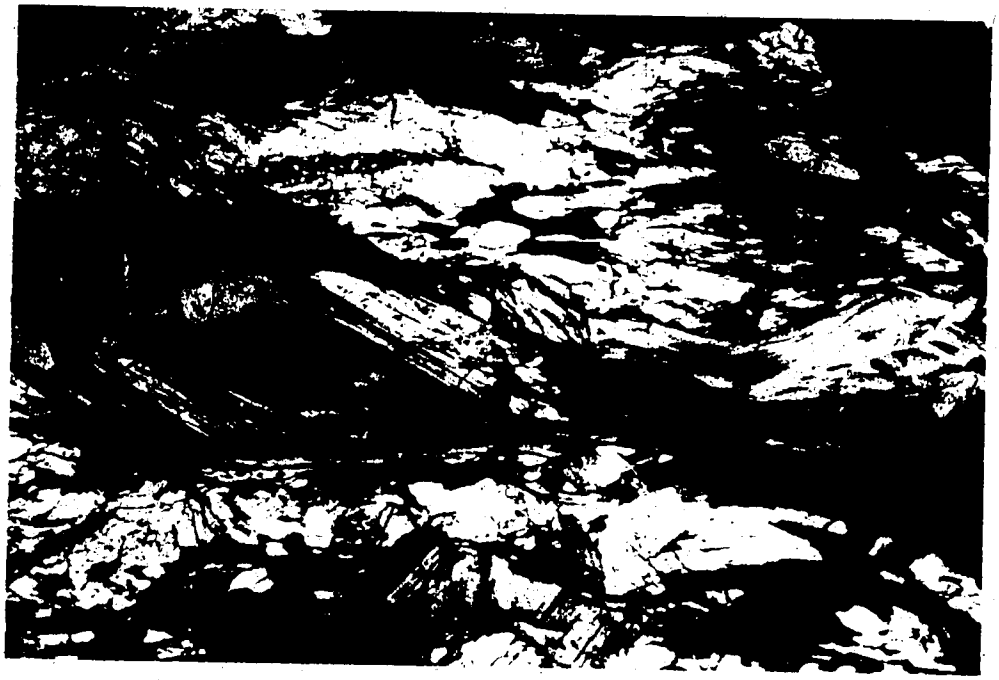

PLATE 12 Schist in the roof pendant and within 1.5 km of the intrusive contact is a high grade assemblage of sillimanite-garnet-biotite-muscovite schist. Sillimanite occurs in felted masses associated with biotite and rarely, as bundles of tiny slender prismatic crystals (shown here). Field of view = 4.5 mm x 2.8 mm.

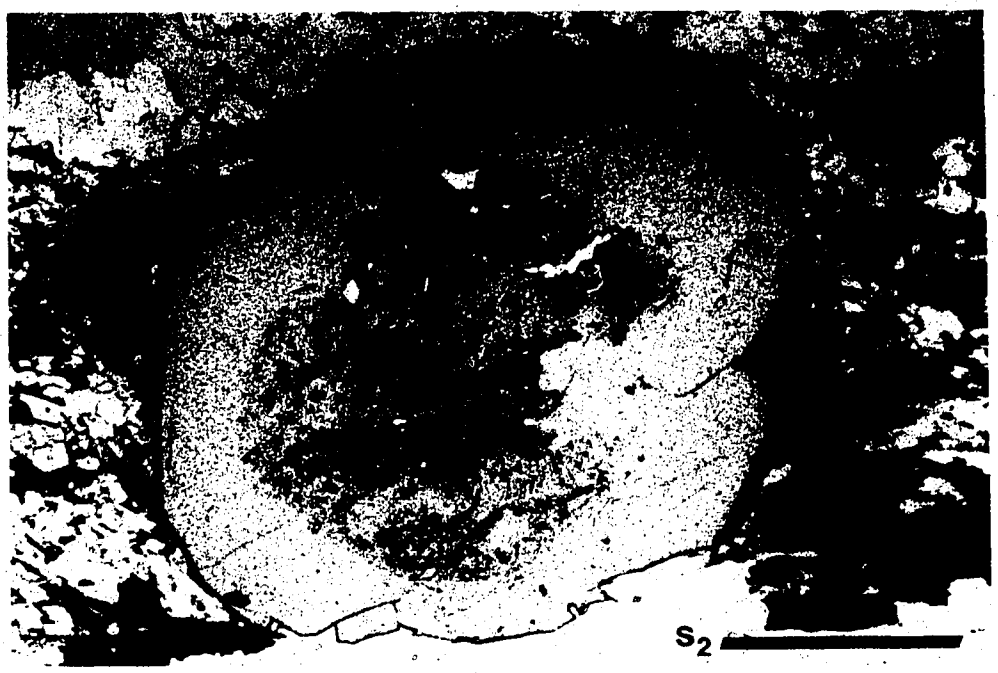

PLATE 13 A garnet porphyroblast includes quartz, ilmenite and graphite (?) inclusions which define a crenulated S_1 (Stage two of crenulation cleavage development). An inclusion-free rim suggests two stages of garnet growth. Field of view = 4.5 mm x 2.8 mm.

PLATE 14 Strongly aligned ilmenite and graphite(?) included in a garnet porphyroblast. An inclusion free zone at the rim of the porphyroblast suggests two stages of garnet growth. S_i parallels S_e but is not continuous with it. S_e wraps around the garnet developing a weak wrap-around texture. The garnet porphyroblast grew after the initiation of S_2 but before the final stages of tightening of the S_2 schistosity. Field of view 4.5 mm × 2.8 mm.

Stage-six-preserving garnets are locally partially dissolved against S_2 due to pressure solution at grain boundaries in contact with the S2 surface. These garnets also have inclusion-free rims (Plates 13 and 14) which indicates a second phase of garnet growth. These porphyroblasts typically have foliation-defining micas forming a wrap-around texture.

The garnets that preserve stage two to stage six of crenulation cleavage development are considered syntectonic with respect to S_2 development. The draping of matrix micas around the porphyroblasts indicates that the porphyroblasts formed after the initial development of S_2 and before final tightening (and possibly reactivation) of S_2.

The garnets described above are normally zoned; with higher concentrations of Mn (and to a lesser extent, Ca) in the core and higher concentrations of Fe and Mg in the rim (Figure 6a). Complex zoning of syntectonic garnets was also observed (Figure 6b).

Other garnet porphyroblasts postdate S_2 homogenization. These grains are quite small, inclusion-free, and show no wrap-around features (i.e. matrix mica is not deflected, Plate 15). Microprobe analysis of these post-tectonic garnets indicates that they are normally zoned (Figures 7a and b).

Staurolite is fine-grained where it first appears at

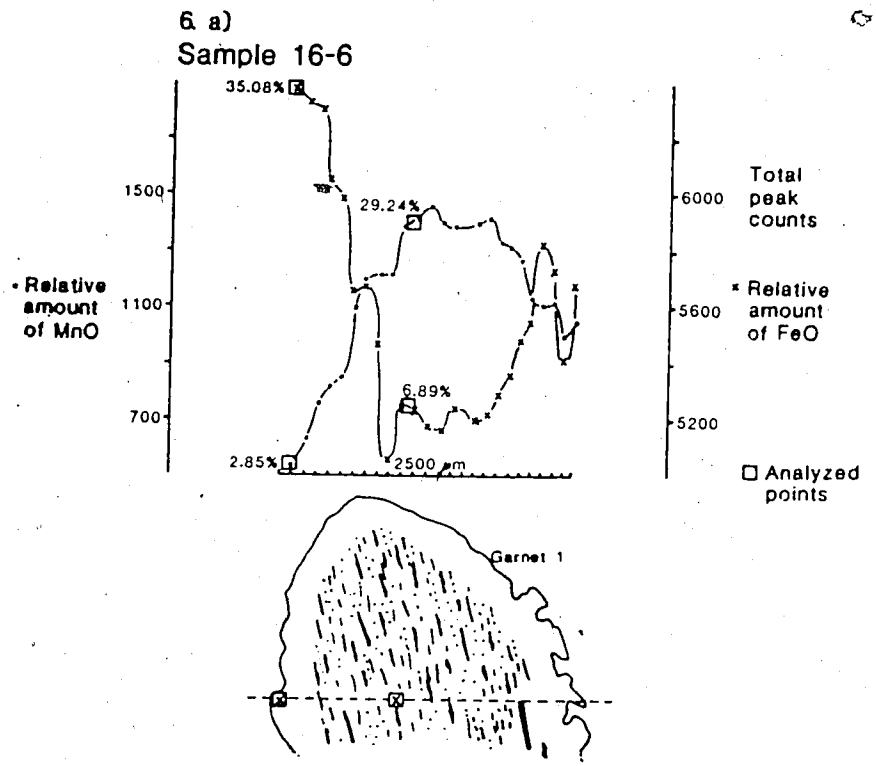

Figure 6. Traverses across syntectonic garnet grains; a) A syntectonic garnet with an inclusion-filled core and an inclusion-free rim. The garnet is normally zoned. Amount of FeO and MnO is relative to the amount of these oxides in the standards used (35.29 wt% and 4.87 wt% respectively).

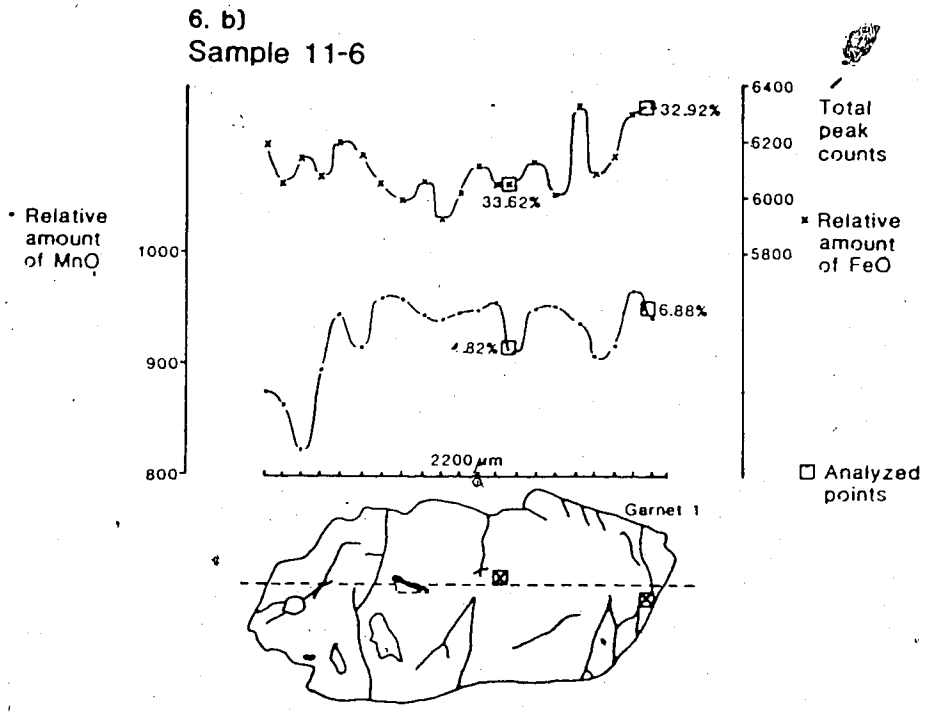

Figure 6. b) A syntectonic garnet with no inclusions. Matrix micas are draped over the porphyroblast developing a wrap-around texture. The garnet is complexly zoned. Scales are separated for clarity. Amount of FeO and MnO is relative to the amount of these oxides in the standards used (35.29 wt% and 4.87 wt% respecitvely).

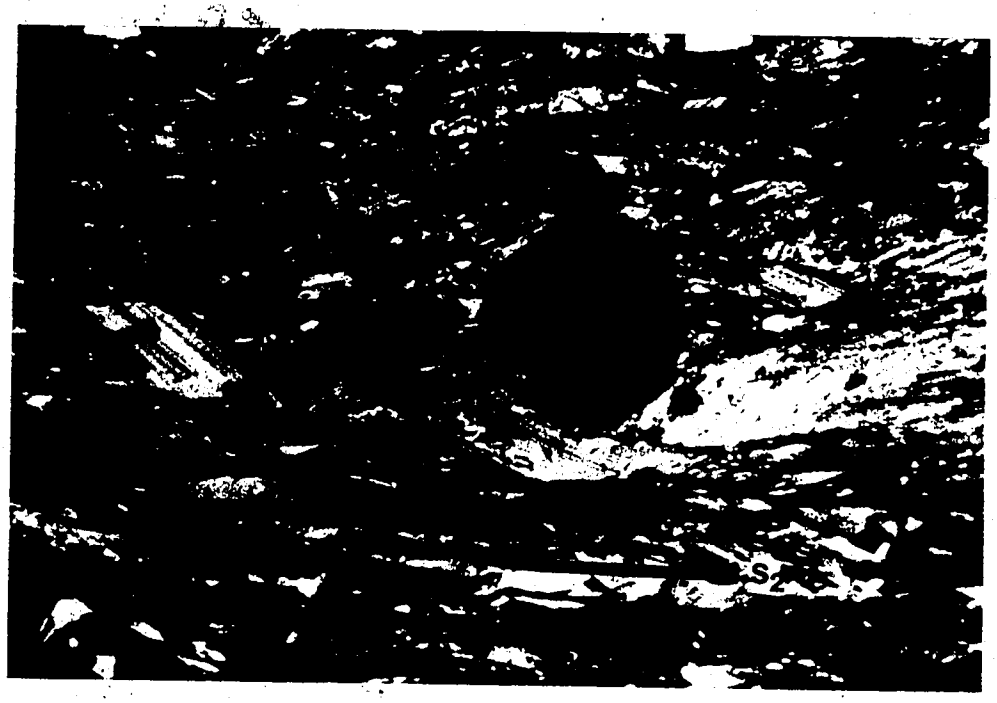

PLATE 15 A post-S_2 garnet porphyroblast. These are small, inclusion-free, and normally zoned. Field of view = 4.5 mm x 2.8 mm.

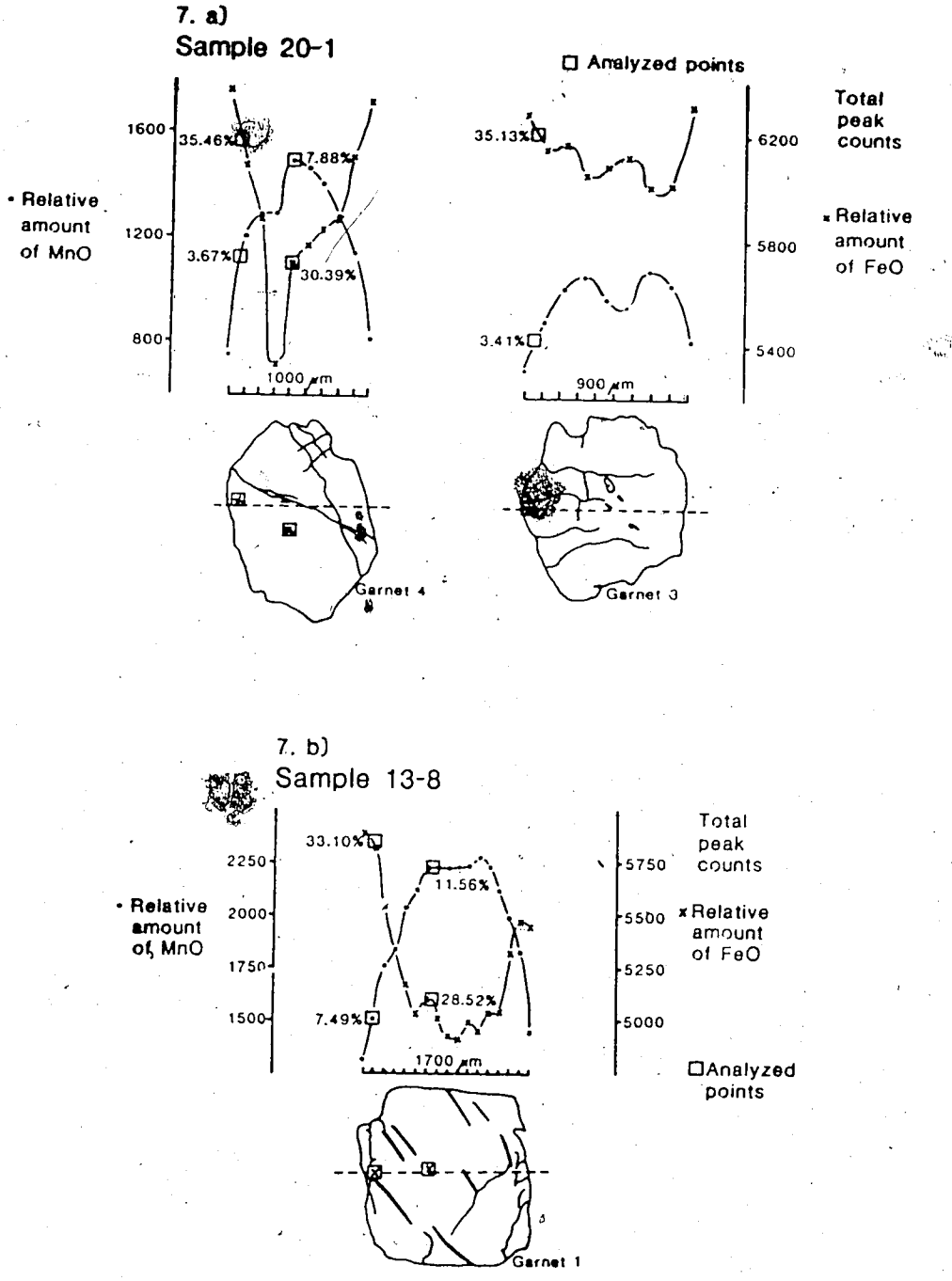

Figure 7. Traverses across two post-tectonic garnet grains; both garnets have few inclusions, show no wrap-around texture, and are normally zoned. Amount of FeO and MnO is relative to the amount of these oxides in the standards used (35.29 wt% and 4.87 wt% respectively).

the intrusive contact and becomes coarser grained (up to 1 cm in length) and more abundant away from the contact. This may reflect increased nucleation away from the contact where fluids may be less abundant. In thin section staurolite commonly exhibits a branching habit, where mineral growth has occurred by segregation (Bard, 1980), both along the mica-rich foliation planes of the main schistosity (S_2) and along the earlier foliation (S_1) (Plate 16). This habit accentuates stage four of foliation development.

Staurolite porphyroblasts are commonly subhedral to euhedral and contain inclusions of garnet, biotite, quartz, ilmenite, tourmaline and graphite. Some are euhedral and include a sigmoidal S_i. S_i is at an angle to S_e (due to relative rotation of S_e and S_i ?). A weakly to well-developed wrap-around texture is commonly developed. Textures preserved by the anhedral branching staurolite and the subhedral staurolite porphyroblasts indicate that staurolite growth occurred during the late stages of crenulation cleavage development.

Other subhedral staurolite porphyroblasts include a slightly sigmoidal S_i which extends into the matrix, where S_e forms crenulations of similar wavelength (Plate 17). These porphyroblasts are subhedral and appear to have been static with respect to S_i. This texture indicates that crystal growth occurred after S_2 homogenization

PLATE 16 "Branching" staurolite grows along mica-rich domains, which define S_2, and along S_1. Staurolite preserves stage four in the development of the new schistosity (S_2). Field of view = 4.5 mm x 2.8 mm.

PLATE 17 Slightly sigmoidal internal inclusion trails in these staurolite porphyroblasts are continuous with the external fabric (S_e) which has undulations of a similar wavelength. Staurolite growth occurred at the end of foliation development (stage six). This explains its static appearance with respect to S_i. Field of view = 4.5 mm x 2.8 mm.

(Bard, 1980).

Staurolite encloses garnet. Staurolite is commonly enclosed and (or) replaced by andalusite. Thus, staurolite growth occurred late in the development of S_2. Locally post-tectonic staurolite is observed.

Andalusite porphyroblasts are most commonly large (6 mm long), anhedral poikiloblasts which include fibrous sillimanite, staurolite, biotite, feldspar, quartz, ilmenite, muscovite, tourmaline, and graphite. Elongate inclusions (ilmenite, quartz, biotite) are parallel to S_e. Subhedral andalusite porphyroblasts are also poikiloblastic. S_i is continuous with S_e which wraps around the subhedral grains (Plate 18). These andalusite poikiloblasts preserve stage six of crenulation cleavage development. They are interpreted to have grown late in the process of S_2 development, after S_2 homogenization.

Andalusite porphyroblasts locally exhibit a branching habit similar to staurolite, outlining both S_1 and S_2 surfaces (Plate 19).

Elongate, dark green-grey pseudomorphs after andalusite are best exposed on weathered foliation surfaces near contacts with phyllite. The pseudomorphs are commonly 4 - 5 cm long and 1 cm across but may be up to 10 cm in length, and are formed of chlorite and/or biotite (?).

Because andalusite frequently mantles staurolite, encloses both feldspar and biotite porphyroblasts, develops

PLATE 18 Andalusite porphyroblast (An) partially enclosing staurolite (St). S_i is continuous with S_e. A strong wrap-around texture is developed in the matrix indicating that porphyroblast growth occurred after the initial development of S_2 but before the final tightening of the S_2 schistosity. Field of view = 4.5 mm x 2.8 mm.

PLATE 19 Andalusite growth by segregation develops a "branching" habit similar to that observed in the late kinematic staurolite porphyroblasts. Andalusite growth occurs along mica-rich S_2 planes. Field of view = 4.5 mm x 2.8 mm.

weak wrap-around texture, and typically preserves stage six of S_2 foliation development, it is considered a late syn-kinematic to post-kinematic mineral.

Biotite typically includes zircon inclusions (with radiation metamict haloes), ilmenite, tourmaline and graphite. Quartz, feldspar, and muscovite also occur locally as inclusions in biotite. Biotite occurs as anhedral grains which define the foliation and as subhedral porphyroblasts. S_i in biotite is commonly planar, parallel, and continuous with S_i in neighbouring andalusite porphyroblasts and with S_e.

Biotite porphyroblasts locally preserve stage three to four of foliation development (Plate 20). The same stage(s) are preserved in the matrix and are less well-preserved in branching staurolite.

S_1 is defined by compositional segregation of mica-rich foliae and quartz + feldspar-rich foliae, and preferred mica orientation. Muscovite is the dominant S_1-defining mica, although minor anhedral biotite grains also define S_1.

As biotite defines S_1 locally, is intimately intergrown with early sillimanite, locally preserves stages three and four of crenulation cleavage development with staurolite, and locally is static with respect to andalusite, it is interpreted to be forming throughout the foliation development process.

PLATE 20 A biotite porphyroblast preserves graphite (?) inclusions, which define S_1, as well as a gently undulating S_2 schistosity. Stage four of the foliation development is preserved. Field of view = 4.5 mm x 2.8 mm.

Rare anhedral to subhedral plagioclase porphyroblasts are observed in the schist. These porphyroblasts include graphite, ilmenite, biotite and muscovite which outline and preserve stage three and four of the foliation development (Plates 21 and 22).

Where plagioclase porphyroblasts coexist with andalusite they do not have well-developed internal inclusions. They are included in the poikiloblastic andalusite which preserves stage three and four of S_2 development.

As plagioclase porphyroblasts preserve stage three and four or are included by a porphyroblast that preserves stage three and four, it is assumed that plagioclase grew between homogeneous S_1 and homogeneous S_2 foliation development.

Porphyroblast - matrix relationships indicate syntectonic growth (with respect to S_2 development) of all porphyroblasts as well as some post-tectonic growth of most porphyroblasts. The timing of porphyroblast development is summarized in Table 2.

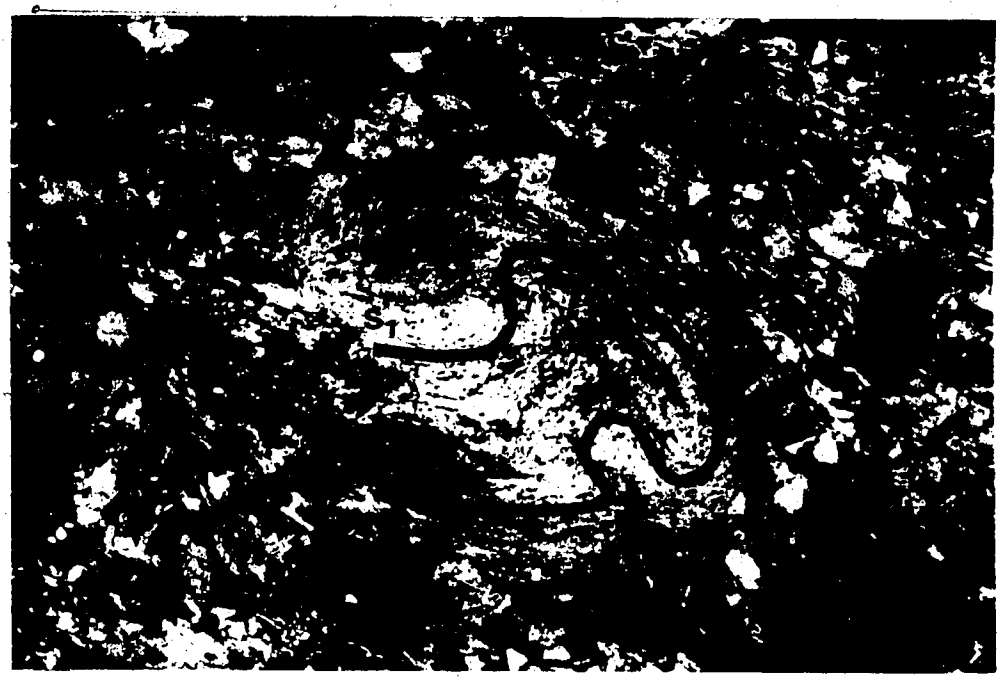

PLATE 21 Rare plagioclase feldspar porphyroblast with intricate opaque inclusion trails (S_1). The porphyroblast preserves Stage two (?) of crenulation cleavage development.
Field of view = 4.5 mm x 2.8 mm

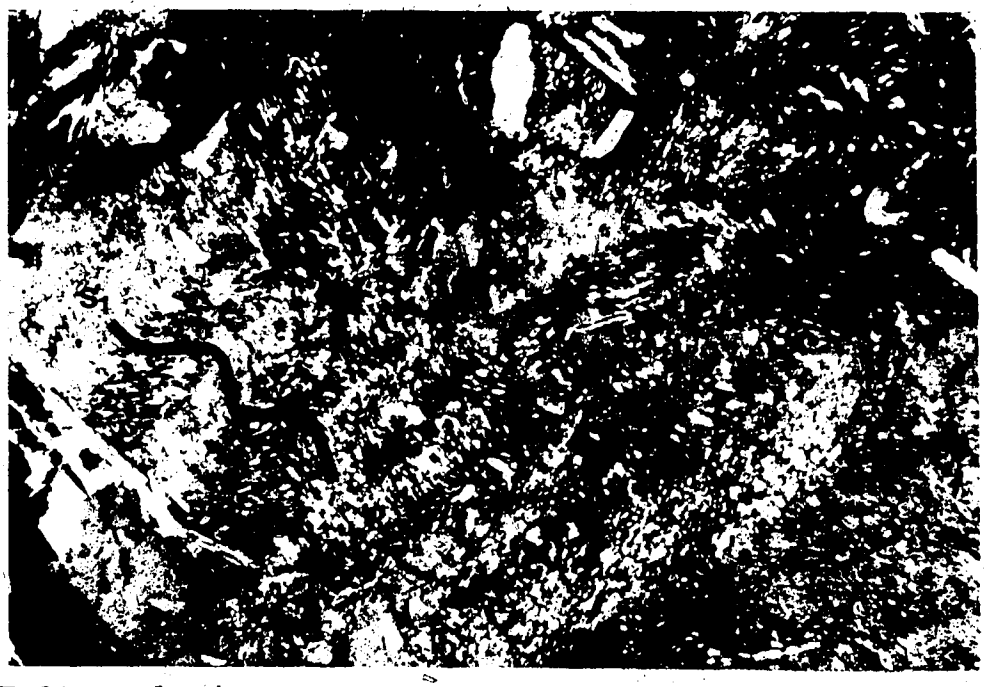

PLATE 22 Plagioclase feldspar porphyroblast includes muscovite, quartz and opaque grains which define a crenulated S_1 (Stage Three).
Field of view = 1.8 mm x 1.0 mm.

TABLE 2. Timing of porphyroblast development with respect to the progressive development of crenulation cleavage (S_2).

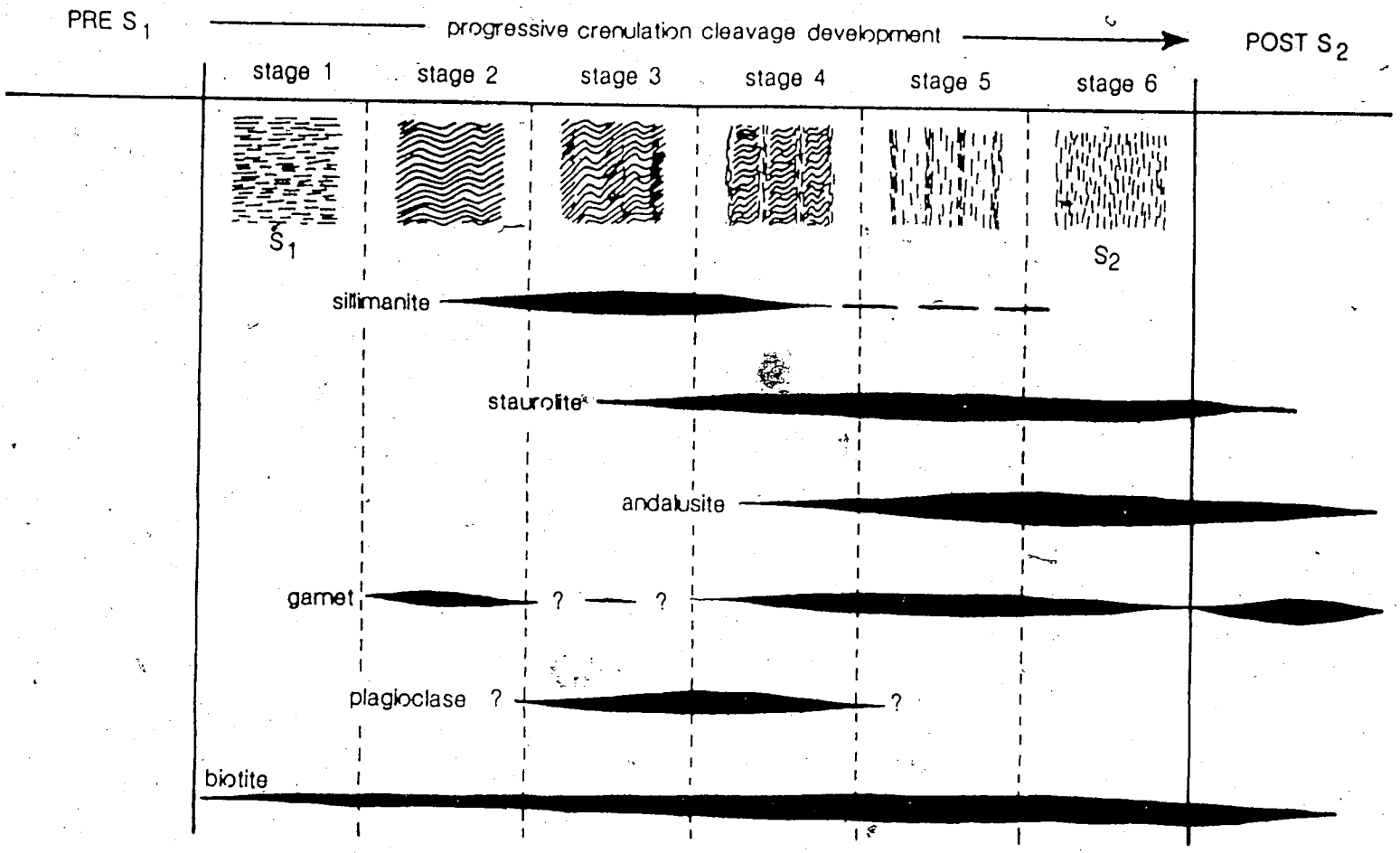

V. GEOTHERMOMETRY AND GEOBAROMETRY

In order to determine a unique temperature and pressure estimate for each mineral assemblage analyzed, the Ferry and Spear (1978) geothermometer and the Ghent et al. (1979) geobarometer were solved iteratively. Temperatures were initially calculated for each garnet-biotite pair assuming 4 kbar pressure. This gives rise to a maximum temperature. Maximum temperature results were than used to calculate pressures for each sample, this in turn, gives rise to a maximum pressure result. Two iterations of this process were carried out. A third iteration resulted in less than 1% change in the pressure result. An average pressure was then determined for the area and used in subsequent geothermometric calculations.

Plagioclase-garnet-Al_2SiO_5-quartz geobarometry

Microprobe data collected from plagioclase-garnet-Al_2SiO_5-quartz assemblages in 8 samples of schist were used in geobarometric calculations. A calibration of the anorthite-grossular geobarometer has been applied to 21 assemblages within the 8 samples.

The equations used are those of Ghent et al. (1979) (Appendix IV). Assuming ideal solid-solution, the activity

of $CaAl_2Si_2O_8$ in the plagioclase is equal to X_{Ca}, with X_{Ca} = atomic Ca/atomic (Ca + Na + K). Similarly, the activity of $Ca_3Al_2Si_3O_{12}$ in the garnet is equal to X_{Ca}^3, with X_{Ca} = atomic Ca/atomic (Ca + Fe + Mn + Mg). Activity-coefficient terms are necessary to account for non-ideality. An empirical activity-coefficient-ratio term ($3\log \gamma_{Gr}/\gamma_{An}$) of -0.4 was estimated by Ghent et al. (1979). This value (-0.4) was used for the activity-coefficient ratio in the geobarometer applied to the assemblages in the schist.

The pressure results are given for each mineral assemblage in Table 3.

Sample 11-6.2 gives an unusually high pressure result. The stoichiometry of the garnet in this sample is poor relative to an ideal garnet. An extreme result is also obtained for sample 27-4. The Ca content in the garnet and plagioclase is much higher in this sample and the activity of Ca in the garnet and plagioclase may not be adequately expressed. For these reasons, the results for these samples (11-6.2, all 27-4 samples) have not been included in the overall pressure estimate for the area.

Remaining results range from 2.8 to 6.5 kbars. The average within-sample standard deviation is 12.62. An average pressure for each sample was calculated. The average of the pressures for each sample is taken to represent the mean pressure in the area. As the data are

TABLE 3. Geobarometry results, where P (bars) is calculated using the Ghent (1976), as modified by Ghent et al (1979), plagioclase-garnet-Al_2SiO_5-quartz geobarometer. S = Sillimanite A = Andalusite

SAMPLE NUMBER	Ca Garnet	Fe Garnet	Mn Garnet	Mg Garnet	Ca Plag	Na Plag	K Plag	X_{Ca} garnet x 10^{-2}	X_{Ca} plag x 10^{-2}	K_S x 10^{-2}	T (°C)	P (bars)	coexisting Al_2SiO_5
8-4.1	0.0665	5.1519	0.4392	0.3686	0.2692	2.7483	0.0241	1.1035	8.8506	0.1938	743	5532	S
8-4.2	0.0748	5.1883	0.4190	0.3738	0.2518	2.7996	0.0209	1.2352	8.1958	1.2352	743	6415	S
8.4-3	0.0545	5.1156	0.4600	0.4438	0.2621	2.7343	0.0376	0.8973	8.6388	0.1121	743	4682	S
11-6.1	0.0963	4.4647	0.9450	0.4307	0.3895	2.6268	0.0267	1.6221	12.800	0.2035	643	4173	S
11-6.2	0.2939	4.4194	0.7204	0.4476	0.3828	2.7260	0.0310	4.9972	12.192	6.8860	643	9102	S
12-8.1	0.2049	4.7528	0.6381	0.4946	0.4953	2.6566	0.0255	3.3643	15.588	1.0053	556	5075	A
12-8.2	0.2515	4.6117	0.6656	0.4366	0.4543	2.7710	0.0209	4.2160	13.995	2.7340	556	6420	A
13-8.1	0.1307	4.5668	1.0463	0.3081	0.4795	2.6931	0.0187	2.1597	15.025	0.2970	543	3217	A
13-8.2	0.1307	4.5668	1.0463	0.3081	0.3745	2.5802	0.1259	2.1597	12.157	0.5607	543	4058	A
13-8.3	0.1472	4.5795	0.9380	0.3596	0.2301	2.6861	0.1565	2.4434	7.4885	3.4739	543	6471	A
13-8.4	0.1472	4.5795	0.9380	0.3596	0.4397	2.6813	0.0396	2.4434	13.912	0.5418	543	4012	A
16-6.1	0.2540	4.7955	0.3945	0.5767	0.8116	2.2286	0.0248	4.2188	26.480	0.4044	655	5319	S
18-6.1	0.2087	4.8785	0.4896	0.5145	0.4044	2.8733	0.0223	3.4262	12.255	2.1855	567	6340	A
18-6.2	0.2087	4.8785	0.4896	0.5145	0.3999	2.8216	0.0231	3.4262	12.325	2.1481	567	6316	A
18-6.3	0.2100	4.7427	0.5814	0.4778	0.4103	2.7757	0.0169	3.4931	12.810	2.0724	567	6237	A
18-6.4	0.2100	4.7427	0.5814	0.4778	0.4287	2.7988	0.0216	3.4931	13.194	1.8555	567	6117	A
27-1.2	0.1999	5.0147	0.3496	0.5644	0.7396	2.2349	0.0187	3.2618	24.709	0.2300	538	2797	A
27-4.1	1.1388	4.2313	0.2592	0.4025	1.1489	1.8252	0.0353	18.880	38.177	12.095	627	10041	A
27-4.2	1.1388	4.2313	0.2592	0.4025	1.3175	1.6703	0.0271	18.880	43.700	8.0643	627	9449	A
27-4.3	1.1414	4.3846	0.2491	0.4166	1.1806	1.8451	0.0283	18.434	38.658	10.844	627	9882	A
27-4.4	1.1414	4.3846	0.2491	0.4166	1.1606	1.8685	0.0431	18.434	37.777	11.619	627	9983	A

not spatially skewed (i.e. a range of pressure results is typical in all parts of the study area), a common pressure is used for the entire area, i.e. 4.9 kbar.

Error on the pressure calculated for each assemblage is ± 1.6 kbar (Ghent et al 1979). Pigage and Anderson (1985) suggested shallow intrusion at low pressure (less than 4 kbar) for the Anvil plutonic suite. This estimate is within error of the result of this study. A pressure of 4.9 ± 1.6 kbar suggests a (stratigraphic ?) cover of about 16 km (± 5 km) during emplacement.

Garnet-biotite geothermometry

Data collected from 38 garnet-biotite pairs in 13 samples was used in the garnet-biotite geothermometer (Ferry and Spear, 1978) (Appendix IV). Results are given in Table 4 and presented graphically in Figure 8.

The highest temperatures are recorded in the roof pendant rocks.

Results range from 509 to 872 °C. The average within-sample standard deviation is 2.82. A general trend of decreasing temperature away from the intrusive is recorded. All previous workers have noted that metamorphic grade decreases rapidly away from the intrusive from upper amphibolite facies to lower greenschist facies.

TABLE 4. Geothermometry results, where T (^{o}C) is calculated using the Ferry and Spear (1978) garnet-biotite geothermometer at 4.9 kbar.

SAMPLE NUMBER	Mg Garnet	Fe Garnet	Mg Biotite	Fe Biotite	Mg/Fe Garnet x 10^{-2}	Mg/Fe Biotite	K	TEMP ^{o}C
8-4.1	0.4542	5.0926	1.0328	3.7159	8.9188	0.2779	0.3208	872
8-4.3	0.4438	5.1156	1.2062	3.5863	8.6754	0.3363	0.2579	757
8-4.4	0.3234	5.1944	1.2062	3.5863	6.2259	0.3363	0.1851	620
8-4.6	0.3633	5.2393	1.0155	3.5058	6.9341	0.2897	0.2394	723
11-6.1	0.4307	4.4647	1.5810	3.3786	9.6468	0.4679	0.2062	657
11-6.2	0.3870	4.2708	1.4751	3.2375	9.0615	0.4556	0.1989	644
11-6.3	0.4476	4.4194	1.5613	3.1011	10.128	0.5035	0.2012	648
11-6.4	0.3864	4.2774	1.6244	3.2639	9.0335	0.4977	0.1815	621
12-8.1	0.4366	4.6117	2.1136	3.0428	9.4672	0.6946	0.1363	523
12-8.2	0.4649	4.6109	1.9802	3.1296	10.083	0.6327	0.1594	570
12-8.3	0.4447	4.7574	1.9969	3.0052	9.3475	0.6645	0.1407	532
12-8.4	0.4946	4.7528	2.0274	3.0393	10.407	0.6671	0.1560	563
12-8.5	0.5347	4.8170	2.0376	3.1472	11.100	0.6474	0.1714	594
13-8.1	0.3081	4.556	1.8099	3.7659	6.7465	0.4806	0.1404	549
13-8.2	0.3596	4.5795	1.8911	3.6729	7.8524	0.5149	0.1525	527
13-8.3	0.3690	4.6374	1.7421	3.3071	7.9570	0.5268	0.1511	552
15-5.1	0.4674	4.5394	1.7053	2.9988	10.297	0.5687	0.1811	612
15-5.2	0.4828	4.5694	1.6914	3.0304	10.566	0.5581	0.1893	628
15-5.3	0.4891	4.4886	1.7329	2.9106	10.896	0.5954	0.1830	615
15-5.4	0.4891	4.4886	1.7329	2.9106	10.896	0.5954	0.1834	616
15-5.5	0.4998	4.6532	1.7592	2.9825	10.741	0.5898	0.1821	614
15-7.1	0.4864	4.575	1.6040	2.7696	10.632	0.5791	0.1836	616
16-6.1	0.5767	4.7955	1.9298	2.9905	12.026	0.6453	0.1864	622
16-6.2	0.6199	4.8162	1.8171	3.1206	12.871	0.5823	0.2210	687
17-11.1	0.4948	4.7061	1.7895	3.0345	10.514	0.5897	0.1283	606
17-11.2	0.4948	4.7061	1.8792	3.0611	10.514	0.6139	0.1713	593
18-6.1	0.4778	4.7427	2.0960	3.0050	10.074	0.6975	0.1444	542
18-6.2	0.5154	4.8785	1.9042	3.0462	10.565	0.6251	0.1690	592
18-6.3	0.5047	4.8612	2.0533	3.0863	10.382	0.6653	0.1561	566
20-1.1	0.5001	4.8981	2.0734	2.6435	10.210	0.7843	0.1302	509
20-1.2	0.5644	5.0147	2.0173	2.9673	11.255	0.6798	0.1656	581
20-1.3	0.4851	4.8085	1.9823	2.7657	10.088	0.7167	0.1407	531
20-1.4	0.4757	4.8435	1.9364	2.7843	9.8214	0.6955	0.1412	532
24-4.1	0.4533	4.7257	1.8267	3.5826	9.5922	0.5099	0.1881	625
25-2.1	0.4121	4.4827	1.6346	3.2472	9.1931	0.5034	0.1826	615
27-4.1	0.4025	4.2313	1.8295	2.9985	9.5124	0.6101	0.1559	562
27-4.2	0.4391	4.3966	1.7454	2.9932	9.9873	0.5831	0.1713	592
27-4.3	0.4708	4.2738	1.5617	3.4231	11.016	0.4562	0.2415	725

Figure 8. Sample locations and geothermometry results.

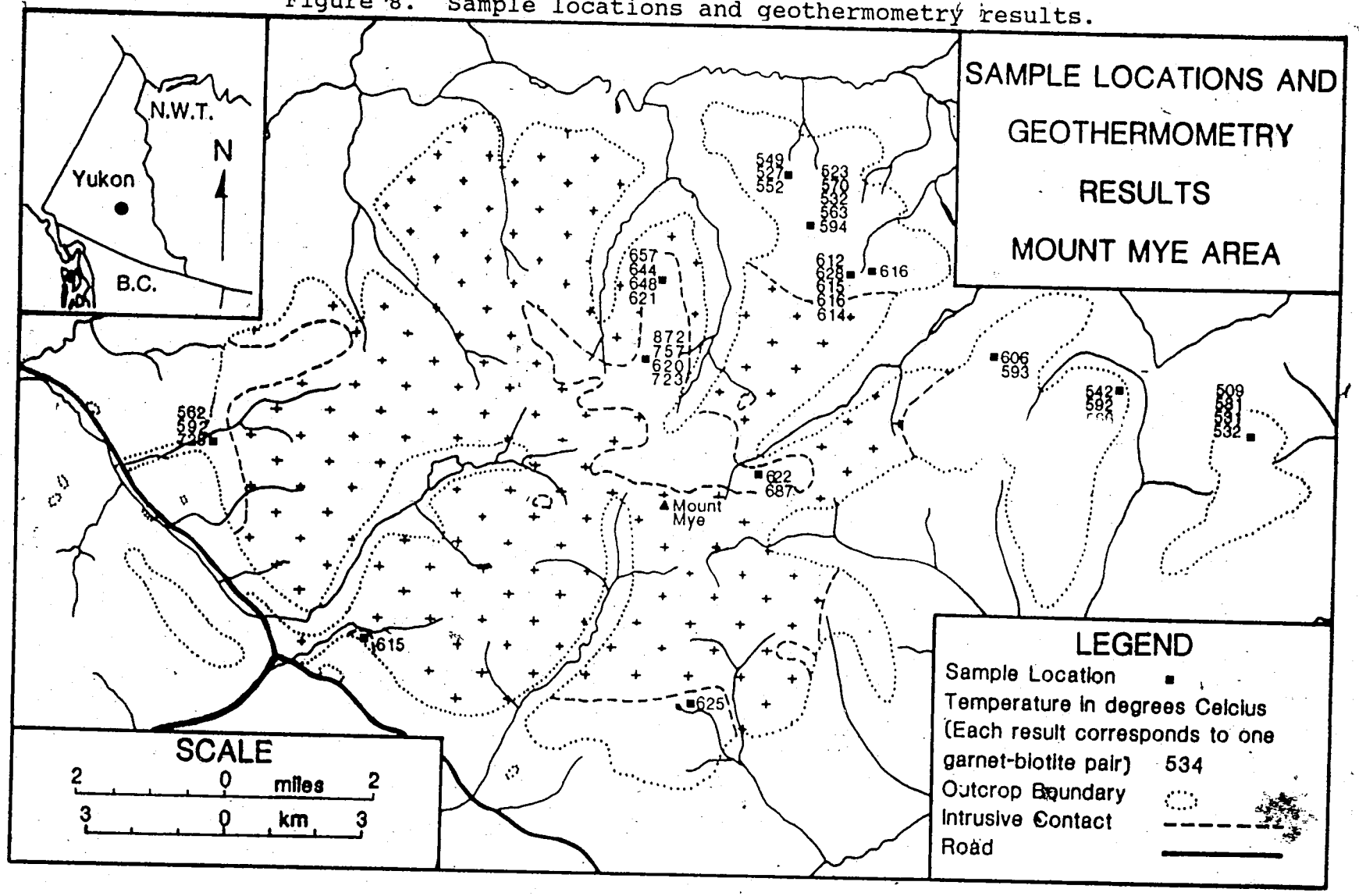

The average P-T determination for each sample is plotted in Figure 9 along with Holdaway's (1971) and Richardson's (1969) phase diagrams for the aluminosilicates. Error bars indicate an error of ± 50 °C (Ferry and Spear, 1978) for the temperature results (the error is larger when the error associated with the geobarometer is also considered) and ± 1.6 kbar (Ghent et al, 1979) for the pressure result.

On Holdaways's (1971) phase diagram, four of the seven points plot within the stability field consistent with mineralogy. Three andalusite-bearing assemblages (12-8, 13-8, 18-6) plot outside the andalusite stability field. In one sample (13-8) the error bar extends into the andalusite field. The average pressure value for these samples is high.

On Richardson's (1969) phase diagram, four of the seven points plot within the stablility field consistent with mineralogy. Two andalusite-bearing (12-8 and 18-6) samples plot above the andalusite field. In both cases the error bar extends into the andalusite field. One sillimanite-bearing assemblage (11-6) plots below the sillimanite stability field, with the error bar extending into the sillmanite field.

Andalusite may be stabilized at higher pressures and coexist with sillimanite due to the presence of minor

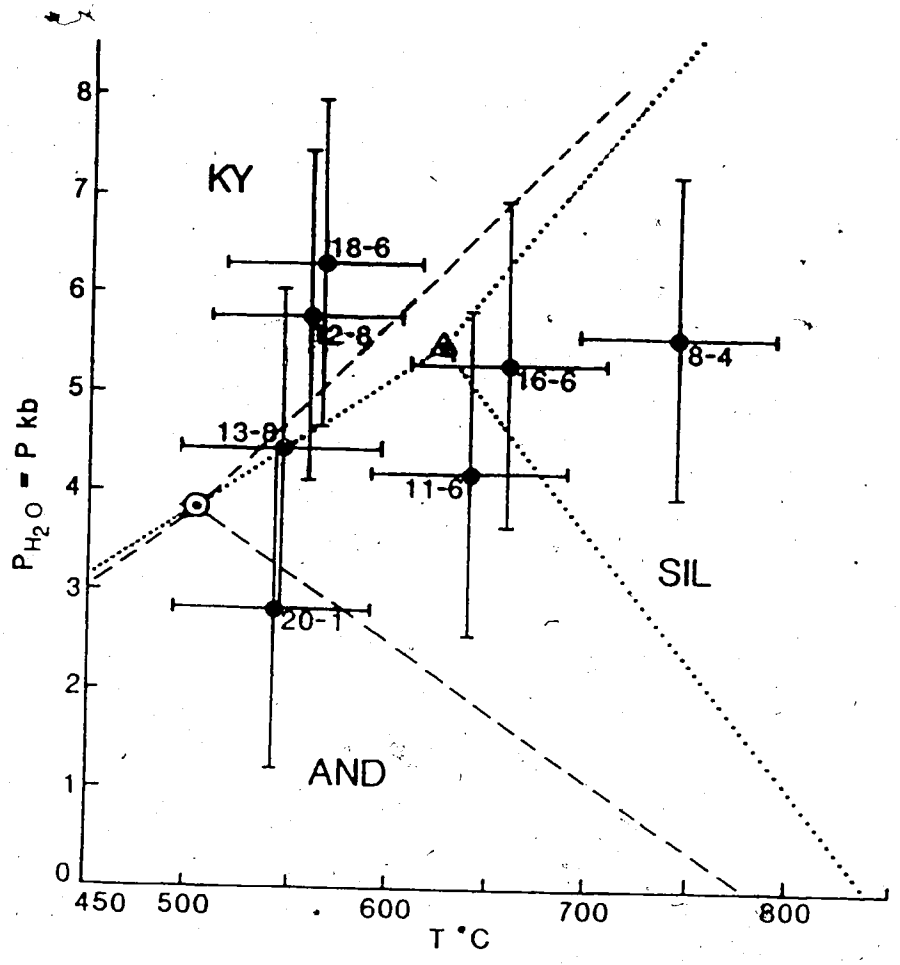

Figure 9. Dots represent the average P-T determination for each sample. Error bars indicate an error of ± 50 °C (Ferry and Spear, 1978) for the temperature results and ± 1.6 kbar (Ghent et al, 1979) for the pressure result. Dashed line represents Holdaway's (1971) phase diagram for the aluminosilicates. Dotted line represents Richardson's (1969) phase diagram for the aluminosilicates.

impurities in the andalusite structure. As a result, sillimanite and andalusite coexist in a divariant field. In sample 12-8 minor fibrolite is observed to coexist with andalusite. Microprobe analysis of andalusite indicates that minor elements make up a very small proportion of the composition (less than 0.6 wt %).

Another possible reason for the high pressure results is that the empirical activity-coefficient-ratio term for Ca ($\gamma = -0.4$) may not be adequate.

The plagioclase-garnet-Al_2SiO_5-quartz assemblage in these samples may not be in equilibrium. Minor retrograde alteration of garnet and biotite to chlorite is observed in sample 13-8. Some retrograde chlorite alteration of garnet and minor sericitic alteration of plagioclase is observed in sample 18-6.

The garnets analyzed in 6 of the samples used for geobarometry are normally zoned. Garnet in the remaining sample, 11-6 (garnet 2), shows a slight (< 0.5 wt %) variation in CaO from core to rim. Biotite and plagioclase grains were not examined for homogeneity.

VI. DISCUSSION

Interpretation of Metamorphic Conditions

The contact aureole of the Anvil batholith is wider than the narrow zones of contact metamorphism around other mid-Cretaceous batholiths in the Cordillera (e.g. Reesor, 1958: Campbell, 1967; Blusson, 1968; Reesor, 1973; Gabrielse et al, 1973; Anderson, 1982; Anderson, 1983; Smit et al, 1985).

Contacts between mid-Cretaceous intrusives and country rock are typically steep, sharp, and discordant. Country rock is not notably deformed. Layering in metasedimentary rocks dips away from the contact. The aureoles are well-developed and characterized by andalusite, cordierite, staurolite, and biotite hornfels or knotted schist in the pelitic units, and by calc-silicate hornfels, skarn or marble in calcareous units. Contact metamorphism affects narrow zones (typically less than 1 km) of country rock.

Although contact relationships are similar, the mineral assemblages in the thermal aureole around the Anvil batholith (i.e. sillimanite zone adjacent to the contact) reflect higher-grade metamorphism than around other mid-Cretaceous intrusives.

The thermal imprint around the Anvil Batholith affects at least a 2200 meter-thick (true thickness) envelope of metasedimentary rocks. Furthermore, the rocks at the contact are not hornfelsed and pelitic rocks have well-developed schistosity.

Two series of contact metamorphism, distinguished by differences in pressure conditions, have been defined by Reverdatto et al. (1970).

The first is the common hornfelsic-rock low-pressure series, or non-abyssal contact metamorphism. This type of contact metamorphism is limited to pressures of less than 3 kbar. In this series the initial temperature of the country rock is low and the temperature reached during metamorphism depends essentially on magma temperature and composition.

The characteristic narrow hornfelsed zones around most Cordilleran mid-Cretaceous intrusives belong to this series.

The second series is a thermally-transformed gneissose rock series, or abyssal contact metamorphism. This type of metamorphism occurs under moderately high pressure, such that the temperature field in the neighbourhood of the intrusive is superimposed on a regional termperature field. This results in larger contact aureoles, and possibly in the development of schistose texture in the rocks. In this series the initial

temperature of the country rocks may be high. Pressure exceeds 3 kbar. The result is rock transformation under conditions of regional metamorphism. The temperature of rocks in direct contact with a granitoid intrusive reach 600 - 700 °C and peripheral parts of the aureoles reach about 400 °C.

The contact aureole around the Anvil batholith fits the description of this abyssal, contact-metamorphic series.

Geothermometry results indicate an average temperature of 685 °C for the roof pendant rocks, an average temperature of 620 °C for rocks adjacent to the intrusive margin, and an average temperature of 550 °C for rocks up to 8.7 km (horizontal distance) from the intrusive contact.

These temperatures would be impossible to attain if the temperature and composition of the magma were the main controls of the temperature in the aureole rocks. At the estimated pressure (4.9 ± 1.6 kbar), the corresponding minimum temperature of water-saturated granite is 660 °C (Figure 10) assuming perfect heat transfer from the intrusive to the country rock. The temperature of the rocks adjacent to the Anvil batholith must have been initially high (under conditions of regional metamorphism) in order for temperatures of 600 - 700 °C to be attained in the aureole.

Geobarometry indicates an average pressure of 4.9 ±

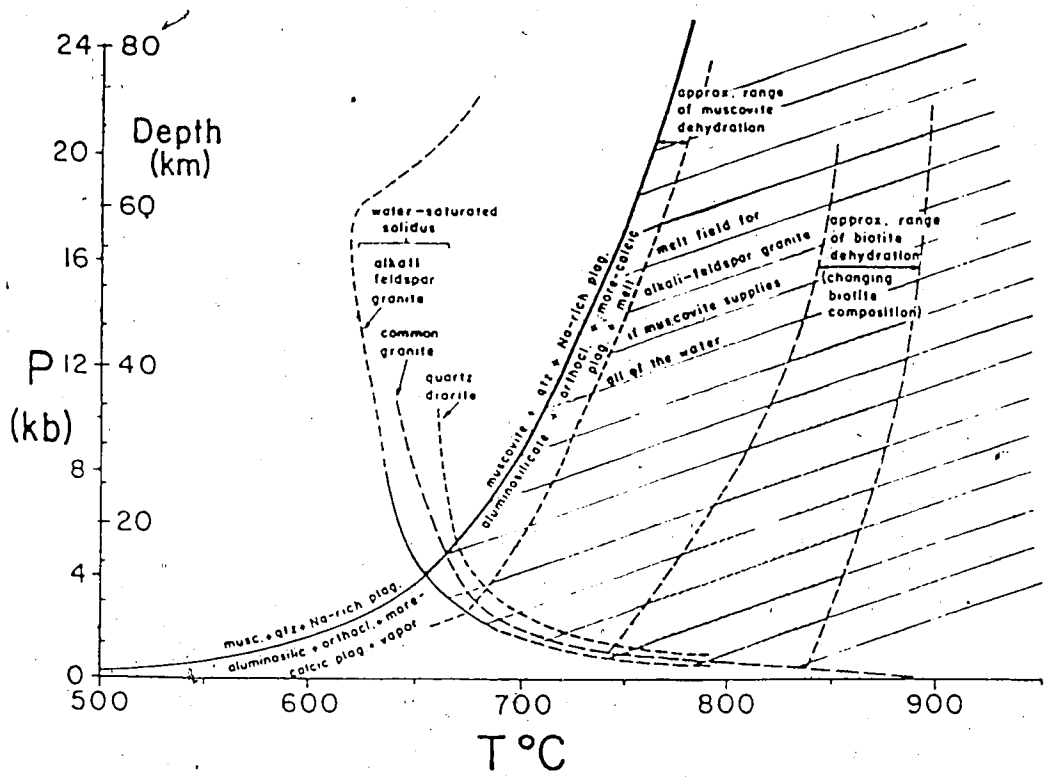

Figure 10. Solidus for a water-saturated common granite, modified after Hyndman (1981).

1.6 kbar. At 600 - 700 °C, the abscence of kyanite does not restrict pressure to less than 4 kbar. Kyanite might be expected as a contact metamorphic mineral only if pressure exceeded 6 kbar (Holdaway, 1971).

Pressure estimates for the area thus imply moderate depths and rock transformation under regional or near-regional metamorphic conditions as characterized by Reverdatto's et al (1970) abyssal contact-metamorphic series. Assuming an average geothermal gradient, rock in the Anvil area was hot (300 °C) at the time of intrusion.

Regional Implications

The pressure estimate together with regional geological relationships provides some constraints on the rate of uplift in the Mt. Mye area.

Unmetamorphosed Paleocene conglomerate (unit 15a - Tempelman-Kluit, 1972) is exposed at several localities in the Pelly River Valley, 28 km west of the study area.

The presence of this conglomerate implies that underlying metamorphosed strata were uplifted between mid-Cretaceous and Paleocene time. If the pressure estimate for the area is realistic, large-scale uplift is implied. Rapid uplift is implied by the K - Ar geochronological results summarized by Pigage and Anderson (1985).

The Paleocene age of the conglomerate does not provide a limiting time for unroofing of the granite as the

conglomerate does not contain granitic clasts. A youngest age for unroofing of the plutonic suite has not been determined. The presence of the large, continuous roof pendant and the fact that isograds are conformable to and dip away from the granitic contact suggests that the presently exposed level of the Anvil batholith is near the top of the pluton.

The granite must have come to its present position at a later time (post-Paleocene) possibly through movement along faults. Uplift may have been facilitated by steeply-dipping, northwest-trending faults that splay from the Tintina and Wangorda faults. This assumes that the conglomerate was deposited in situ and was not transported to its present location. The conglomerate is, in places, separated from the granitic intrusive by strike slip faults. If the conglomerate was transported to its present location by fault movement, or if the metamorphism of the underlying strata is associated with the earliest deformation event (i.e. the S_1-forming event), then no precise time constraints for uplift can be inferred.

Post-Paleocene unroofing of the granite would imply lower rates of uplift. In any case, the average pressure estimate for the area indicates that some 16 km of overlying cover has been removed since the mid-Cretaceous. The overlying cover may have been a structurally-thickened stratigraphic pile, i.e. a series of Mesozoic nappes.

The proposed spatial, temporal and geochemical link between some phases of the Anvil batholith and the South Fork volcanics (Pigage and Anderson, 1985) conflicts with this evidence of large-scale uplift and erosion in the area.

Rapid uplift (since the mid-Cretaceous) of the Yukon-Tanana terrane to the southwest of the study area cannot be demonstrated. Similarly, the Tantalus Formation, an Upper Jurassic to Lower Cretaceous unmetamorphosed conglomerate, lies unconformably across Yukon Crystalline Terrane and Whitehorse Trough strata (Tempelman-Kluit, 1980).

The estimated average pressure for the Mt. Mye area indicates large-scale uplift for the region. In view of the lack of evidence for similar uplift in neighbouring Yukon-Tanana terrane and the proposed relationships between the Anvil plutonic suite and the South Fork volcanics, the pressure estimate for the area may be high. However, even at the lower limit of error associated with the pressure estimate (3.3 kbar), relatively large-scale uplift (removal of at least 11 km of (stratigraphic) cover is implied. Significant differential uplift across Tintina fault in this area since the mid-Cretaceous is also implied.

VII. CONCLUSIONS

1. The isograds are concentric to the pluton in the study area.

2. Isograds dip away from the pluton at the present level of exposure. Isograd surfaces are steeply-dipping where the intrusive contact is steeply-dipping and shallowly-dipping where the intrusive contact is shallowly-dipping. This accounts for the variation in the width of the metamorphic zone. The dip of the isograds lessens with distance from the intrusive contact. The dip of the granitic contacts is similarly interpreted to lessen with distance.

3. As granitic sills are injected along the S_2 foliation plane in the schist, and as foliation developed in the granitic sills at intrusive margins is parallel with S_2 in the schist, the Anvil batholith must have been emplaced after formation of the S_2 surface and before the final stages of the S_2-forming deformation event.

4. All porphyroblast-matrix relationships indicate syntectonic growth (with respect to S_2) of porphyro-

blasts, as well as some post-tectonic growth.

5. The average pressure for the Mount Mye area is 4.9 ± 1.6 kbar. A pressure of this magnitude suggests a maximum thickness of cover during emplacement of about 16 km (± 5 km).

6. Temperatures ranged from 509 to 872 ^{o}C ± 50 ^{o}C. The highest temperatures are recorded in roof pendant rocks. A general trend of decreasing temperature away from the intrusive margins is recorded.

7. The contact aureole developed adjacent to the Anvil batholith is distinct from contact aureoles around other Cordilleran mid-Cretaceous intrusives. The intrusive contact is sharp, locally steep, and discordant. The high-grade nature and extent of contact metamorphism, as well as the presence of a well-developed schistosity in pelitic rocks, is unique to the aureole around the Anvil Batholith.

8. The characteristics of the contact aureole developed in the pelitic schists around the Anvil batholith are those of a thermally-transformed gneissose rock series (abyssal contact metamorphism). This type of contact metamorphism occurs under moderately high

pressure, and the temperature field around the intrusive is superimposed on a regional field.

9. Large-scale uplift in the Mt. Mye area is implied by the geobarometry results. Even at the lowermost end of the error associated with the average pressure estimate for the area, removal of 11 km of overlying cover since the mid-Cretaceous is implied. Previously proposed relationships between the Anvil plutonic suite and the South Fork volcanics, and the present evidence for large-scale uplift and erosion in the area cannot be reconciled.

10. There is no evidence for similar large-scale uplift since the mid-Cretaceous in the neighbouring Yukon-Tanana terrane. Significant differential uplift across Tintina fault in this area is implied.

REFERENCES

Anderson, R.G. 1982. Geology of the Mactung pluton in Niddery Lake map area and some of the plutons in Nahanni map area, Yukon Territory and District of Mackenzie; in Current Research, Part A, Geological Survey of Canada, Paper 82-1A, 299-304.

Anderson, R.G. 1983. Selwyn plutonic suite and its relationship to tungsten mineralization, southeastern Yukon and District of Mackenzie; in Current Research, Part B, Geological Survey of Canada, Paper 83-1B, 151-163.

Bard, J.P. 1980. Microtextures of igneous and metamorphic rocks; S.W. Morel (editor), Kluwer Academic Publishers, Norwell, Mass., 264p.

Bell, T.H. and Rubenach, M.J. 1983. Sequential porphyroblast growth and crenulation cleavage development during progressive deformation; Tectonophysics, 92, 171-194.

Bell, T.H. 1985. Deformation partitioning and porphyroblast rotation in metamorphic rocks: a radical interpretation; Journal of Metamorphic Geology, 3, 109-118.

Bell, T.H. 1986 Foliation development and refraction of earlier foliations and decrenulation due to shifting patterns of deformation partitioning; Journal of Metamorphic Geology, 4, 1-24.

Bell, T.H. Rubenach, M.J., and Fleming, P.D. 1986. Porphyroblast nucleation, growth and dissolution in regional metamorphic rocks as a function of deformation partitioning during foliation development; Journal of Metamorphic Geology, 4, 37-67.

Blusson, S.L. 1966. Frances Lake, Yukon Territory and District of Mackenzie; Geological Survey of Canada, Map 8-1976.

Blusson, S.L. 1967. Tekwi Mountain, Nahanni and Frances

Lake map-areas; in Report of activities May to October, 1966, Geological Survey of Canada, Paper 67-1, part A, 44-45.

Bostock, H.S. and Lees, E.J. 1938. Laberge map-area, Yukon; Geological Survey of Canada, Memoir 217.

Campbell, R.B. 1967. Geology of the Glenlyon map area; Geological Survey of Canada, Memoir 352, 92p.

Carmichael, I.S.E., Turner, F.J. and Verhoogen, J. 1974. Ingeous petrology. McGraw-Hill, New York, 739p.

Colby, J.W. 1968. Advancements in X-Ray Analysis, 11, 287-305.

Coney P.J., Jones D.L. and Monger, J.W.H. 1980. Cordilleran suspect terranes; Nature, 288, 329-333.

Cox, F.C. 1969. Inclusions in garnets: discussion and suggested mechanism of growth for syntectonic garnets; Geological Magazine, 106, 57-62.

Dixon, J.M. 1976. Apparent "double rotation" of porphyroblasts during a single progressive deformation; Tectonophysics, 34, 101-116.

Ferry, J.M. and Spear, F.S. 1978. Experimental calibration of the partitioning of Fe and Mg between biotite and garnet; Contributions to Mineralogy and Petrology, 66, 113-117.

Gabrielse, H. and Blusson, S.L. 1969. Geology of Coal River map area, Yukon Territory and District of Mackenzie (95 D); Geological Survey of Canada, Paper 68-38, 22p.

Gabrielse H. and Reesor J.E. 1974. Geochronology of plutonic rocks in two areas of the Canadian Cordillera; Royal Society of Canada, Special Publication, 8, Geochronology in Canada, 96-138.

Gabrielse, H., Blusson, S.L. and Roddick, J.A. 1973. Geology of Flat River, Glacier Lake and Wrigely Lake map areas; Geological Survey of Canada, Memoir 366, 153p.

Ghent, E.D. 1976. Plagioclase-garnet Al_2SiO_5-quartz: a potential geobarometer-geothermometer; American Mineralogist, 61, 710-714.

Ghent E.D., Robbins, D.B. and Stout, M. Z. 1979. Geothermometry, geobarometry, and fluid compositions of metamorphosed cal-silicates and pelites, Mica Creek, British Columbia; American Mineralogist, 64, 874-885.

Gordey, S.P., 1978. Stratigraphy and structure of the Summit Lake area, Yukon and Northwest Territories; in Current Research, Part A, Geological Survey of Canada, Paper 78-1A, 43-48.

Gordey, S.P. 1983. Thrust faults in the Anvil Range and a new look at the Anvil Range Group, south central Yukon Territory; in Current Research, Part A, Geological Survey of Canada, Paper 83-1A, 225-227.

Holdaway, M.J. 1971. Stability of andalusite and the aluminum silicate phase diagram; American Journal of Science, 271, 97-131.

Hyndman, D.W. 1981. Controls on source and depth of emplacement of granitic magma, Geology, 9, 244-249.

Jennings, D.S., Jilson, G.A. and Pigage, L.C. 1980. Anvil Range stratigraphy, south-central Yukon Territory; Geological Association of Canada, Cordilleran Section, Programme and Abstracts, 16-

Jennings D. S. and Jilson G.A. 1986. Geology and sulphide depositis of Anvil Range, Yukon Territory; in Mineral deposits of northern cordillera, J.Morin (editor), Canadian Institute of Mining and Metallurgy, special volume 37, 378p.

Jilson, G.A. 1984. Summary of the geology and sulphide deposits of the Anvil Range, Yukon Territory; unpublished internal report, Cyprus Anvil Mining Development Corporation 59p.

Lister, G.S. and Williams, P.F. 1983. The partitioning deformation in flowing rock masses; Tectonophysics 92, 1-34.

Mortenson, J.K. and JIlson, G.A. 1983. Evolution of the Yukon-Tanana terrane: evidence from southeastern Yukon Territory; Geology, 13, 806-810.

Olesen, N.O. 1978. Distinguishing between inter-kinematic and syn-kinematic porphyroblastesis. Geologische Rundschau, 67, 278-287.

Pigage L. C. and Anderson, R. G. 1985. The Anvil plutonic suite, Faro, Ykon Territory; Canadian Journal of Earth Sciences, 22, 1204-1216.

Pigage L.C. and Jilson, G.A. 1985. Major extensional faults, Anvil Pb-Zn district, Yukon; Geological Society of America, Cordilleran Section Annual Meeting, Abstracts with Programs p.400.

Powell, D. and Treagus, J.E. 1970. Rotational fabrics in metamorphic minerals; Mineralogical Magazine, 37, 801-814.

Roddick, J.A. and Green, L.H. 1961. Tay River map area, Yukon Territory; Geological Survey of Canada, Map 13-1961.

Reesor, J.E. 1958. Dewar Creek map-area with special emphasis on the White Creek Batholith, British Columbia; Geological Survey of Canada, Memoir 292,78p.

Reesor, J.E. 1973. Geology of the Lardeau map-area, east half, British Columbia; Geological Survey of Canada, Memoir, 369.

Reverdatto, V.V., Sharapov, V.N. and Melamed, V.G. 1970. The controls and selected peculiarities of the origin of contact metamorphic zonation; Contributions to Mineralogy and Petrology, 29, 310-337.

Richardson, S.W., Gilbert, M.C. and Bell, P.M. 1969. Experimental determination of kyanite-andalusite and andalusite-sillimanite equilibria: the aluminium silicate triple point; American Journal of Science, 267, 259-272.

St-Onge, M.R. 1984. Geothermometry and geobarometry in pelitic rocks of north-central Wopmay Orogen (early Proterozoic), Northwest Territories, Canada; Geological Society of America Bulletin, 95, 196-208.

Schoneveld, C. 1977. A study of some typical inclusion patterns in strongly paracrystalline rotated garnets; Tectonophysics, 39, 453-471.

Smit, H., Armstrong, R.L. and van der Heyden, P. 1985. Petrology, chemistry and radiogenic isotope (K-Ar, Rb-Sr, and U-Pb) study of the Emerald Lake pluton, eastern Yukon Territory; in Current research, Part B, Geological Survey of Canada, Paper 85-1B, 347-359

Spry, A. 1963. The chronological analysis of crystallization and deformation of some Tasmanian Precambrian rocks; Journal of the Geological Society of Australia, 10, 193-208.

Spry, A. 1969. Metamorphic textures. Pergamon Press, Oxford.

Tempelman-Kluit, D.J. 1972. Geology and origin of the Faro, Vangorda, and Swim concordant zinc-lead deposits, central Yukon Territory; Geological Survey of Canada, Bulletin 208, 73p.

Tempelman-Kluit, D.J. 1974. Reconnaissance geology of Aishihik lake, Snag and part of Stewart River map-areas, west-central Yukon (115H, 115K-J and 115N-O); Geological Survey of Canada, Paper 73-41.

Tempelman-Kluit, D.J. 1977. Quiet Lake (105 F) and Finlayson Lake (105 G) map areas, Yukon Territory; Geological Survey of Canada, Open File 486.

Tempelman-Kluit, D.J. 1979. Transported cataclasite, ophiolite and granodiorite in Yukon: evidence of arc-continent collision; Geological Survey of Canada, Paper 79-14, 29p.

Tempelman-Kluit, D.J. 1980. Geology and Mineral deposits of southern Yukon, in Yukon Geology and Exploration 1979-80, Department of Indian and Northern Affairs, Whitehorse, Yukon, 7-31.

Vernon, R.H. 1978. Porphyroblast-matrix microstructural relationships in deformed metamorphic rocks; Geologische Rundschau, 67, 288-305.

Wheeler, J.O. 1961. Whitehorse map-area, Yukon Territory 105 D; Geological Survey of Canada, Memoir 312, 156p.

Williams, P.J. and Schoneveld, C. 1981. Garnet rotation and the development of axial plane crenulation cleavage; Tectonophysics, 70, 307-334.

Zwart, H.J. 1960. The chronological succession of folding and metamorphism in the central Pyrenees; Geologische Rundschau, 50, 203-218.

Zwart, H.J. 1962. On the determination of polymetamorphic associations and its application to the Bosost area (central Pyrenees); Geologische Rundschau, 52, 38-65.

APPENDIX 1. SAMPLE LOCATIONS

SAMPLE NUMBER	EASTING	NORTHING
2-1	597950 E	6912675 N
2-2	597850 E	6912600 N
2-3	597100 E	6912625 N
2-4	597125 E	6912675 N
3-1	598175 E	6913325 N
3-2	597800 E	6913400 N
3-3	598075 E	6914100 N
3-4	598100 E	6914225 N
3-5	598125 E	6914300 N
3-6	598125 E	6914475 N
3-7	598200 E	6915500 N
3-8	598200 E	6915500 N
4-1	597975 E	6910950 N
4-2	597975 E	6910950 N
4-3	597800 E	6910850 N
4-4	597800 E	6910850 N
4-5	598100 E	6910625 N
4-6	598200 E	6910450 N
4-7	598675 E	6910175 N
4-8	598675 E	6910175 N
4-9	598875 E	6910200 N
4-10	599300 E	6910725 N
4-11	599625 E	6911075 N
5-1	599500 E	6912000 N
5-2	599500 E	6911825 N
5-3	600400 E	6913050 N
5-4	600400 E	6913050 N
5-5	601400 E	6914750 N
5-6	600750 E	6913750 N
6-1	597075 E	6911800 N
6-2	596650 E	6911950 N
6-3	596650 E	6911950 N
6-4	596500 E	6912550 N
6-5	596450 E	6912500 N
6-6	596100 E	6912800 N
6-7	597700 E	6913300 N

SAMPLE NUMBER	EASTING	NORTHING
7-1	600125 E	6915300 N
7-2	600150 E	6918000 N
7-3	599300 E	6918525 N
7-4	599375 E	6918150 N
7-5	599600 E	6917625 N
7-6	599775 E	6917500 N
7-7	600125 E	6917325 N
7-8	600225 E	6917275 N
7-9	600975 E	6916350 N
7-10	600725 E	6916000 N
8-1	597900 E	6912600 N
8-2	597625 E	6912400 N
8-3	597525 E	6912400 N
8-4	596925 E	6912550 N
8-5	597375 E	6913025 N
9-1	599525 E	6911975 N
9-2	599800 E	6912050 N
9-3	600175 E	6912450 N
9-4	600400 E	6912675 N
9-5	601400 E	6915000 N
9-6	601300 E	6915500 N
9-7	601325 E	6915650 N
9-8	601375 E	6915750 N
9-9	601450 E	6916125 N
10-1	598975 E	6911150 N
10-2	599250 E	6910750 N
10-3	598150 E	6910550 N
10-4	598150 E	6910550 N
10-5	598100 E	6910675 N
10-6	598000 E	6910900 N
10-7	598075 E	6911775 N
11-1	598500 E	6913925 N
11-2	598500 E	6913925 N
11-3	598450 E	6914075 N
11-4	598600 E	6914400 N
11-5	598175 E	6915250 N
11-6	598125 E	6915025 N
11-7	598125 E	6914575 N
11-8	598125 E	6914575 N
11-9	598125 E	6914375 N
11-10	597900 E	6913600 N
12-1	601325 E	6917250 N
12-2	601525 E	6917400 N
12-3	602200 E	6917700 N
12-4	602075 E	6916950 N
12-5	602050 E	6916900 N

SAMPLE NUMBER	EASTING	NORTHING
12-6	601850 E	6916500 N
12-7	601700 E	6916275 N
12-8	601425 E	6916225 N
12-9	601350 E	6916500 N
12-10	601325 E	6916700 N
13-1	601250 E	6917150 N
13-2	601250 E	6917150 N
13-3	601250 E	6917025 N
13-4	601250 E	6916925 N
13-5	601300 E	6916775 N
13-6	601100 E	6916850 N
13-7	601100 E	6916850 N
13-8	600600 E	6917300 N
13-9	600400 E	6917450 N
13-10	600650 E	6918250 N
13-11	601150 E	6917300 N
14-1	603225 E	6919625 N
14-2	603325 E	6919650 N
14-3	603325 E	6919650 N
15-1	601475 E	6916350 N
15-2	601400 E	6915575 N
15-3	601425 E	6915150 N
15-4	601425 E	6914900 N
15-5	601700 E	6914900 N
15-6	602000 E	6914925 N
15-7	602150 E	6915050 N
15-8	602450 E	6915150 N
15-9	602775 E	6915500 N
15-10	603200 E	6915450 N
15-11	602550 E	6916250 N
15-12	602400 E	6916300 N
15-13	602025 E	6916350 N
15-14	601400 E	6917125 N
16-1	601650 E	6911275 N
16-2	601400 E	6911175 N
16-3	600950 E	6911075 N
16-4	600550 E	6910975 N
16-5	600400 E	6910875 N
16-6	600350 E	6910775 N
16-7	600750 E	6911050 N
17-1	604750 E	6913275 N
17-2	604900 E	6913450 N
17-3	605025 E	6913575 N
17-4	605425 E	6914000 N
17-5	605900 E	6914125 N
17-6	606500 E	6914050 N

SAMPLE NUMBER	EASTING	NORTHING
17-7	606900 E	6914025 N
17-8	606150 E	6913825 N
17-9	605575 E	6913525 N
17-10	605400 E	6913325 N
17-11	605300 E	6913150 N
17-12	604725 E	6912500 N
18-1	605000 E	6912475 N
18-2	605600 E	6912200 N
18-3	605825 E	6912125 N
18-4	606300 E	6911825 N
18-5	607150 E	6912425 N
18-6	606475 E	6912850 N
18-7	606700 E	6911700 N
18-8	606550 E	6911300 N
18-9	606300 E	6911600 N
19-1	604525 E	6911150 N
19-2	605050 E	6911900 N
19-3	605950 E	6912025 N
19-4	605950 E	6911300 N
19-5	606350 E	6910975 N
19-6	606700 E	6910450 N
19-7	606650 E	6910875 N
19-8	606200 E	6911300 N
19-9	603500 E	6912100 N
20-1	611000 E	6912225 N
20-2	611150 E	6911000 N
20-3	611350 E	6911225 N
20-4	610275 E	6910125 N
20-5	609900 E	6909900 N
21-1	591225 E	6913325 N
21-2	590625 E	6913525 N
21-3	590625 E	6913375 N
21-4	590425 E	6913300 N
21-5	589900 E	6912900 N
21-6	589425 E	6912700 N
21-7	589200 E	6912500 N
21-8	588400 E	6911525 N
22-1	588500 E	6910675 N
23-1	596700 E	6905000 N
23-2	596500 E	6905150 N
23-3	596350 E	6905525 N
23-4	596625 E	6905625 N
23-5	597775 E	6906000 N
23-6	598000 E	6905800 N
23-7	597975 E	6905650 N

SAMPLE NUMBER	EASTING	NORTHING
23-8	597300 E	6905050 N
24-1	596275 E	6904275 N
24-2	598775 E	6905075 N
24-3	598600 E	6906000 N
24-4	598375 E	6906050 N
24-5	598900 E	6906625 N
24-6	599400 E	6906800 N
24-7	599825 E	6906650 N
24-8	599550 E	6906200 N
24-9	598950 E	6906150 N
24-10	599100 E	6905600 N
24-11	598950 E	6905350 N
25-1	591675 E	6906750 N
25-2	591900 E	6907050 N
25-3	587200 E	6909275 N
26-1	589000 E	6906425 N
26-2	588150 E	6906675 N
26-3	588000 E	6906950 N
26-4	587975 E	6907200 N
26-5	587700 E	6907425 N
26-6	587500 E	6907575 N
26-7	586675 E	6908325 N
26-8	585000 E	6909075 N
27-1	586475 E	6910625 N
27-2	586900 E	6910750 N
27-3	587125 E	6910800 N
27-4	588300 E	6910725 N
27-5	587775 E	6909350 N
27-6	588400 E	6910125 N
29-2	582800 E	6913350 N
29-3	583000 E	6913250 N
29-4	585400 E	6911900 N

APPENDIX 2. MINERAL ASSEMBLAGES

SAMPLE NO.	ROCK TYPE	Ch	Bt	Ms	Gt	Si	An	St	Hb	Qz	Fs	Zr	Ti	To	Ct	Cz	Di	Vs	Tr	Ru	Opq
2-1	sch		x	x	x	x				x	x	x									
2-2	skn	x			x						x		x				x				
2-3	int			x	x					x	x										
2-4	int										x										
2-5	sch		x	x	x					x	x	x		x							x
2-6	skn				x												x	x			
3-1	sch	x	x	x		x				x	x	x		x							
3-4	sch		x	x		x				x	x	x		x							
3-7	int		x	x						x	x										
3-8	sch		x	x	x	x				x	x	x		x							
4-1	int				x					x	x										
4-3	int		x	x		x				x	x	x									
4-6	sch		x			x				x	x										
4-10	sch		x	x		x				x	x	x									
5-2	amph								x	x	x		x								x
5-5	sch		x	x	x	x				x	x			x							
6-4	sch		x		x					x	x										
6-6	int								x	x	x				x						
6-7	amph					x			x	x	x					x					x
7-2	phyl	x		x						x	x										x
7-3	phyl	x		x						x	x										x
7-5	skn		x							x			x		x		x		x		x
7-8	skn		x							x	x		x		x		x		x		x
7-9	sch		x	x	x		x	x		x	x			x							x
7-10	sch		x	x		x				x	x			x							
8-2	sch		x	x		x				x	x										x
8-4	sch		x		x	x				x	x			x							x
8-5	sch			x						x				x							x
9-1	skn									x	x		x		x		x				
9-2	int		x	x						x	x										
9-3	sch		x	x		x				x	x	x		x							
9-4	skn				x						x		x				x				
9-5	sch		x		x	x				x	x										
9-6	sch		x	x	x	x				x	x	x		x							x
9-8	sch		x	x		x		x		x	x										
10-1A	sch		x		x	x				x	x	x		x							
10-2	sch		x	x		x				x	x			x							x
10-4	sch		x	x	x	x				x	x			x							x
10-4	sch		x	x	x	x				x	x			x							x
10-5	sch		x	x	x	x				x	x			x							
10-6B	sch		x	x	x	x				x	x			x							x
10-7	sch		x			x				x	x									x	x
11-1	skn				x					x	x		x				x		x		
11-3	sch		x	x		x				x	x			x						x	x
11-4	sch		x	x	x	x				x	x			x							
11-6	sch		x	x	x	x				x	x			x							
11-7	skn		x							x									x		x
11-8	sch			x						x				x							x
11-9A	skn				x						x		x		x		x	x			
11-10B	sch		x	x	x	x				x	x			x							
12-1	phyl	x	x							x	x										x

SAMPLE NO.	ROCK TYPE	Ch	Bt	Ms	Gt	Si	An	St	Hb	Qz	Fs	Zr	Ti	To	Ct	Cz	Di	Vs	Tr	Ru	Opq
12-2	phyl	x	x	x			x			x	x			x							x
12-3	phyl	x		x						x											
12-5	phyl	x		x						x	x										x
12-6	skn	x	x	x					x	x	x				x		x		x		
12-7	skn									x	x		x		x		x				x
12-8	sch		x	x	x		x	x		x	x			x							
12-9	skn	x								x	x		x				x				x
13-3	sch	x	x	x			x	x		x	x										
13-5	skn									x	x				x		x				x
13-6	skn									x	x				x		x				
13-7	sch	x	x	x	x			x		x	x										x
13-8	sch		x	x	x		x			x	x										x
13-9	sch		x	x			x	x		x										x	x
13-10	phyl	x		x						x											x
																					x
14-1	phyl	x								x	x				x			x			
14-3	lmst									x	x				x						x
																					x
15-1	sch		x		x			x		x	x			x							
15-5	sch		x	x	x	x				x	x										
15-6	sch		x		x					x	x										
15-7C	sch		x	x	x	x				x	x										
15-8	sch		x	x		x	x	x		x	x	x		x							x
15-9	sch		x	x	x		x	x		x	x			x						x	x
15-10	sch		x	x	x		x	x		x	x			x							x
15-12	sch		x	x			x	x		x	x			x							x
15-13	sch		x	x				x		x	x										
15-14A	skn		x							x	x				x		x				x
16-1	skn				x					x	x				x		x				
16-2	skn	x			x					x	x		x				x				
16-4	sch		x	x		x				x				x							x
16-6	sch			x	x	x		x		x	x			x							x
16-7	sch		x	x		x				x	x										
17-1	sch	x	x	x	x	x				x	x			x							x
17-3	sch		x	x	x			x		x	x			x							x
17-4	sch		x	x			x	x		x	x			x							x
17-7	sch		x	x	x		x	x		x	x										x
17-8	sch		x	x			x	x		x	x										x
17-9	sch		x	x			x	x		x	x			x							x
17-11	sch		x	x	x			x		x	x			x							x
17-12	sch		x	x	x	x	x	x		x	x			x							
																					x
18-2	sch		x	x	x			x		x											x
18-4	sch		x	x	x		x	x		x	x			x							x
18-6	sch		x	x	x		x	x		x	x			x							x
18-7	sch		x	x				x		x	x										x
18-8	sch		x	x				x		x	x										x
																					x
19-1B	sch		x	x		x				x	x			x							x
19-3	sch		x	x	x			x		x	x			x						x	x
19-4	sch		x	x	x			x		x	x										
19-6	sch		x	x			x	x		x	x									x	x
19-9	sch		x	x		x				x	x			x							
20-1	sch		x	x	x		x	x		x	x	x		x							x
20-3	sch		x	x			x	x		x	x										x
20-5	sch		x	x	x		x	x		x	x			x							x

SAMPLE NO.	ROCK TYPE	Ch	Bt	Ms	Gt	Si	An	St	Hb	Qz	Fs	Zr	Ti	To	Ct	Cz	Di	Vs	Tr	Ru	Opq
21-1	sch		x							x	x										x
21-2B	skn				x					x	x		x				x				x
21-4A	sch		x							x	x			x							x
21-5B	sch		x	x		x				x	x			x							x
21-7	sch		x	x		x				x	x			x							
21-8	sch		x	x	x					x	x			x							x
22-1	skn		x	x	x			x		x	x		x	x			x				x
23-1B	sch		x	x			x	x		x				x							x
23-2	skn		x							x	x		x				x		x		x
23-3	sch		x							x	x		x				x		x		x
23-4	int		x	x						x	x										
23-5A	sch		x							x	x	x	x								x
23-5B	sch		x	x						x	x	x		x							
23-7	phyl		x	x						x	x			x							x
23-8	phyl		x	x						x	x			x							x
24-1	phyl		x	x						x											x
24-2	sch		x	x				x		x	x			x							x
24-3	skn	x	x							x	x		x				x				x
24-4A	skn		x							x	x		x				x				
24-4B	sch		x	x	x		x	x		x	x			x							x
24-5	skn	x								x	x		x				x				x
24-6	sch		x	x				x		x	x										x
24-7	skn	x		x						x	x						x				x
24-10	phyl	x	x	x	x					x											
25-2A	skn										x				x		x				
25-2B	sch		x		x			x		x	x						x				
25-3	sch		x	x			x	x		x	x			x							x
26-3	sch		x	x				x		x	x										x
26-4	sch		x	x	x		x	x		x	x			x							x
26-5	amph								x	x	x										x
26-6	sch	x	x	x			x			x	x										x
27-1	sch		x	x			x	x		x	x										x
27-2	sch	x	x	x	x					x	x			x							x
27-4	sch	x	x	x	x		x	x		x	x										x
27-5	sch		x	x				x		x	x										
27-6	lmst		x							x	x				x						x
29-2	phyl	x		x						x											x
29-3	phyl		x							x	x				x						
29-4	phyl		x	x			x			x	x										x

APPENDIX 3. ANALYTICAL METHODS AND MICROPROBE DATA BASE

Analytical Methods

Analyses of garnet, plagioclase and biotite were done at the University of Alberta by the wavelength dispersive technique using an automated ARL-SEMQ electron microprobe. An accelerating voltage of 15 kev, an aperature current of 0.6×10^{-7} amperes and a probe current of 0.079×10^{-7} amperes was used for all analyses. The beam was rastered over an area of 5×10^{-8} to 10×10^{-8} cm^2 for plagioclase analyses. All other analyses were done with a beam spot area of 2×10^{-8} cm^2. Counting time for both the standards and the samples was 100 seconds. Background counting time was 40 seconds.

For garnet analysis the standards used were: grossular for Si, Al, Ca; chromite for Cr, Fe; willemite for Mn; pyrope for Mg; and rutile for Ti. For plagioclase analysis the standards used were: sanidine for Si, K; pyrope for Al and Fe; diopside for Ca, Mg; and tugtupite for Na. For biotite analysis the standards used were: diopside for Si, Ca, Mg; ilmenite for Ti, Fe; kyanite for Al; lemite for Mn; and sanidine for Na and K.

ZAF corrections were applied and ionic proportions

calculated by the program MAGIC IV (Colby, 1968). The detection of the analyses is 0.1 wt%. The statistical error at the 99% confidence level is nearly ± 1% of the amount present for the major elements and up to ± 10% for minor elements.

Microprobe data base

Garnet Analyses

Sample No.	8-4.1	8-4.3 Mean	8-4.4 Mean	8-4.5	8-4.6	8-4.7	8-4.8	8-4.8	11-6.1	11-6.1	11-6.1 Mean	11-6.2
Analysis No.	RIM 1 Garnet	RIM 1&2 Garnet	RIM 1&2 Garnet	RIM 1 Garnet	RIM 1 Garnet	RIM 1 Garnet	RIM 1 Garnet	CORE 1 Garnet	RIM 1 Garnet	RIM 2 Garnet	CORE 1&2 Garnet	RIM 1 Garnet
SiO_2	35.602	34.565	33.441	35.732	35.196	36.126	35.601	34.554	37.323	38.028	38.326	38.959
TiO_2	0.075	0.004	0.015	0.000	0.008	0.014	0.018	0.058	0.000	0.000	0.008	0.014
Al_2O_3	21.121	21.148	21.506	21.322	21.269	21.070	20.811	20.967	20.752	20.622	20.470	20.633
Cr_2O_3	0.048	0.000	0.023	0.039	0.000	0.032	0.000	0.050	0.047	0.049	0.027	0.034
FeO	36.806	36.349	36.337	37.428	37.760	37.879	37.500	36.681	32.921	31.705	33.615	32.205
MnO	2.791	3.228	3.294	3.150	2.875	3.020	3.239	3.478	6.879	6.742	4.816	6.895
MgO	1.842	1.769	1.269	1.502	1.469	1.531	1.348	2.003	1.782	1.612	1.698	1.632
CaO	0.429	0.302	0.371	0.377	0.414	0.426	0.453	0.438	0.554	1.685	2.479	1.358
TOTAL	98.713	97.365	96.256	99.550	98.991	100.100	98.969	98.228	100.258	100.443	101.439	101.730

Number of ions on the basis of 24 O

Si	5.8903	5.8167	5.7148	5.8811	5.8396	5.9168	5.9081	5.7832	6.0526	6.1252	6.1214	6.1874
Al	4.1183	4.1943	4.3324	4.1361	4.1590	4.0671	4.0704	4.1359	3.9661	3.9146	3.8533	3.8621
Cr	0.0062	0.0000	0.0032	0.0051	0.0000	0.0042	0.0000	0.0066	0.0060	0.0062	0.0035	0.0042
Ti	0.0093	0.0005	0.0020	0.0000	0.0010	0.0017	0.0023	0.0073	0.0000	0.0000	0.0009	0.0017
Fe	5.0926	5.1156	5.1944	5.1519	5.2393	5.1883	5.2046	5.1342	4.4647	4.2708	4.4900	4.2774
Mn	0.3911	0.4600	0.4769	0.4392	0.4040	0.4190	0.4553	0.4930	0.9450	0.9197	0.6516	0.9276
Mg	0.4542	0.4438	0.3234	0.3686	0.3633	0.3738	0.3334	0.4997	0.4907	0.3870	0.4041	0.3864
Ca	0.0760	0.0545	0.0380	0.0665	0.0736	0.0748	0.0805	0.0785	0.0963	0.2908	0.4242	0.2311
(Si,Al)	6.0000	6.0000	6.0000	6.0000	6.0000	6.0000	6.0000	6.0000	0.0526	6.1252	6.1214	6.1874
(Al,Ti,Cr)	4.0241	4.0115	4.0524	4.0223	3.9996	3.9898	3.9808	3.9330	3.9721	3.9208	3.8577	3.8680
(Mn,Mg,Ca,Fe)	6.0139	6.0739	6.0327	6.0262	6.0802	6.0559	6.0738	6.2054	5.9367	5.8683	5.9699	5.8225
Pyr	0.0755	0.0730	0.0536	0.0612	0.0598	0.0617	0.0549	0.0805	0.0725	0.0659	0.0677	0.0664
Alm	0.8468	0.8422	0.8610	0.8549	0.8617	0.8567	0.8569	0.8274	0.7520	0.7278	0.7521	0.7346
Sp	0.0650	0.0757	0.0790	0.0729	0.0664	0.0692	0.0750	0.0794	0.1592	0.1567	0.1091	0.1593
Gro	0.0126	0.0090	0.0063	0.0110	0.0121	0.0124	0.0132	0.0126	0.0162	0.0495	0.0710	0.0397

Garnet Analyses

Sample No.	13-8.3	13-8.3	13-8.4	13-8.4	15-1.1	15-1.1	15-5.1	15-5.1	15-5.1	15-5.2	15-5.2	15-5.3
Analysis No.	Mean RIM 1&2 Garnet	CORE 1 Garnet	RIM 1 Garnet	CORE 1 Garnet	Mean RIM 1&2 Garnet	Mean CORE 1&2 Garnet	RIM 1 Garnet	CORE 1 Garnet	RIM 2 Garnet	RIM 1 Garnet	CORE 1 Garnet	Mean RIM 1&2 Garnet
SiO_2	34.426	35.007	36.026	36.479	37.096	37.215	37.111	36.747	37.642	36.542	36.792	37.156
TiO_2	0.041	0.083	0.040	0.051	0.038	0.046	0.036	0.037	0.031	0.031	0.304	0.021
Al_2O_3	20.791	20.641	20.788	20.595	20.144	19.930	19.490	19.196	19.538	19.883	18.324	19.036
Cr_2O_3	0.063	0.013	0.017	0.043	0.006	0.010	0.026	0.012	0.032	0.026	0.064	0.027
FeO	32.708	28.169	32.165	28.098	34.883	33.218	32.952	32.203	33.376	33.631	31.630	33.026
MnO	6.381	10.798	7.733	11.766	4.314	5.491	5.244	6.153	5.074	4.306	6.125	5.147
MgO	1.460	1.004	1.387	0.996	2.257	1.909	1.904	1.969	1.979	2.027	1.906	1.986
CaO	0.841	1.353	1.136	1.241	0.663	1.200	1.957	1.329	1.437	1.829	2.060	1.712
TOTAL	96.711	97.138	99.291	99.269	99.403	99.019	98.720	97.645	99.108	98.275	97.205	98.111
Number of ions on the basis of 24 O												
Si	5.8362	5.9104	5.9377	6.0059	6.0659	6.1046	6.1131	6.1245	6.1621	6.0455	6.1663	6.1584
Al	4.1540	4.0990	4.0381	3.9963	3.8822	3.8531	3.7838	3.7706	3.7695	3.8770	3.6194	3.7184
Cr	0.0069	0.0018	0.0022	0.0056	0.0007	0.0014	0.0034	0.0016	0.0042	0.0034	0.0085	0.0036
Ti	0.0052	0.0105	0.0050	0.0063	0.0047	0.0057	0.0045	0.0046	0.0038	0.0039	0.0383	0.0026
Fe	4.6374	3.9694	4.4335	3.8688	4.7703	4.5570	4.5394	4.4886	4.5694	4.6532	4.4334	4.5778
Mn	0.9164	1.5411	1.0795	1.6408	0.5975	0.7630	0.7317	0.8687	0.7036	0.6034	0.8695	0.7227
Mg	0.3690	0.2521	0.3406	0.2444	0.5501	0.4668	0.4674	0.4891	0.4828	0.4998	0.4762	0.4906
Ca	0.1528	0.2443	0.2006	0.2188	0.1162	0.2110	0.3454	0.237[illegible]	0.2520	0.3243	0.3699	0.3039
(Si,Al)	6.0000	6.0000	6.0000	6.0059	6.0659	6.1046	6.1131	6.1245	6.1621	6.0455	6.1663	6.1584
(Al,Ti,Cr)	4.0023	4.0217	3.9830	4.0082	3.8876	3.8603	3.7917	3.7768	3.7775	3.8843	3.6662	3.7246
(Mn,Mg,Ca,Fe)	6.0756	6.0069	6.0542	5.9728	6.0341	5.[illegible]78	6.0839	6.083[illegible]	6.[illegible]78	6.0807	6.1490	6.0950
Pyr	0.0607	0.0420	0.0563	0.0409	0.[illegible]12	0.0778	0.0768	0.0804	0.0804	0.0822	0.0774	0.0805
Alm	0.7633	0.6608	0.7323	0.6477	[illegible]905	0.7598	0.7461	0.7378	0.7606	0.7652	0.7210	0.7511
Sp	0.1508	0.2565	0.1783	0.2747	0.0990	0.1272	0.1203	0.1428	0.1171	0.0992	0.1414	0.1186
Gro	0.0251	0.0407	0.0331	0.0366	0.0192	0.0352	0.0568	0.0390	0.0419	0.0533	0.0601	0.0498

Garnet Analyses

Sample No.	15-5.3	15-7c.1 Mean	15-7c.1 Mean	16-6.1 Mean	16-6.1	16-6.2	16-6.2	17-11.1 Mean	17-11.1	17-11.1 Mean	18-6.1 Mean	18-6.1
Analysis No.	CORE 1 Garnet	RIM 1&2 Garnet	CORE 1&2 Garnet	RIM 1&2 Garnet	CORE 1 Garnet	RIM 1 Garnet	CORE 1 Garnet	RIM 1&2 Garnet	MID 1 Garnet	CORE 1&2 Garnet	RIM 1&2 Garnet	RIM 3 Garnet
SiO_2	36.739	36.019	36.253	36.262	36.211	35.378	36.382	38.131	37.936	37.879	36.728	37.330
TiO_2	0.032	0.031	0.047	0.016	0.095	0.002	0.035	0.011	0.095	0.240	0.066	0.082
Al_2O_3	19.182	21.135	21.125	21.150	20.491	21.179	20.719	20.841	20.758	20.708	21.129	21.021
Cr_2O_3	0.042	0.008	0.015	0.036	0.009	0.019	0.043	0.007	0.000	0.029	0.031	0.007
FeO	32.335	33.530	36.273	35.076	29.241	34.777	34.054	35.282	32.312	30.871	36.135	36.265
MnO	6.260	5.183	2.974	2.849	6.888	2.915	3.202	3.970	7.148	8.873	3.580	3.644
MgO	1.940	2.005	2.073	2.367	1.083	2.512	2.432	2.082	1.564	1.273	2.138	2.113
CaO	1.640	2.012	1.744	1.450	4.867	1.319	2.259	1.282	1.699	1.701	1.206	1.135
TOTAL	98.169	99.923	100.504	99.206	98.885	98.102	99.127	101.606	101.512	101.574	101.013	101.597
Number of ions on the basis of 24 O												
Si	6.1028	5.8829	5.8885	5.9278	5.9558	5.8583	5.9507	6.0817	6.0721	6.0681	5.9281	5.9834
Al	3.7554	4.0637	4.0443	4.0750	3.9722	4.1334	3.9941	3.9176	3.9158	3.9097	4.0201	3.9710
Cr	0.0055	0.0010	0.0019	0.0046	0.0012	0.0025	0.0056	0.0008	0.0000	0.0037	0.0040	0.0009
Ti	0.0040	0.0038	0.0057	0.0021	0.0117	0.0003	0.0043	0.0012	0.0114	0.0289	0.0080	0.0098
Fe	4.4920	4.5750	4.9273	4.7955	4.0222	4.8162	4.6581	4.7061	4.3254	4.1359	4.8785	4.8612
Mn	0.8807	0.7160	0.4092	0.3945	0.9596	0.4089	0.4436	0.5363	0.9690	1.2040	0.4896	0.4948
Mg	0.4803	0.4864	0.5020	0.5767	0.2656	0.6199	0.5928	0.4948	0.3733	0.3039	0.5145	0.5083
Ca	0.2919	0.3519	0.3036	0.2540	0.8576	0.2341	0.3958	0.2191	0.2914	0.2920	0.2087	0.1950
(Si,Al)	6.1028	6.0000	6.0000	6.0000	6.0000	6.0000	6.0000	6.0831	6.0721	6.0681	6.0000	6.0000
(Al,Ti,Cr)	3.7649	3.9514	3.9404	4.0095	3.9409	3.9945	3.9448	3.9196	3.9272	3.9423	3.9605	3.9651
(Mn,Mg,Ca,Fe)	6.1449	6.1293	6.1421	6.0207	6.1050	6.0791	6.0903	5.9563	5.9591	5.9358	6.0913	6.0557
Pyr	0.0782	0.0793	0.0817	0.0958	0.0435	0.1020	0.0973	0.0831	0.0626	0.0512	0.0845	0.0833
Alm	0.7310	0.7464	0.8022	0.7965	0.6588	0.7922	0.7648	0.7901	0.7258	0.6968	0.8009	0.8027
Sp	0.1433	0.1168	0.0666	0.0655	0.1572	0.0673	0.0728	0.0900	0.1626	0.2028	0.0804	0.0817
Gro	0.0475	0.0574	0.0494	0.0422	0.1405	0.0385	0.0650	0.0368	0.0489	0.0492	0.0343	0.0322

Garnet Analyses

Sample No.	18-6.1	18-6.1 Mean	18-6.2 Mean	18-6.2	18-6.2 Mean	20-1.1	20-1.1	20-1.2	20-1.2	20-1.3	20-1.4	20-1.4
Analysis No.	MID 1 Garnet	CORE 1&2 Garnet	RIM 1&2 Garnet	MID 1 Garnet	CORE 1&2 Garnet	RIM 1 Garnet	CORE 1 Garnet	RIM 1 Garnet	CORE 1 Garnet	RIM 1 Garnet	RIM 1 Garnet	CORE 1 Garnet
SiO_2	37.406	36.933	37.496	37.295	37.487	36.475	35.223	35.465	33.487	35.252	35.563	33.567
TiO_2	0.041	0.079	0.054	0.091	0.102	0.060	0.059	0.055	0.045	0.076	0.033	0.177
Al_2O_3	21.073	20.822	21.183	20.785	20.886	20.972	21.404	21.069	22.144	21.978	21.734	22.728
Cr_2O_3	0.032	0.059	0.013	0.005	0.032	0.002	0.009	0.020	0.002	0.018	0.060	0.043
FeO	34.844	32.732	35.480	32.531	29.435	35.901	33.424	36.331	34.402	35.127	35.460	30.387
MnO	5.060	7.583	4.295	7.705	10.672	2.982	5.371	2.501	3.502	3.410	3.666	7.875
MgO	1.778	1.454	2.006	1.441	1.194	2.957	1.534	2.294	1.996	1.988	1.954	1.342
CaO	1.281	1.203	1.226	1.326	1.562	1.286	1.553	1.130	1.529	1.775	1.496	1.424
TOTAL	101.516	100.865	101.753	101.179	101.370	99.736	98.577	98.866	97.107	99.624	99.966	97.542
	Number of ions on the basis of 24 O											
Si	6.0003	5.9843	5.9933	6.0162	6.0302	5.9505	5.8365	5.8532	5.6382	5.7702	5.8083	5.6242
Al	3.9840	3.9763	3.9904	3.9516	3.9598	4.0324	4.1801	4.0983	4.3942	4.2398	4.1836	4.4881
Cr	0.0040	0.0073	0.0017	0.0006	0.0042	0.0003	0.0012	0.0026	0.0003	0.0023	0.0077	0.0057
Ti	0.0049	0.0097	0.0065	0.0111	0.0123	0.0073	0.0074	0.0068	0.0057	0.0093	0.0041	0.0223
Fe	4.6745	4.4354	4.7427	4.3887	3.9598	4.8981	4.6319	5.0147	4.8441	4.8085	4.8435	4.2579
Mn	0.6875	1.0408	0.5814	1.0528	1.4540	0.4121	0.7539	0.3496	0.4994	0.4728	0.5072	1.1176
Mg	0.4252	0.3512	0.4778	0.3464	0.2861	0.5001	0.3788	0.5644	0.5010	0.4851	0.4757	0.3352
Ca	0.2202	0.2088	0.2100	0.2292	0.2691	0.2249	0.2757	0.1999	0.2759	0.3113	0.2618	0.2556
(Si,Al)	6.0003	6.0000	6.0000	6.0162	6.0302	6.0000	6.0000	6.0000	6.0000	6.0000	6.0000	6.0000
(Al,Ti,Cr)	3.9929	3.9776	3.9919	3.9633	3.9763	3.9905	4.0252	3.9609	4.0384	4.0216	4.0037	4.1403
(Mn,Mg,Ca,Fe)	6.0074	6.0362	6.0119	6.0171	5.9690	6.0352	6.0403	6.1286	6.1204	6.0777	6.0882	5.9663
Pyr	0.0708	0.0582	0.0795	0.0576	0.0479	0.0829	0.0627	0.0921	0.0818	0.0798	0.0781	0.0562
Alm	0.7781	0.7348	0.7889	0.7294	0.6634	0.8116	0.7668	0.8182	0.7915	0.7912	0.7956	0.7137
Sp	0.1144	0.1724	0.0967	0.1750	0.2436	0.0683	0.1248	0.0570	0.0816	0.0778	0.0833	0.1873
Gro	0.0366	0.0346	0.0349	0.0381	0.0451	0.0373	0.0456	0.0326	0.0451	0.0512	0.0430	0.0428

Garnet Analyses

Sample No.f Analysis No.	24-4b.1 Mean RIM 1&2 Garnet	24-4b.1 Mean CORE 1&2 Garnet	25-2.1 Mean RIM 1&2 Garnet	25-2.1 CORE 1 Garnet	27-4.1 RIM 1 Garnet	27-4.1 CORE 1 Garnet	27-4.2 RIM 1 Garnet	27-4.2 RIM 2 Garnet	27-4.2 CORE 1 Garnet	27-4.3 RIM 1 Garnet	27-4.3 CORE 1 Garnet
SiO_2	38.459	38.189	37.051	39.916	37.612	37.119	36.578	35.518	35.949	35.583	35.960
TiO_2	0.023	0.021	0.024	0.015	0.088	0.065	0.067	0.085	0.099	0.061	0.060
Al_2O_3	21.206	21.424	20.116	20.900	21.048	21.054	21.133	21.349	21.069	21.544	21.458
Cr_2O_3	0.053	0.025	0.010	0.000	0.042	0.045	0.018	0.013	0.014	0.004	0.000
FeO	35.831	35.593	32.846	28.536	31.711	31.908	32.470	32.068	31.680	31.262	31.365
MnO	4.210	4.095	4.163	4.072	1.918	2.098	1.747	1.799	1.881	2.244	1.995
MgO	1.928	2.122	1.695	1.337	1.693	1.572	1.820	1.710	1.580	1.932	1.618
CaO	1.187	1.165	3.564	3.708	6.662	7.031	5.832	6.516	6.820	6.108	7.021
TOTAL	102.897	102.634	99.472	98.484	100.773	100.891	99.664	99.057	99.092	98.737	99.476
	Number of ions on the basis of 24 O										
Si	6.0651	6.0314	6.0468	6.3831	6.0011	5.9411	5.9222	5.8071	5.8669	5.8166	.8393
Al	3.9416	3.9878	3.8694	3.9389	3.9580	3.9716	4.0325	4.1137	4.0524	4.1506	4.1066
Cr	0.0066	0.0031	0.0013	0.0000	0.0053	0.0056	0.0023	0.0017	0.0003	0.0006	0.0000
Ti	0.0027	0.0025	0.0030	0.0018	0.0105	0.0078	0.0081	0.0105	0.0121	0.0075	0.0073
Fe	4.7257	4.7012	4.4827	3.8162	4.2313	4.2711	4.3966	4.3846	4.3239	4.2738	4.2595
Mn	0.5622	0.5478	0.5759	0.5516	0.2592	0.2844	0.2396	0.2491	0.2601	0.3107	0.2743
Mg	0.4533	0.4994	0.4121	0.3188	0.4025	0.3751	0.4391	0.4166	0.3844	0.4708	0.3915
Ca	0.2005	0.1972	0.6235	0.6353	1.1388	1.2058	1.0118	1.1414	1.1925	1.0697	1.2216
(Si,Al)	6.0651	6.0314	6.0468	6.3831	6.0011	6.0000	6.0000	6.0000	6.0000	6.0000	6.0000
(Al,Ti,Cr)	3.9509	3.9934	3.8737	3.9407	3.9738	3.9261	3.9651	3.9330	3.9331	3.9753	3.9532
(Mn,Mg,Ca,Fe)	5.9417	5.9459	6.0942	5.3219	6.0318	6.1364	6.0871	6.1917	6.1609	6.1250	6.1469
Pyr	0.0763	0.0840	0.0676	0.0599	0.0677	0.0463	0.0721	0.0673	0.0624	0.0507	0.0637
Alm	0.7953	0.7907	0.7356	0.7171	0.7015	0.6960	0.7223	0.7081	0.7018	0.6978	0.6929
Sp	0.0946	0.0921	0.0945	0.1036	0.0430	0.0611	0.0394	0.0402	0.0422	0.0769	0.0446
Gro	0.0337	0.0332	0.1023	0.1194	0.1888	0.1965	0.1662	0.1843	0.1935	0.1746	0.1987

Biotite Analyses

Sample No.	8-4.1	8-4.2	8-4.3	8-4.4	8-4.6	8-4.8	11-6.1	11-6.2	11-6.3	11-6.4	12-8.1 Mean	12-8.2 Mean
Analysis No.	RIM 1 Biotite	RIM 1 Biotite	RIM 1 Biotite	RIM 1 Biotite	RIM 1 Biotite	RIM 1 Biotite	RIM 1 Biotite	RIM 1 Biotite	RIM 1 Biotite	RIM 1 Biotite	RIM 1&2 Biotite	RIM 1&2 Biotite
SiO_2	34.258	34.292	33.194	34.453	33.654	34.364	33.434	33.531	34.558	32.786	32.135	31.344
TiO_2	1.830	0.937	1.403	2.045	2.263	2.023	2.582	2.903	2.451	2.817	1.107	1.345
Al_2O_3	20.638	21.059	21.084	21.043	21.737	21.200	19.881	20.142	19.712	19.801	20.575	20.702
FeO	26.194	25.488	24.877	25.073	24.742	24.382	23.771	22.685	21.802	22.661	20.897	21.228
MnO	0.100	0.108	0.088	0.070	0.113	0.106	0.265	0.320	0.278	0.242	0.124	0.081
MgO	4.085	4.692	4.694	4.148	4.021	4.373	6.241	5.799	6.159	6.328	8.144	7.537
CaO	0.059	0.013	0.006	0.000	0.006	0.008	0.014	0.009	0.004	0.000	0.000	0.010
Na_2O	0.138	0.170	0.204	0.230	0.219	0.210	0.304	0.260	0.277	0.288	0.253	0.231
K_2O	8.555	8.527	8.431	8.535	8.643	8.750	8.783	8.547	8.682	8.887	8.732	8.601
TOTAL	95.856	95.285	93.982	95.597	95.399	95.414	95.274	94.196	93.924	93.810	91.967	91.079
Number of ions on the basis of 24 O												
Si	5.8111	5.8270	5.7219	5.8205	5.7019	5.8064	5.6822	5.7222	5.8777	5.6467	5.5951	5.5249
Al	4.1260	4.2174	4.2834	4.1899	4.3406	4.2217	3.9822	4.0512	3.9513	4.0193	4.2219	4.3012
Ti	0.2335	0.1197	0.1819	0.2598	0.2883	0.2570	0.3300	0.3726	0.3135	0.3648	0.1450	0.1786
Fe	3.7159	3.6220	3.5863	3.5425	3.5058	3.4454	3.3786	3.2375	3.1011	3.2639	3.0428	3.1296
Mn	0.0143	0.0155	0.0129	0.0101	0.0163	0.0152	0.0381	0.0463	0.0400	0.0354	0.0183	0.0231
Mg	1.0328	1.1883	1.2062	1.0445	1.0155	1.1012	1.5810	1.4751	1.5613	1.6244	2.1136	1.9802
Ca	0.0107	0.0023	0.0011	0.0000	0.0011	0.0014	0.0025	0.0017	0.0007	0.0001	0.0000	0.0017
Na	0.0454	0.0560	0.0681	0.0755	0.0718	0.0687	0.1001	0.0859	0.0914	0.0962	0.0854	0.0790
K	1.8512	1.8484	1.8539	1.8394	1.8681	1.8860	1.9042	1.8606	1.8837	1.9524	1.9394	1.9142
(Si,Al)	8.0000	8.0000	8.0000	8.0000	8.0000	8.0000	8.0000	8.0000	8.0000	8.0000	8.0000	8.0000
(Al,Ti,Fe, Mn,Mg)	6.9336	6.9849	6.9926	6.8673	6.8684	4.8188	6.9921	6.9049	6.8449	6.9545	7.1367	7.1376
(Ca,Na,K)	1.9073	1.9067	1.9231	1.9149	1.9410	1.9561	2.0068	1.9482	1.9758	2.0487	2.0248	2.0149
(F,OH)												
Phl	0.2168	0.2462	0.2510	0.2272	0.2238	0.2414	0.3163	0.3100	0.3320	0.3299	0.4084	0.3858
Ann	0.7801	0.7505	0.7463	0.7706	0.7726	0.7553	0.6760	0.6803	0.6595	0.6629	0.5880	0.6097
Mn	0.0030	0.0032	0.0027	0.0022	0.0036	0.0033	0.0076	0.0097	0.0085	0.0072	0.0035	0.0045

Biotite Analyses

Sample No.	12-8.3	12-8.4	12-8.5	13-8.1	13-8.2	13-8.3	15-5.1	15-5.2	15-5.3	15-5.4	15-5.5	15-7c.1
Analysis No.	Mean RIM 1&2 Biotite	Mean RIM 1&2 Biotite	Mean RIM 1&2 Biotite	Mean RIM 1&2 Biotite	RIM 1 Biotite	RIM 1 Biotite	RIM 1 Biotite	RIM 1 Biotite	Mean RIM 1&2 Biotite	Mean RIM 1&2 Biotite	RIM 1 Biotite	Mean RIM 1&2 Biotite
SiO_2	31.965	31.776	31.155	31.338	31.993	33.765	34.637	34.669	33.925	33.141	33.169	35.729
TiO_2	1.779	1.532	1.358	1.183	1.349	1.478	2.619	2.497	2.363	2.591	2.619	2.910
Al_2O_3	20.815	20.188	20.438	20.823	21.337	19.945	19.872	18.891	20.023	20.301	20.143	20.272
FeO	20.688	20.630	21.233	25.769	25.595	23.107	21.266	21.490	20.289	20.712	20.735	19.833
MnO	0.102	0.139	0.131	0.197	0.127	0.140	0.262	0.249	0.269	0.210	0.217	0.199
MgO	7.712	7.721	7.715	6.949	7.394	6.830	6.785	6.730	6.777	6.790	6.862	6.448
CaO	0.008	0.028	0.009	0.010	0.062	0.016	0.030	0.012	0.003	0.095	0.000	0.017
Na_2O	0.306	0.356	0.349	0.120	0.257	0.152	0.317	0.282	0.255	0.301	0.313	0.361
K_2O	8.775	8.525	8.235	6.134	5.151	8.529	8.671	8.748	8.719	8.386	8.775	8.453
TOTAL	92.150	90.895	90.623	92.523	93.265	93.961	94.459	94.568	92.623	92.527	92.834	94.222
Number of ions on the basis of 24 O												
Si	5.5509	5.5978	5.5202	5.4742	5.4895	5.7784	5.8404	5.8456	5.8194	5.7042	5.7048	5.9630
Al	4.2610	4.1914	4.2676	4.2870	4.3150	4.0228	3.9490	3.9528	4.0481	4.1186	4.0831	3.9865
Ti	0.2323	0.2028	0.1808	0.1551	0.1740	0.1902	0.3321	0.3166	0.3048	0.3354	0.3388	0.3651
Fe	3.0052	3.0393	3.1472	3.7659	3.6729	3.3071	2.9988	3.0304	2.9106	2.9818	2.9825	2.7696
Mn	0.0150	0.0209	0.0196	0.0292	0.0185	0.0203	0.0374	0.0356	0.0390	0.0306	0.0316	0.0281
Mg	1.9969	2.0274	2.0376	1.8099	1.8911	1.7421	1.7053	1.6914	1.7329	1.7422	1.7592	1.6047
Ca	0.0015	0.0054	0.0017	0.0037	0.0113	0.0029	0.0054	0.0022	0.0004	0.0174	0.0000	0.0030
Na	0.1028	0.1217	0.1197	0.0404	0.0855	0.0505	0.1037	0.0920	0.0851	0.1005	0.1044	0.1168
K	1.9443	1.9158	1.8612	1.3678	1.1276	1.8619	1.8652	1.8817	1.9080	1.8414	1.9253	1.7998
(Si,Al)	8.0000	8.0000	8.0000	8.0000	8.0000	8.0000	8.0000	8.0000	8.0000	8.0000	8.0000	8.0000
(Al,Ti,Fe, Mn,Mg)	7.0613	7.0796	7.1730	7.5212	7.5610	7.0609	6.8630	6.8724	6.8548	6.9128	6.9000	6.7170
(Ca,Na,K)	2.0486	2.0429	1.9826	1.4120	1.2244	1.9153	1.9743	1.9759	1.9935	1.9593	2.0297	1.9196
(F,OH)												
Phl	0.3980	0.3985	0.3915	0.3229	0.3388	0.3436	0.3596	0.3550	0.3701	0.3664	0.3686	0.3645
Ann	0.5990	0.5974	0.6047	0.6719	0.6579	0.6523	0.6325	0.6370	0.6216	0.6271	0.6248	0.6291
Mn	0.0030	0.0041	0.0038	0.0052	0.0033	0.0040	0.0079	0.0075	0.0083	0.0064	0.0066	0.0064

Plagioclase Analyses

Sample No.	8-4.1	8-4.2	8-4.2	8-4.3	11-6.1	11-6.2	12-8.1	12-8.2	13-8.1	13-8.2	13-8.3	13-8.4
Analysis No.	RIM 1 Plag	RIM 1 Plag	CORE 1 Plag	RIM 1 Plag	RIM 1 Plag	RIM 1 Plag	Plag 1	Plag 1	Plag 1	Plag 1	Plag 1	Plag 1
SiO_2	65.029	65.055	65.872	65.538	64.946	63.341	62.979	61.149	62.528	63.020	62.653	61.924
Al_2O_3	21.763	21.627	22.300	21.707	21.856	22.570	23.948	23.522	23.080	23.323	22.948	23.291
FeO	0.280	0.145	0.000	0.149	0.197	0.068	0.202	0.044	0.221	0.353	0.741	0.443
MgO	0.041	0.025	0.029	0.024	0.041	0.053	0.019	0.000	0.006	0.004	0.031	0.027
CaO	1.899	1.773	1.963	1.856	2.753	2.679	3.515	3.138	3.353	2.630	1.601	3.058
Na_2O	10.710	10.892	10.517	10.701	10.260	10.541	10.416	10.577	10.406	10.012	10.324	10.306
K_2O	0.143	0.124	0.364	0.224	0.159	0.182	0.152	0.121	0.110	0.743	0.914	0.231
TOTAL	99.865	99.641	101.045	100.199	100.212	99.434	101.231	98.550	99.703	100.086	99.211	99.280
Number of ions on the basis of 24 O												
Si	8.6066	8.6242	8.6041	8.6368	8.5759	8.4490	8.2843	8.2629	8.3462	8.3761	8.4076	8.3097
Al	3.3947	3.3790	3.4330	3.3715	3.4014	3.5483	3.7127	3.7460	3.6308	3.6535	3.6294	3.6835
Fe	0.0310	0.0161	0.0000	0.0164	0.0217	0.0076	0.0222	0.0050	0.0247	0.0392	0.0831	0.0497
Mg	0.0081	0.0049	0.0056	0.0047	0.0081	0.0105	0.0038	0.0000	0.0012	0.0008	0.0061	0.0054
Na	2.7483	2.7996	2.6634	2.7343	2.6268	2.7260	2.6566	2.7711	2.6931	2.5802	2.6861	2.6813
Ca	0.2692	0.2518	0.2747	0.2621	0.3895	0.3828	0.4953	0.4543	0.4795	0.3745	0.2301	0.4397
K	0.0241	0.0209	0.0607	0.0376	0.0267	0.0310	0.0255	0.0209	0.0187	0.1259	0.1565	0.0396
Ab	0.9036	0.9112	0.8882	0.9012	0.8632	0.8682	0.8361	0.8536	0.8438	0.8375	0.8742	0.8484
An	0.0885	0.0819	0.0916	0.0864	0.1280	0.1219	0.1559	0.1399	0.1503	0.1216	0.0749	0.1391
Or	0.0079	0.0068	0.0202	0.0124	0.0088	0.0099	0.0080	0.0064	0.0059	0.0409	0.0509	0.0125

Biotite Analyses

Sample No.	25-2.1	27-4.1	27-4.2	27-4.3
Analysis No.	RIM 1 Biotite	RIM 1 Biotite	RIM 1 Biotite	RIM 1 Biotite
SiO_2	33.064	33.804	33.630	34.369
TiO_2	1.805	1.736	2.094	2.007
Al_2O_3	21.856	20.750	20.962	19.143
FeO	23.010	21.165	21.168	24.087
MnO	0.162	0.131	0.230	0.254
MgO	6.499	7.245	6.926	6.166
CaO	0.019	0.001	0.020	0.017
Na_2O	0.152	0.147	0.156	0.136
K_2O	8.635	9.432	9.542	9.308
TOTAL	95.203	94.410	94.728	95.487
Number of ions on the basis of 24 O				
Si	5.5794	5.7266	5.6861	5.8402
Al	4.3468	4.1429	4.1772	3.8339
Ti	0.2291	0.2212	0.2662	0.2565
Fe	3.2472	2.9985	2.9932	3.4231
Mn	0.0232	0.0187	0.0329	0.0366
Mg	1.6346	1.8295	1.7454	1.5617
Ca	0.0035	0.0002	0.0036	0.0030
Na	0.0498	0.0483	0.0511	0.0449
K	1.8588	2.0382	2.0580	2.0176
(Si,Al)	8.0000	8.0000	8.0000	8.0000
(Al,Ti,Fe, Mn,Mg)	7.0603	6.9374	6.9010	6.9520
(Ca,Na,K)	1.9121	2.0867	2.1127	2.0655
(F,OH)				
Phl	0.3333	0.3775	0.3658	0.3110
Ann	0.6620	0.6187	0.6373	0.6817
Mn	0.0047	0.0038	0.0069	0.0073

Plagioclase Analyses

Sample No.	16-6.1	18-6.1	18-6.2	18-6.3	18-6.4	20-1.2	27-4.1	27-4.2	27-4.3	27-4.4
Analysis No.	RIM 1 Plag	Plag 1	Plag 1	Plag 1	Plag 1	Plag 1	Plag 1	Plag 1	Plag 1	Plag 1
SiO_2	61.099	63.365	64.384	64.294	61.656	61.075	58.820	54.968	57.547	54.655
Al_2O_3	24.314	22.313	22.487	23.188	23.464	25.520	26.566	28.955	26.785	28.439
FeO	0.196	0.076	0.133	0.165	0.133	0.083	0.141	0.154	0.225	0.047
MgO	0.049	0.000	0.000	0.000	0.000	0.002	0.048	0.033	0.063	0.041
CaO	5.680	2.833	2.838	2.928	2.977	5.219	8.061	9.084	8.194	7.904
Na_2O	8.618	11.123	11.065	10.948	10.741	8.715	7.077	6.364	7.077	7.032
K_2O	0.146	0.131	0.138	0.101	0.126	0.111	0.208	0.157	0.165	0.247
TOTAL	100.102	99.841	101.045	101.624	99.097	100.724	100.921	99.714	100.055	98.364
Number of ions on the basis of 24 O										
Si	8.1487	8.4420	8.4675	8.4074	8.2858	8.0783	7.8242	7.4405	7.7386	7.4900
Al	3.8217	3.5035	3.4854	3.5736	3.7164	3.9782	4.1648	4.6192	4.2451	4.5933
Fe	0.0219	0.0085	0.0147	0.0181	0.0149	0.0091	0.0157	0.0174	0.0253	0.0054
Mg	0.0098	0.0000	0.0000	0.0000	0.0000	0.0005	0.0096	0.0066	0.0126	0.0084
Na	2.2286	2.8733	2.8216	2.7757	2.7988	2.2349	1.8252	1.6703	1.8451	1.8685
Ca	0.8116	0.4044	0.3999	0.4103	0.4287	0.7396	1.1489	1.3175	1.1806	1.1606
K	0.0248	0.0223	0.0231	0.0169	0.0216	0.0187	0.0353	0.0271	0.0283	0.0431
Ab	0.7271	0.8707	0.8696	0.8666	0.8614	0.7467	0.6065	0.5540	0.6041	0.6082
An	0.2648	0.1225	0.1233	0.1281	0.1319	0.2471	0.3818	0.4370	0.3866	0.3778
Or	0.0081	0.0068	0.0071	0.0053	0.0066	0.0062	0.0117	0.0090	0.0093	0.0140

Biotite Analyses

Sample No.	16-6.1	16-6.2	17-11.1	17-11.2	18-6.1	18-6.2	18-6.3 Mean	20-1.1	20-1.2 Mean	20-1.3	20-1.4 Mean	24-4b.1
Analysis No.	RIM 1 Biotite	RIM 1 Biotite	RIM 1 Biotite	RIM 1 Biotite	RIM 1 Biotite	RIM 1 Biotite	RIM 1&2 Biotite	RIM 1 Biotite	RIM 1&2 Biotite	RIM 1 Biotite	RIM 1&2 Biotite	RIM 1 Biotite
SiO_2	32.185	31.709	37.355	34.855	34.079	34.778	33.376	35.338	34.564	35.244	34.997	32.255
TiO_2	2.260	2.324	1.816	1.717	1.396	1.950	1.866	1.639	1.497	1.202	1.894	1.196
Al_2O_3	20.808	20.097	19.815	19.619	20.237	19.631	19.824	21.509	19.765	21.290	20.468	20.637
FeO	20.731	21.077	22.417	21.685	21.281	21.630	21.606	19.187	20.829	19.886	19.839	24.698
MnO	0.092	0.148	0.113	0.104	0.128	0.113	0.090	0.074	0.071	0.102	0.092	0.119
MgO	7.506	6.886	7.418	7.469	8.329	7.587	8.066	8.444	7.945	7.997	7.742	7.066
CaO	0.013	0.057	0.000	0.005	0.042	0.012	0.045	0.028	0.052	0.007	0.005	0.031
Na_2O	0.112	0.123	0.285	0.399	0.285	0.332	0.338	0.448	0.205	0.283	0.234	0.080
K_2O	9.184	7.731	8.826	8.567	8.574	8.625	8.460	8.395	7.828	8.566	8.692	6.554
TOTAL	92.890	90.151	98.045	94.419	94.351	94.658	93.671	95.062	92.756	94.578	93.963	92.635
Number of ions on the basis of 24 O												
Si	5.5516	5.6136	6.0462	5.8832	5.7540	5.8564	5.6989	5.8217	5.8879	5.8611	5.8732	5.5946
Al	4.2301	4.1931	3.7800	3.9028	4.0270	3.8961	3.9898	4.1763	3.9681	4.1727	4.0486	4.2187
Ti	0.2931	0.3093	0.2210	0.2180	0.1773	0.2469	0.2396	0.2031	0.1918	0.1504	0.2389	0.1560
Fe	2.9905	3.1206	3.0345	3.0611	3.0050	3.0462	3.0863	2.6435	2.9673	2.7657	2.7843	3.5826
Mn	0.0135	0.0221	0.0155	0.0149	0.0183	0.0161	0.0128	0.0104	0.0102	0.0143	0.0131	0.0176
Mg	1.9298	1.8171	1.7895	1.8792	2.0960	1.9042	2.0533	2.0734	2.0173	1.9823	1.9364	1.8267
Ca	0.0024	0.0108	0.0000	0.0008	0.0076	0.0021	0.0081	0.0049	0.0095	0.0013	0.0080	0.0057
Na	0.0374	0.0421	0.0896	0.1305	0.0934	0.1084	0.1118	0.1432	0.0676	0.0914	0.0759	0.0268
K	2.0208	1.7458	1.8223	1.8447	1.8466	1.8528	1.8433	1.7644	1.7010	1.8173	1.8606	1.4500
(Si,Al)	8.0000	8.0000	8.0000	8.0000	8.0000	8.0000	8.0000	8.0000	8.0000	8.0000	8.0000	8.0000
(Al,Ti,Fe, Mn,Mg)	7.0086	7.0758	6.8867	6.9592	7.0776	6.9659	7.0807	6.9284	7.0426	6.9465	6.8945	7.3962
(Ca,Na,K)	2.0606	1.7987	1.9119	1.9760	1.9476	1.9633	1.9632	1.9125	1.7781	1.9100	1.9445	1.4825
(F,OH)												
Phl	0.3911	0.3663	0.3698	0.3792	0.4088	0.3834	0.3985	0.4386	0.4039	0.4162	0.4900	0.3366
Ann	0.6061	0.6292	0.6270	0.6177	0.5876	0.6133	0.5990	0.5592	0.5941	0.5807	0.5882	0.6602
Mn	0.0027	0.0045	0.0032	0.0030	0.0036	0.0032	0.0025	0.0022	0.0020	0.0030	0.0028	0.0032

APPENDIX 4. GEOTHERMOBAROMETRY CALCULATIONS

Plagioclase-garnet-Al_2SiO_5-Quartz Geobarometer, Ghent (1976)

for the reaction:

$$3CaAl_2Si_2O_8 = Ca_3Al_2Si_3O_{12} + 2Al_2SiO_5 + SiO_2$$

the equilibrium can described by:

$$0 = \frac{-2551.4}{T(^oK)} + 7.1711 - \frac{0.2842(P(bars) - 1)}{T(^oK)}$$

where sillimanite is the Al_2SiO_5 polymorph and by:

$$0 = \frac{-2817.2}{T(^oK)} + 7.4351 - \frac{0.2678(P(bars) - 1)}{T(^oK)}$$

where andalusite is the Al_2SiO_5 polymorph.

For the discussion of the derivation of equilibrium constant equations, see Carmichael et al. (1974, p.107 et seq.).

Since the minerals are not pure phases, terms for activity of anorthite in plagioclase and activity of grossular in garnet must be added,

$$0 = \frac{-2551.4}{T(^{o}K)} + 7.1711 - \frac{0.2842(P(bars) - 1)}{T(^{o}K)} + \log K_S + \log K_\gamma$$

where sillimanite is the Al_2SiO_5 polymorph

and $K_\gamma = \frac{(\gamma_{Gr})^3}{(\gamma_{An})^3}$

and $K_S = \frac{(X_{Gr})^3}{(X_{An})^3}$

In the absence of experimental data, Ghent et al. (1979) proposed the use of an empirical activity coefficient, K_γ , and estimate $K_\gamma = -0.4$.

The solids activity product, K_S, varies systematically as a function of the Al_2SiO_5 polymorph present,

$$X_{Gr} = \frac{Ca}{Ca + Mg + Fe + Mn}$$

(where total Fe is treated as ferrous iron)

and,

$$X_{An} = \frac{Ca}{Ca + Na + K}$$

The garnet-plagioclase-Al_2SiO_5-quartz geobarometer has a resolution of approximately ± 1.6 kbar Ghent et al. (1979).

The Garnet-Biotite Geothermometer, Ferry and Spear (1978)

for the cation exchange reaction:

$$Fe_3Al_2Si_3O_{12} + KMg_3AlSi_3O_{10}(OH)_2 = Mg_3Al_2Si_3O_{12} + KFe_3AlSi_3O_{12}(OH)_2$$

$$\Delta\bar{G} = \Delta\bar{H} - T\Delta\bar{S} + P\Delta\bar{V} + 3RT\ln K = 0 \qquad (1)$$

where $K = (Mg/Fe)_{garnet}/(Mg/Fe)_{biotite}$

Preferred estimates for H and S of the exchange reaction are 12,454 cal and 4.662 e.u., respectively. $\Delta\bar{V} = +0.057$ cal/bar

Ferry and Spear's (1978) results are consistent with the following expression:

$$\ln K = -2109/T(^{o}K) + 0.782 \qquad (2)$$

by substituting $\Delta\bar{H}$, $\Delta\bar{S}$, and $\Delta\bar{V}$ into equation (1), we get:

$$12{,}454 - 4.662T(^{o}K) + 0.057P(bars) + 3RT\ln K = 0$$

Fe and Mg are assumed to mix ideally. Fe and Mg mix ideally in biotite and garnet solid solutions at least in the composition interval $0.80 \leq Fe/(Fe + Mg) \leq 1.00$.

The Ferry and Spear (1978) calibration may be used on natural assembalges for components up to 0.1 (Ca/Ca + Mn + Fe + Mg), 0.3 (Ca + Mn)/(Ca + Mn + Fe + Mg) in garnet and up to 0.15 $(Al^{VI} + Ti)/(Al^{VI} + Ti + Fe + Mg)$ in biotite.

The geothermometer has a maximum practical resolution of $\pm$ 50 ^{o}C, which corresponds to the error in temperature that results when $\pm$ 0.01 errors in X_{ann}, X_{phl}, X_{alm} and X_{py} are propagated through equation (2).

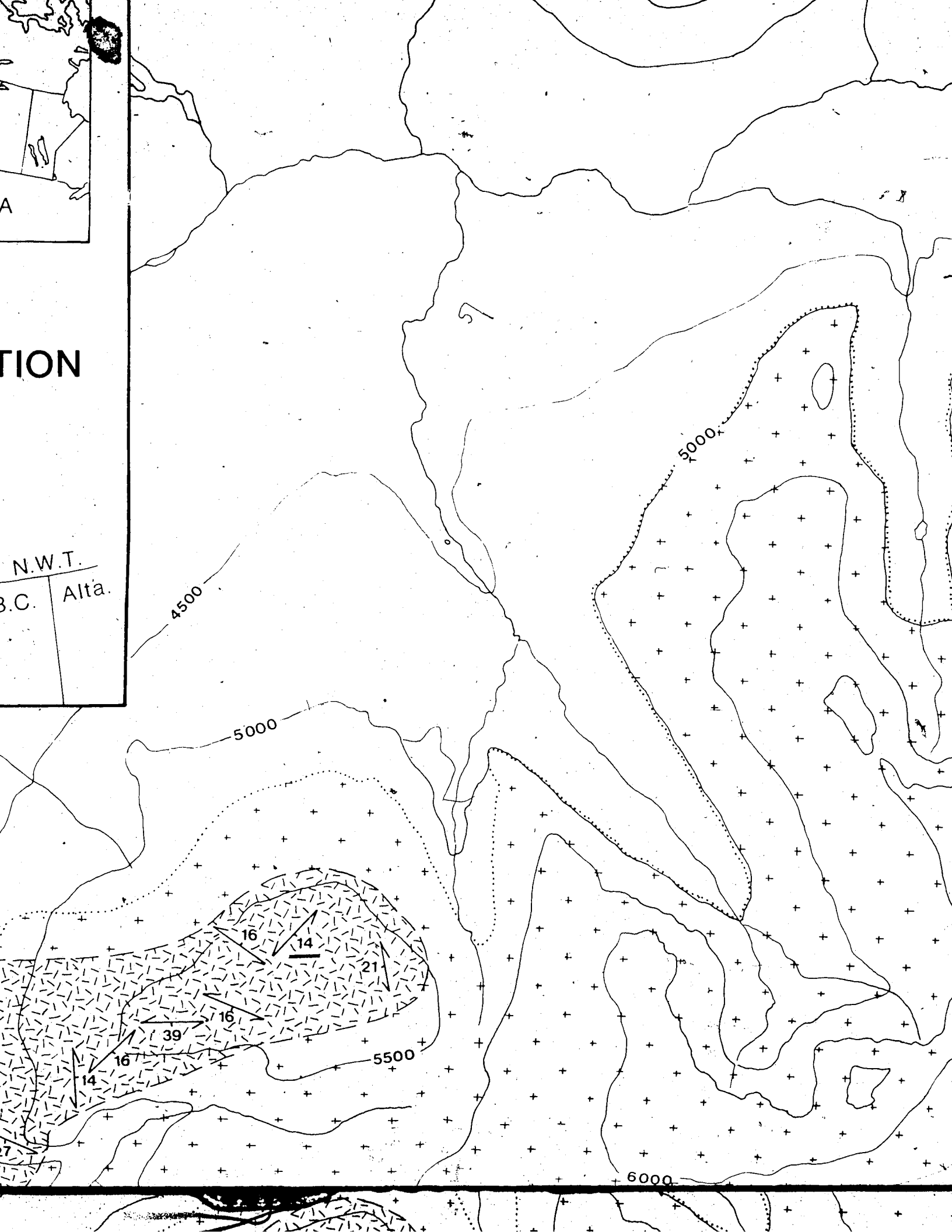
A
TION
N.W.T.
B.C.
Alta.
4500
5000
5000
16
14
21
16
39
16
14
5500
6000

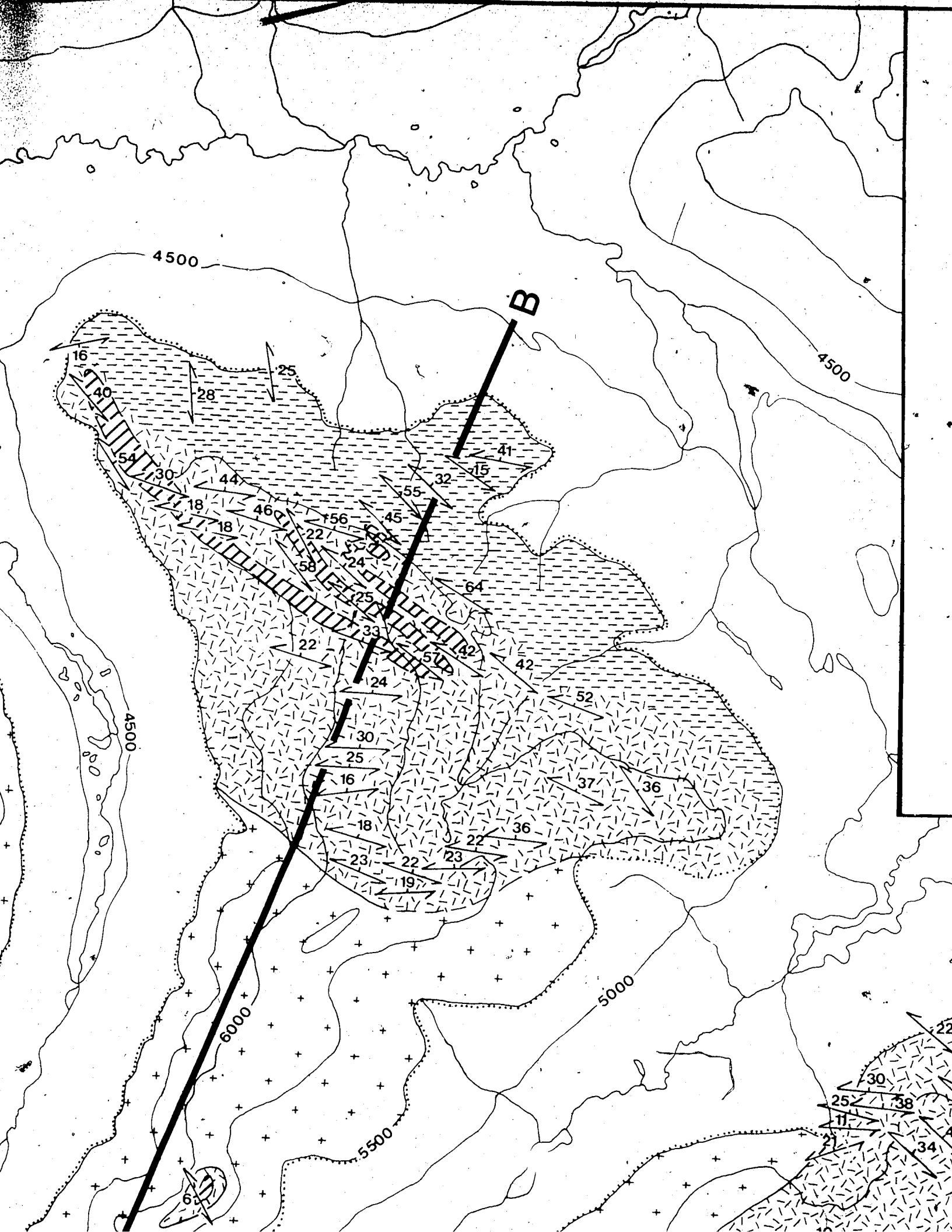
B
4500
4500
4500
5000
6000
5500
16
40
28
25
54
30
44
18
46
18
56
45
55
32
41
15
22
58
24
64
25
33
22
42
42
52
24
30
25
16
18
36
22
23
22
23
19
37
36
30
25
38
11
21
34

GEOLOGY MAP
OF THE
MOUNT MYE AREA
ANVIL RANGE DISTRICT
YUKON TERRITORY

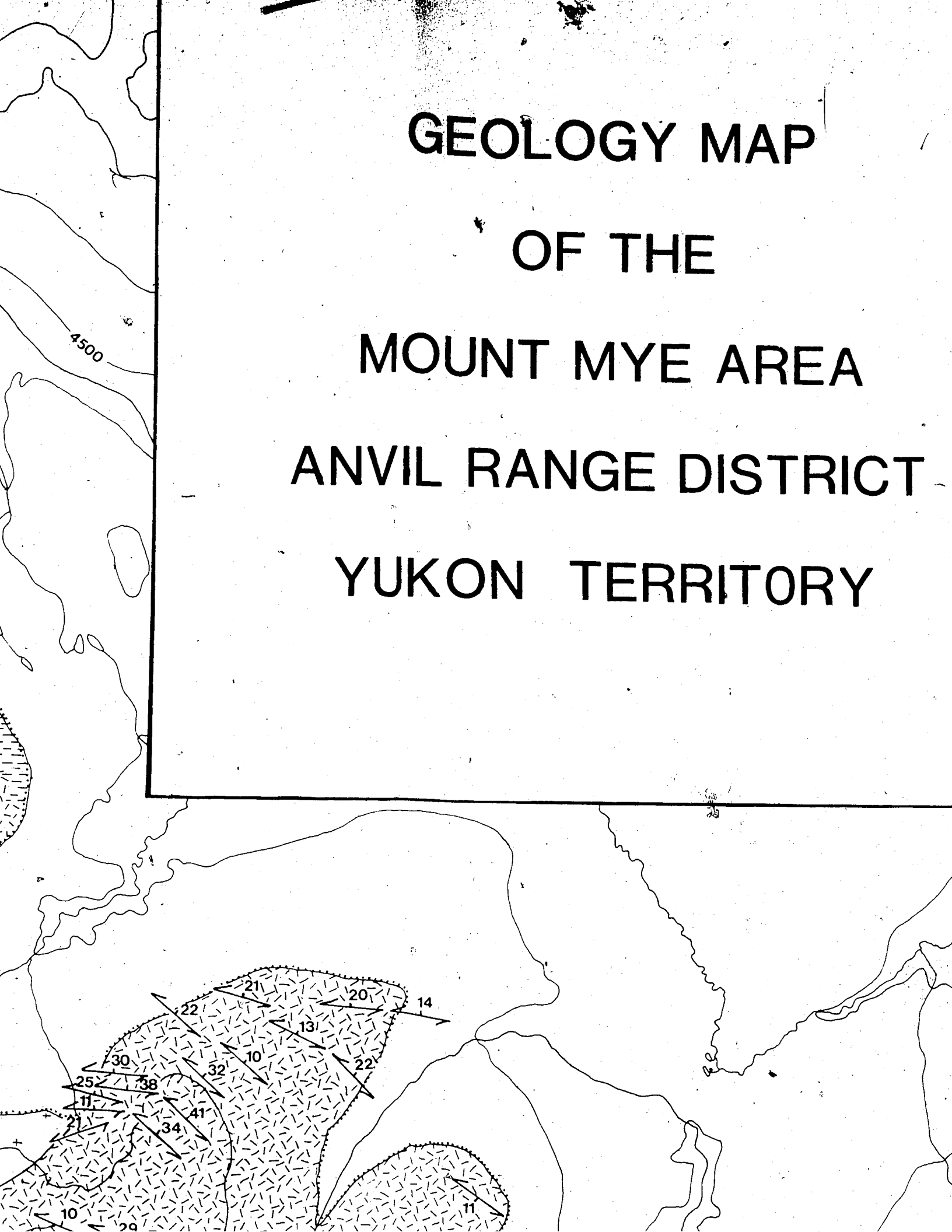

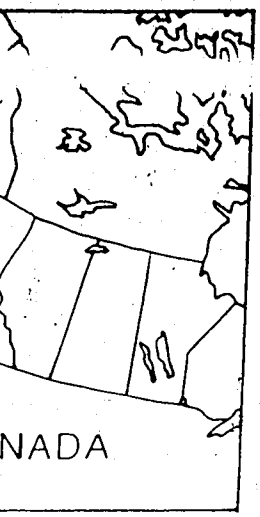

NADA

CATION

N.W.T.

B.C. | Alta.

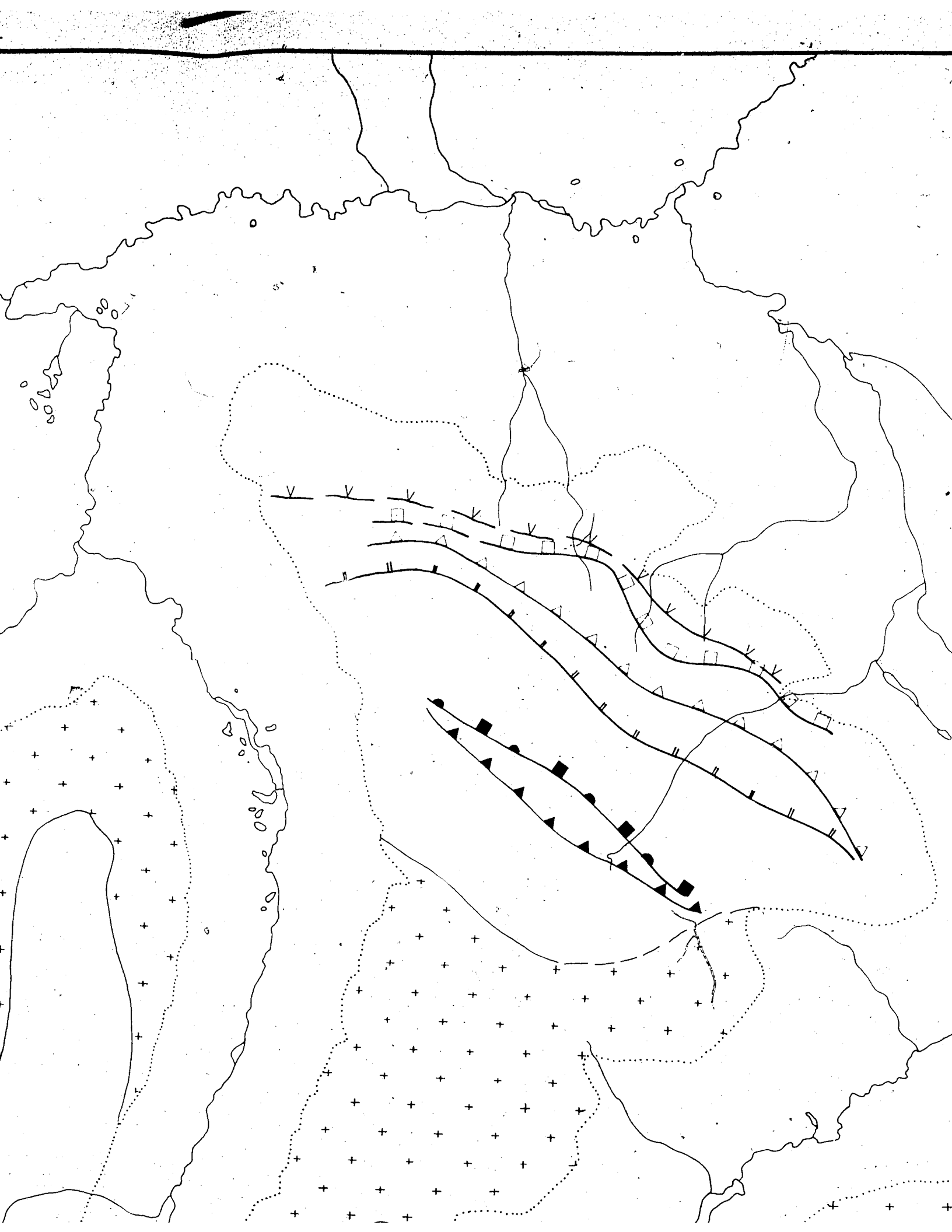

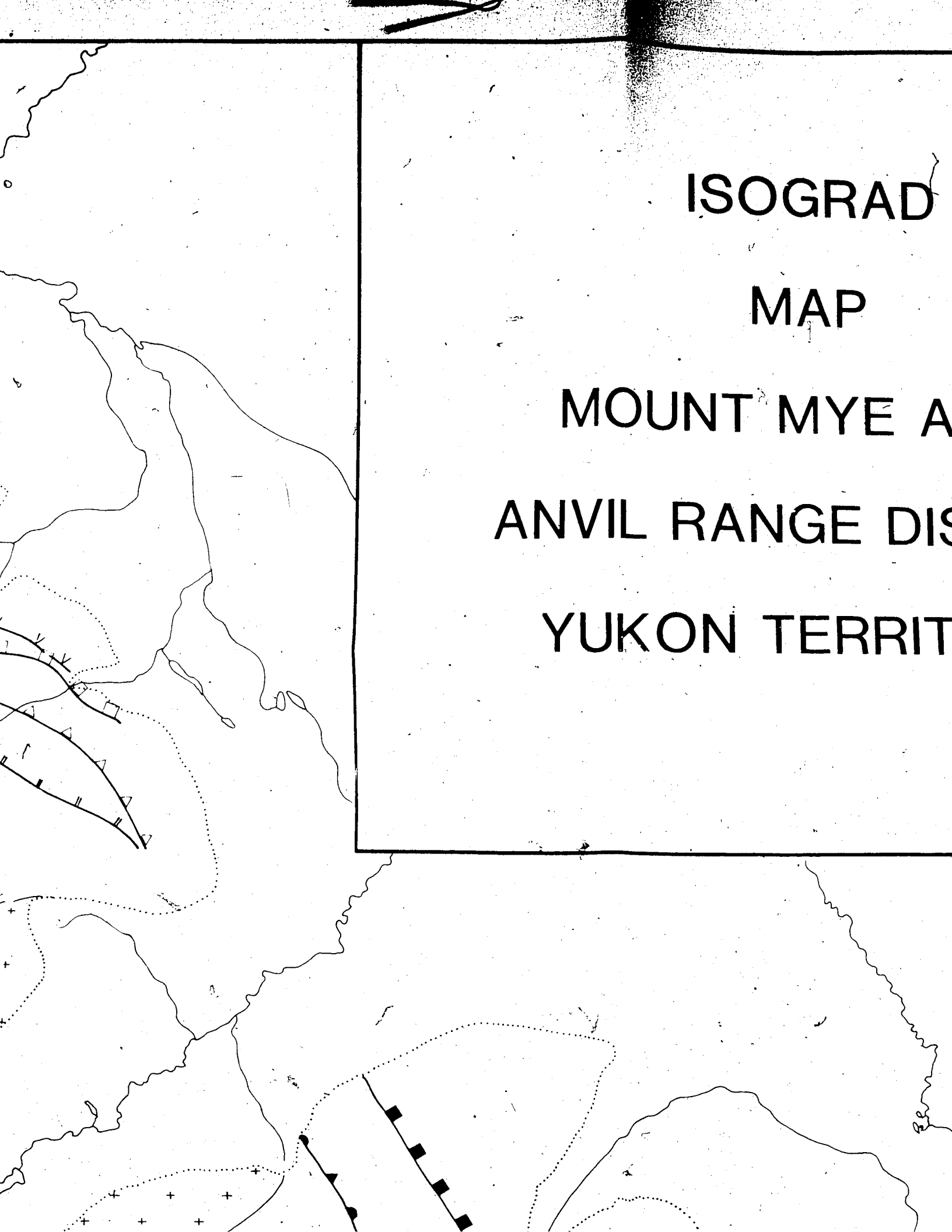
ISOGRAD
MAP
MOUNT MYE A
ANVIL RANGE DIS
YUKON TERRIT

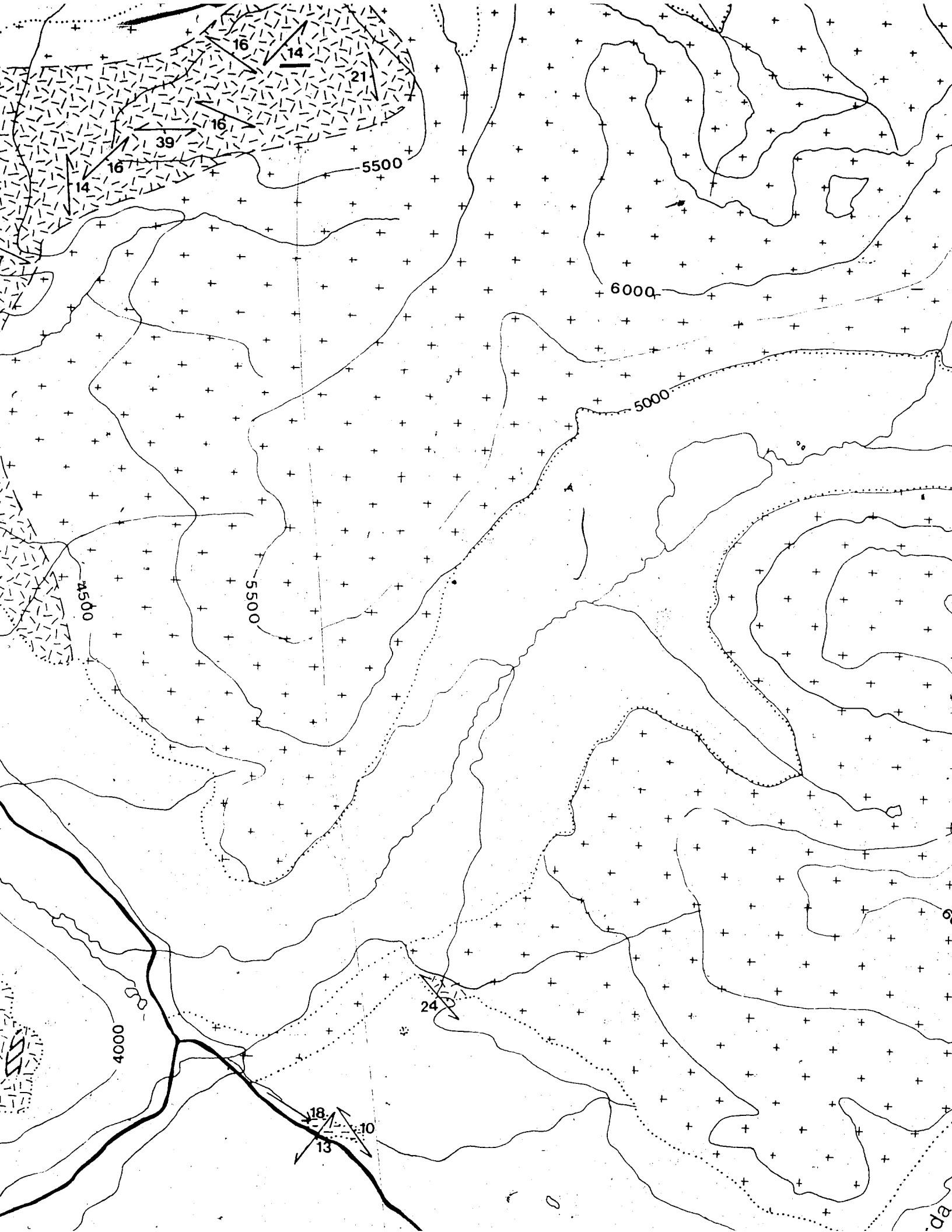
16
14
21
16
39
16
14
5500
6000
5000
5500
5500
4000
24
18
10
13

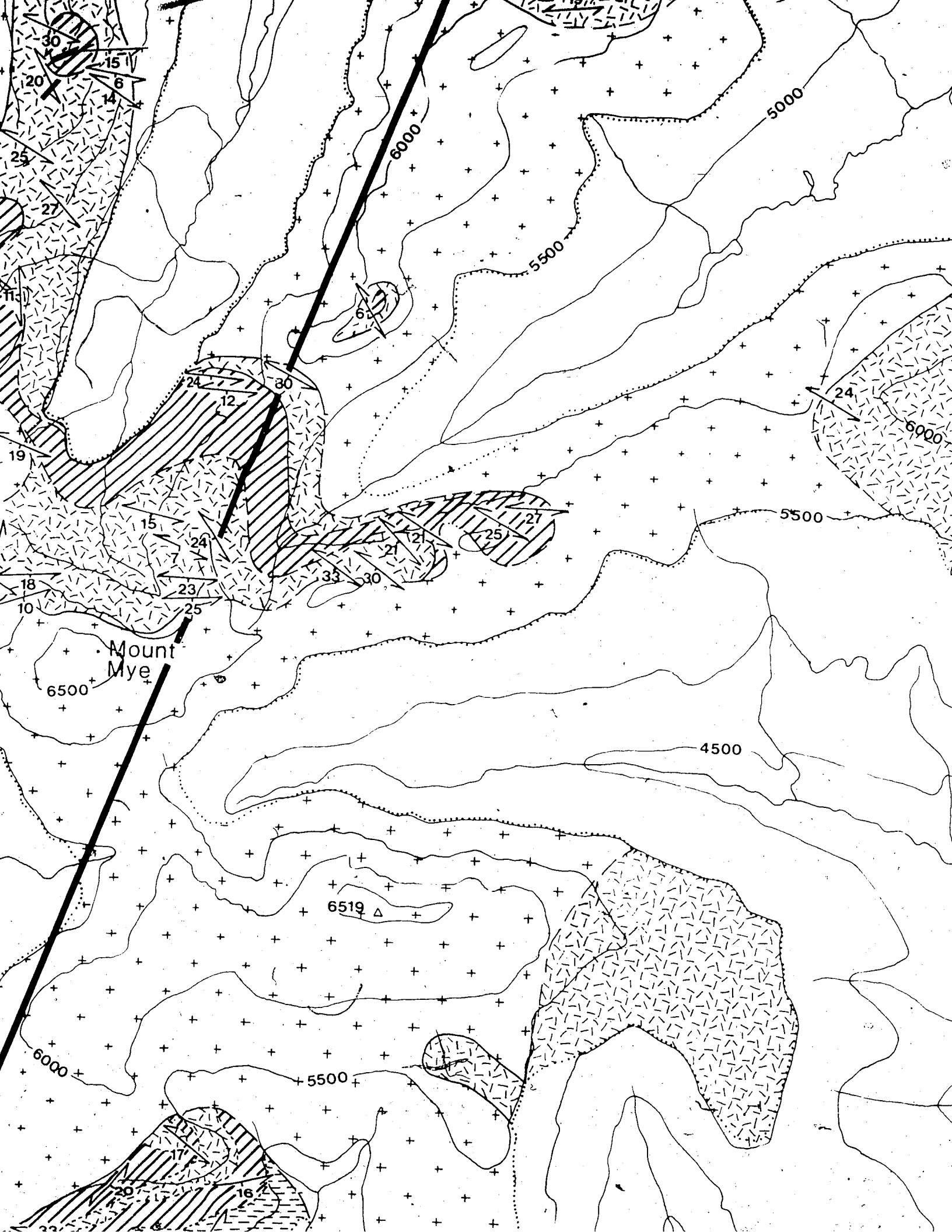
Mount
Mye
6519
6500
6000
5500
5000
4500

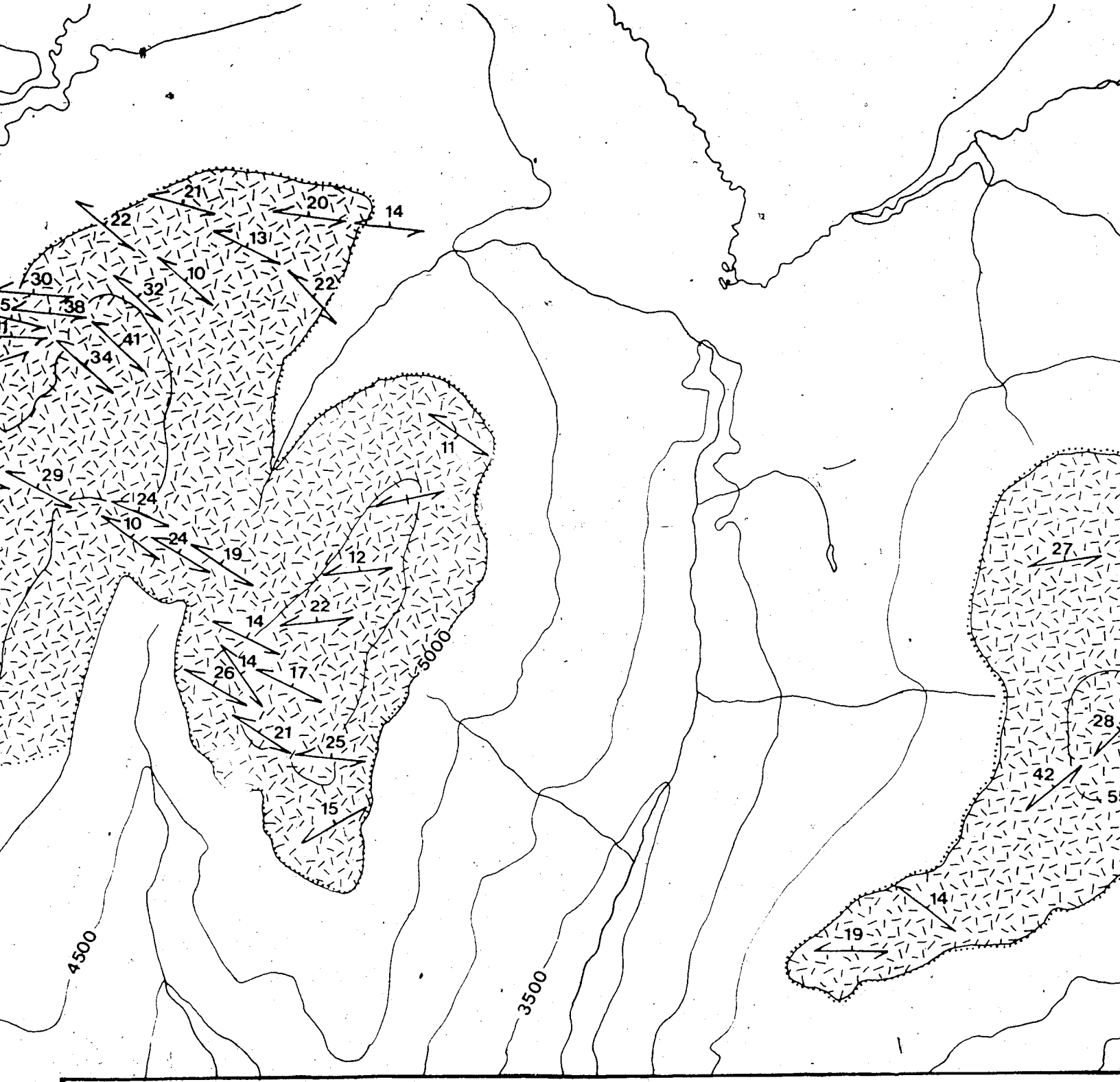

LEGEND

MAP UNITS

CRETACEOUS OR TERTIARY

Diorite dykes

SYMBOLS

Outcrop area

Geologic boundary

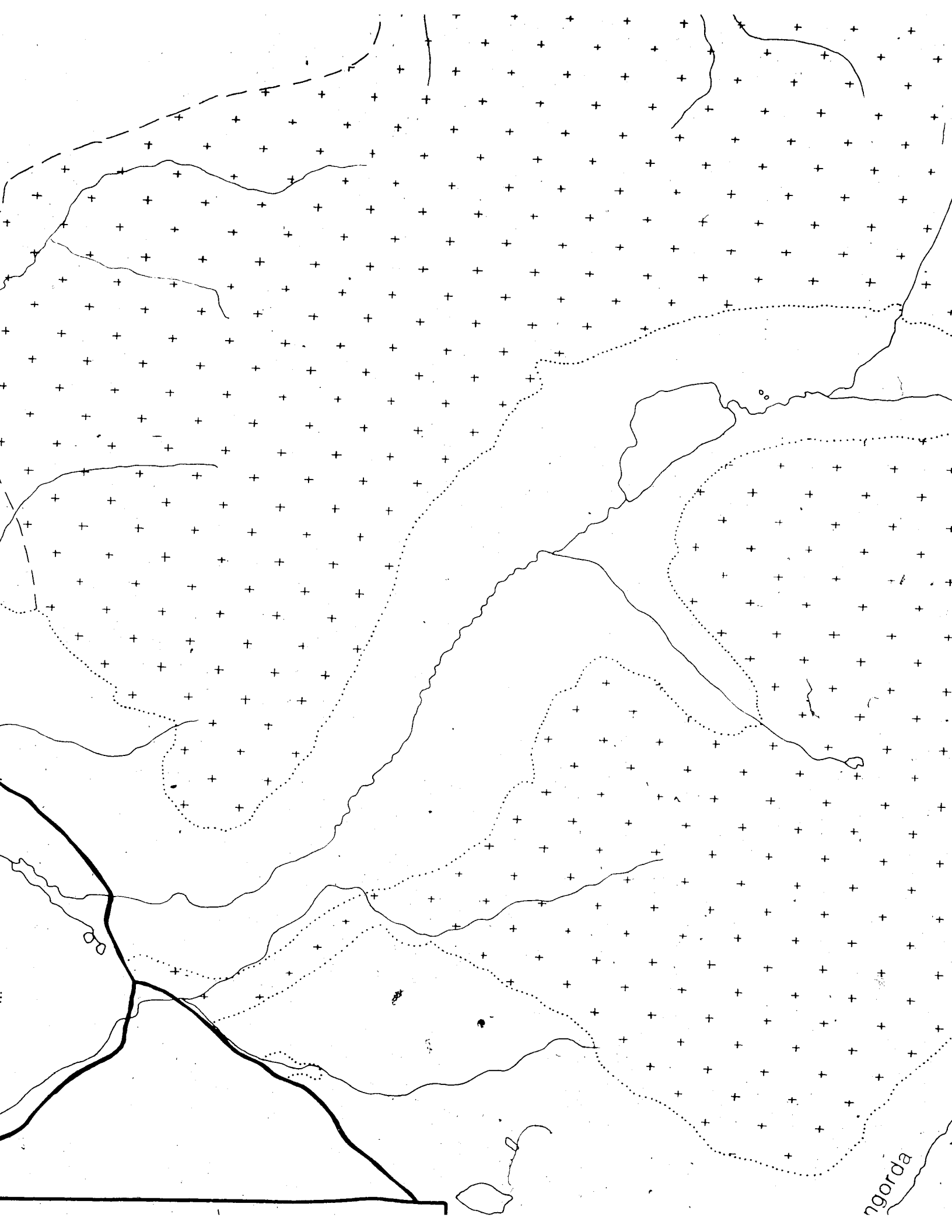
ngorda

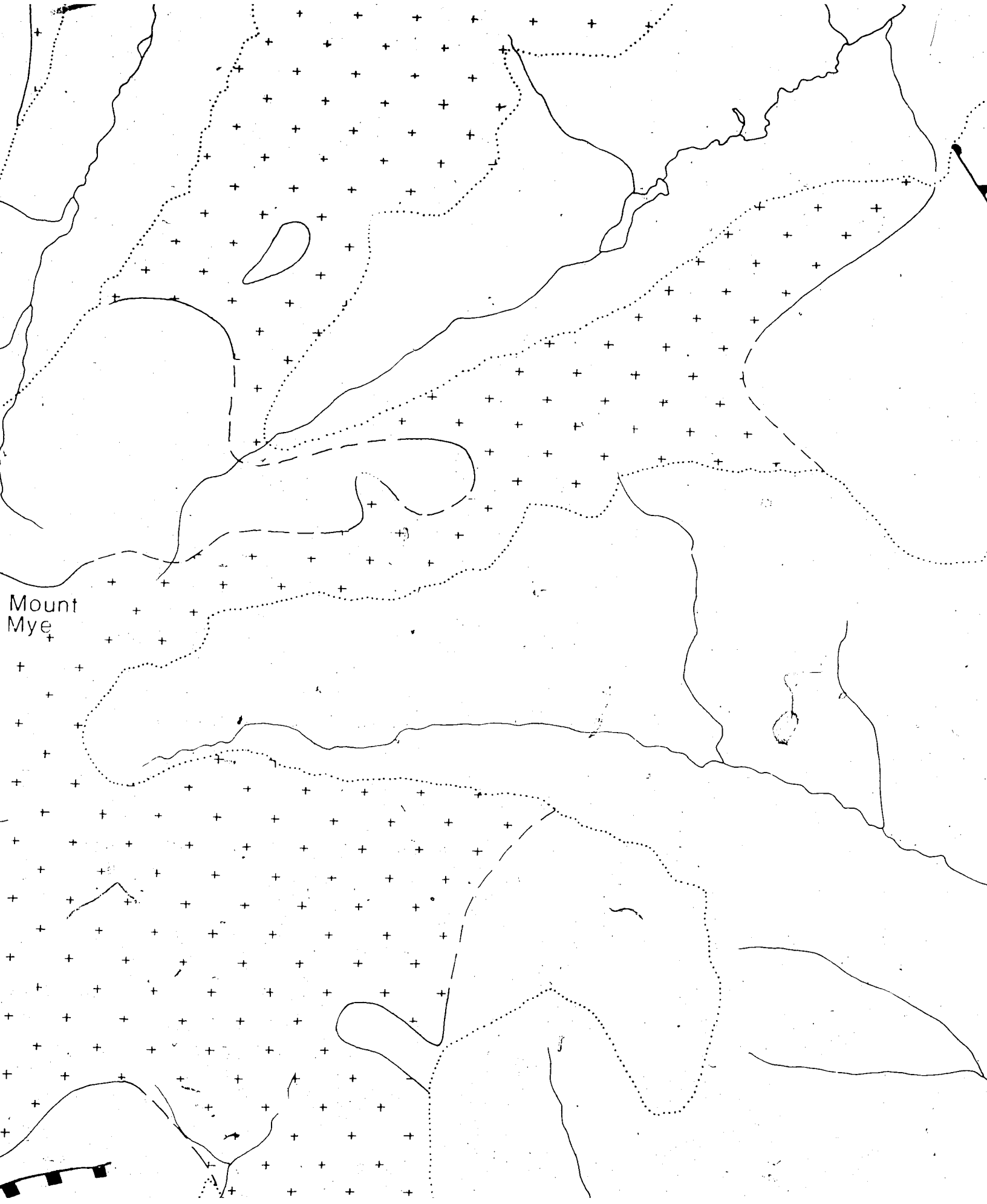
Mount
Mye


LEGEND
CRETACEOUS

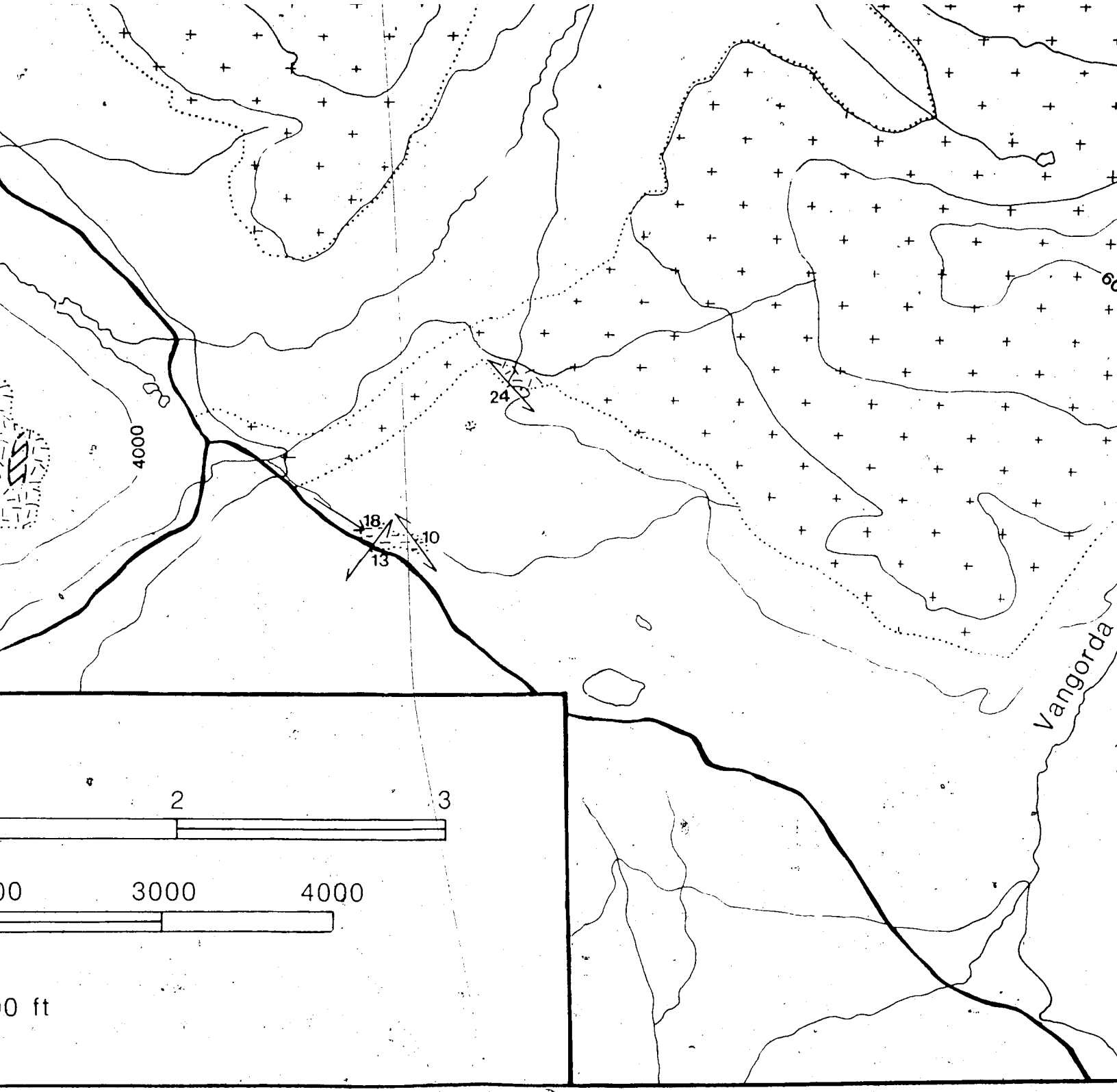
4000
24
18
10
13
Vangorda
2
3
00
3000
4000
0 ft

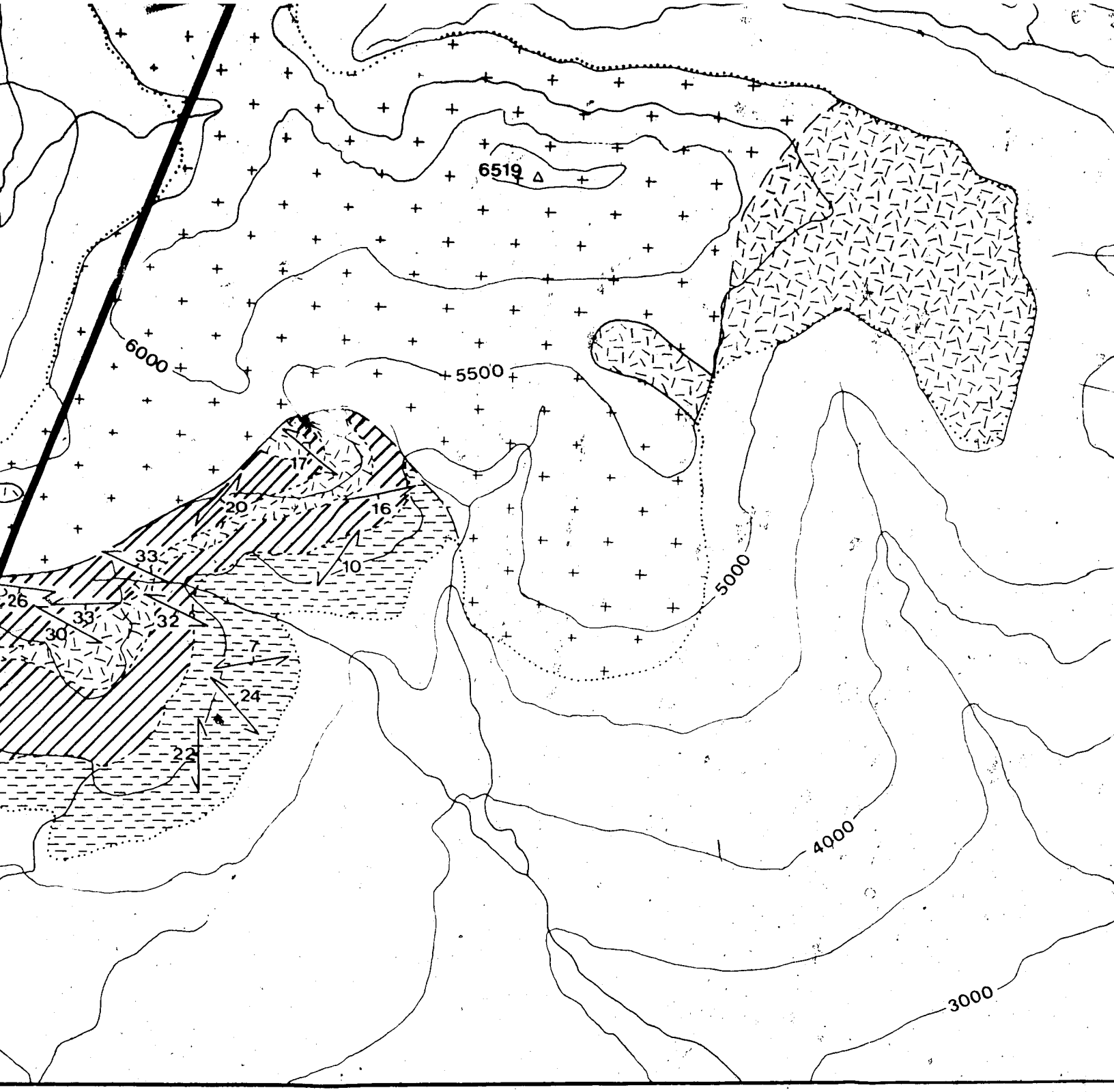
6519
6000
5500
5000
4000
3000
17
20
16
33
10
26
33
32
30
7
24
22

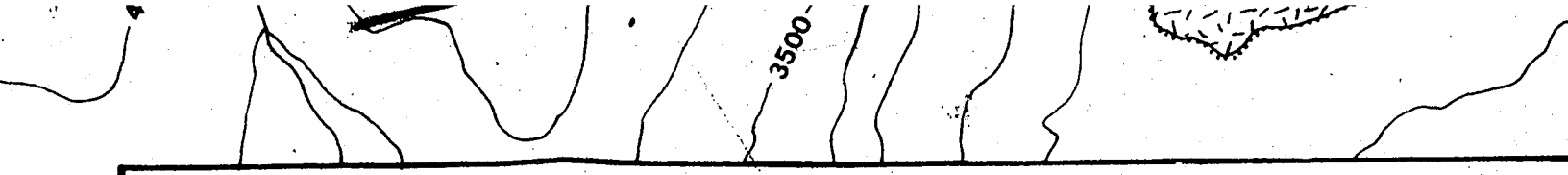

LEGEND

MAP UNITS

CRETACEOUS OR TERTIARY

Diorite dykes

CRETACEOUS

Medium grained biotite-muscovite granite

(?) CAMBRIAN AND (?) ORDOVICIAN

Silver-grey lustrous chlorite-muscovite-quartz phyllite, locally graphitic or calcareous, grades to schist described below

Laminated biotite-garnet-diopside-plagioclase quartz skarn and coarsely crystalline marble

Sillimanite-, staurolite-, and andalusite-garnet-biotite-muscovite schist, includes foliated amphibolite pods

SYMBOLS

Outcrop area

Geologic bounda
(defined, assume

Foliation (incline

Lineation

Fault (approxima

Road

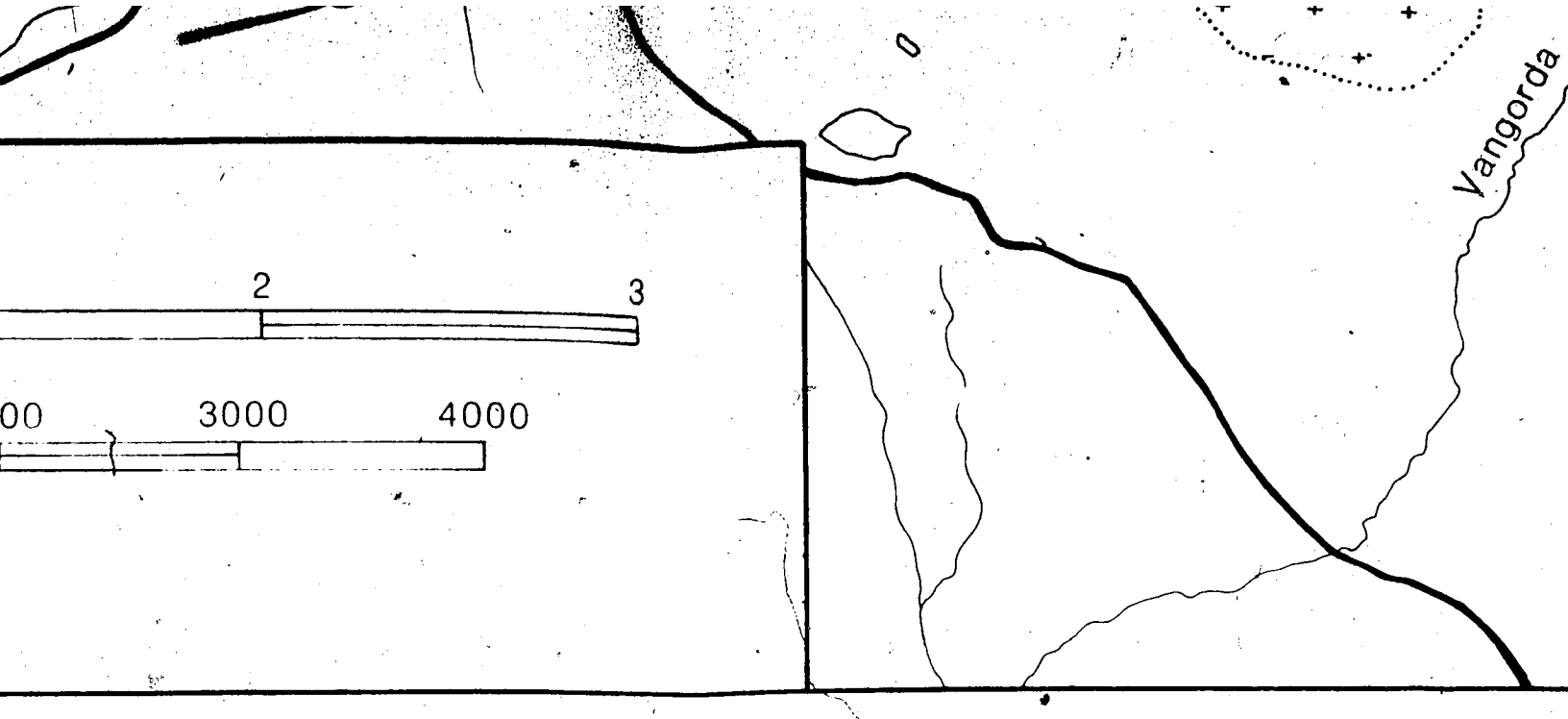
2
3
00
3000
4000
Vangorda

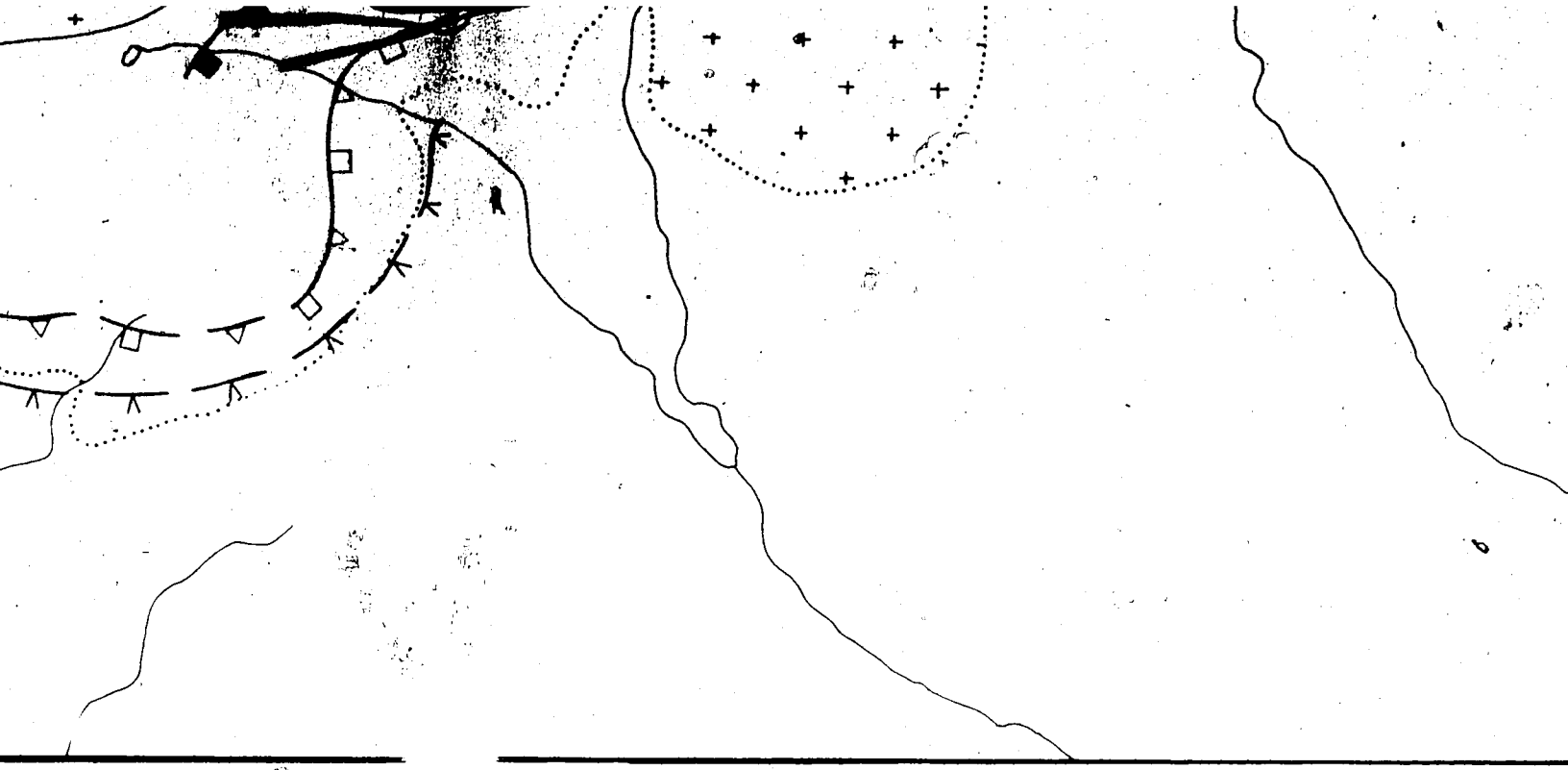

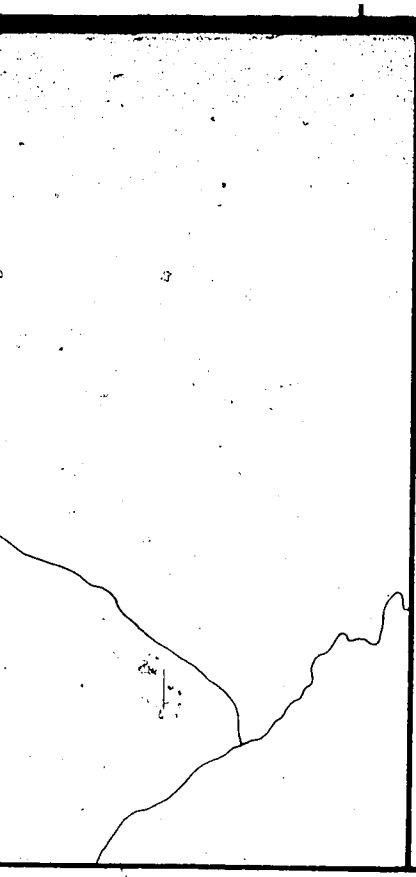

LEGEN

CRETACEOUS

Medium grained biotite-muscovite granite

Outcrop area

Geologic boundary
(defined, assumed, approximate)

Road